Mechanistic Understanding of Selectivity in Methanol-to-Hydrocarbons Conversion on Zeolites

A DISSERTATION
SUBMITTED TO THE FACULTY OF THE GRADUATE SCHOOL
OF THE UNIVERSITY OF MINNESOTA
BY

Samia Ilias

IN PARTIAL FULFILLMENT OF THE REQUIREMENTS
FOR THE DEGREE OF
Doctor of Philosophy

Advised by Aditya Bhan

May 2013

Acknowledgements

I would like to thank my adviser Professor Aditya Bhan, who has been a constant source of guidance for me. The countless hours he has spent critiquing my research, manuscripts, and presentations have helped me to become the researcher I am now.

I was incredibly fortunate to work alongside wonderful Bhan group members, who have always been there to bounce ideas of off and to help me in the lab when I was unable to move a 700-lb liquid nitrogen tank by myself. In particular, I would like to thank Rachit Khare who helped me collect and analyze many of the results presented in Chapter 4. Additionally, I'd like to thank my fellow classmates in the Bhan group, Dr. Hsu Chiang, Dr. Elizabeth Mallon, Ian Hill, and Mark Mazar. They have always been there to encourage me when I was down and to celebrate with me when things were going well.

I'd like to thank all my friends in CEMS, especially Kat Völzing, Milana Trifkovich, Alex Marvin, Bryan Paulsen, and Maroof Adil - Minneapolis has felt like home because of them.

Lastly, I would like to thank my family, for their unconditional love and support, particularly, my father, without whom, I may never have studied chemical engineering.

To my family

Abstract

The methanol-to-hydrocarbons (MTH) process over acid zeolite catalysts has seen renewed interest in recent years both for its ability to grow carbon chains and because methanol can be produced via a syngas intermediate from any gasifiable carbon-based feedstock. MTH proceeds through an indirect mechanism known as the hydrocarbon pool mechanism, involving two catalytic cycles: one in which olefins are repeatedly methylated to form branched species which are susceptible to cracking and another in which aromatics are repeatedly methylated and dealkylated to form light olefins. While the observed product distribution of MTH can be rationalized as an effect of the relative propagation of these two cycles, the current understanding of this chemistry is limited. In MTH conversion, the relationship between zeolite structure, its effect on the kinetics and mechanism, and observed product selectivity of MTH is not fully understood. In this dissertation, the link between the mechanism of MTH and the observed product selectivity is investigated with a focus on how selectivity can be controlled through manipulation of the mechanism and also give insight into the mechanism.

The product selectivity of dimethyl ether (DME) conversion to hydrocarbons on H-ZSM-5, a medium-pore zeolite, was systematically tuned by co-feeding small amounts of ^{13}C-propene and ^{13}C-toluene (4 kPa) with ^{12}C-DME (70 kPa) at iso-conversion conditions (20.8-22.7 C%) at 548 K. The selectivity to ethene (14.5-18 C%) and aromatics (7.1-33.7 C%) increased while selectivity to C_4-C_7 aliphatics (42.8-16.9 C%) decreased with increasing amounts of toluene (0-4 kPa) in the co-feed. Similar trends are also observed at lower conversions (4.6-5.1 C%) at 548 K and at higher temperatures (623 K) on H-ZSM-5. The relative propagation of the olefin- and aromatic-based cycle on H-BEA, a large-pore zeolite, was also tuned through the use of olefin and aromatic co-feeds. The addition of propene resulted in a four-fold increase in selectivity for C_3-C_7 aliphatics compared to the addition of 1,2,4-triMB at 623 K on H-BEA. By changing the ratio of olefins and aromatics in the co-feed, the selectivity of MTH over both H-ZSM-5 and H-BEA can be systematically tuned at iso-conversion, showing that the olefin:aromatic ratio can be used as a parameter to propagate the olefin- and aromatic-based carbon pools to varying extents within the range of conditions studied in this work. On H-SAPO-34, a zeotype material with large cages connected with small windows, the aromatic-based cycle dominates over the olefin-based cycle. Unlike H-ZSM-5 and H-BEA, however, the product selectivity of MTH conversion on H-SAPO-34 could not be tuned through the use of olefin co-feeds, most likely due to aromatics entrained within the catalyst blocking access to the active sites.

The ratio of ethene to 2-methylbutane + 2-methyl-2-butene (ethene/2MB) yield can be used to describe the propagation of aromatic and olefin methylation/cracking cycles. At

iso-conversion conditions at 548 K, propene is co-fed with DME to increase propagation of the olefin-based cycle and correspondingly a 1.7-fold decrease in the ethene/2MB yield is observed. Similarly, the co-reaction of toluene with DME increases propagation of the aromatic-based cycle and a 2.1-fold increase in the ethene/2MB yield is observed. The ethene/2MB yield also increased by a factor of 2 as DME conversion increased from 5-62%, which is consistent with the observed concurrent increase in selectivity to ethene and methylbenzenes. For the reaction of DME alone, increasing the temperature from 548 K to 723 K increases the propagation of the olefin-based cycle and a corresponding decrease in the ethene/2MB yield from 4.7 to 1.3 is also observed. The ethene/2MB yield varies systematically with feed composition, conversion, and temperature, showing that this ratio describes the relative propagation of the aromatic to olefin methylation/cracking cycles in MTH conversion on H-ZSM-5.

Co-reactions of ∼8 kPa of DME with 4 kPa of toluene, p-xylene, and 4-ethyltoluene on H-ZSM-5 at 523-723 K with varying isotopic feed compositions of $^{13}C/^{12}C$ show varying incorporation of $^{13}C/^{12}C$-atoms into ethene and propene. Three distinct aromatic dealkylation mechanisms have previously been reported in the literature (paring, side-chain, and ring expansion mechanism) and were used to predict the ^{13}C-contents of ethene and propene based on the experimentally observed isotopologue distribution of 1,2,4-trimethylbenzene, 1,2,4,5-tetramethylbenzene, and 4-ethyltoluene. The predicted ^{13}C-content of ethene and propene from 1,2,4-trimethylbenzene and 1,2,4,5-tetramethylbenzene from the paring mechanism most closely match the experimentally observed ^{13}C-contents of ethene and propene, compared to the other mechanisms. This work, for the first time, quantitatively shows that aromatic dealkylation to form ethene and propene on H-ZSM-5, occurs through the paring mechanism.

CONTENTS

LIST OF TABLES

LIST OF FIGURES

CHAPTER

ONE

INTRODUCTION

1.1 Motivation

Non-traditional carbon-based feedstocks will be critical in supplying the planet with fuel and chemicals in the future. The conversion of methanol-to-hydrocarbons (MTH) over an acidic zeolite catalyst has received considerable attention since its discovery by Mobil Research Laboratories in 1976, both for its ability to grow carbon chains and because methanol can be produced from any gasifiable carbon-based feedstock, including natural gas, coal, and biomass. Using either methanol or its dehydration product, dimethyl ether (DME), as a feed, a wide variety of hydrocarbons can be formed, such as gasoline-range hydrocarbons (methanol-to-gasoline, MTG) and light olefins (methanol-to-olefins, MTO).[12–15] MTH proceeds through an indirect mechanism known as the hydrocarbon pool mechanism in which two catalytic cycles are at work (Figure 1.1): one in which olefins are repeatedly methylated to form species which are susceptible to cracking and another in which aromatics are repeatedly methylated and dealkylated to form light olefins.[16–20]

The emergence of this dual cycle mechanism has contributed significantly to the general understanding of the hydrocarbon pool mechanism. Previous mechanistic understanding of MTH provided a relationship between zeolite topology and MTH product distribution in very specific cases, such as H-SAPO-34 (CHA framework), which has narrow 8-member ring (MR) openings that hinder diffusion of molecules larger than linear C_4 hydrocarbons out of the 12-MR cages, and H-ZSM-22 (TON framework), where narrow 10-MR pores hinder aromatic dealkylation reactions. For other zeolite frameworks, structure-function relationships have not been fully developed. Elucidating the identity of the hydrocarbon pool on various zeolites now provides further insight into how zeolite topology affects the MTH product distribution, but as Figure 1.2 shows, the missing steps in developing structure-function relationships include an understanding of the kinetic behavior of hydrocarbon pool

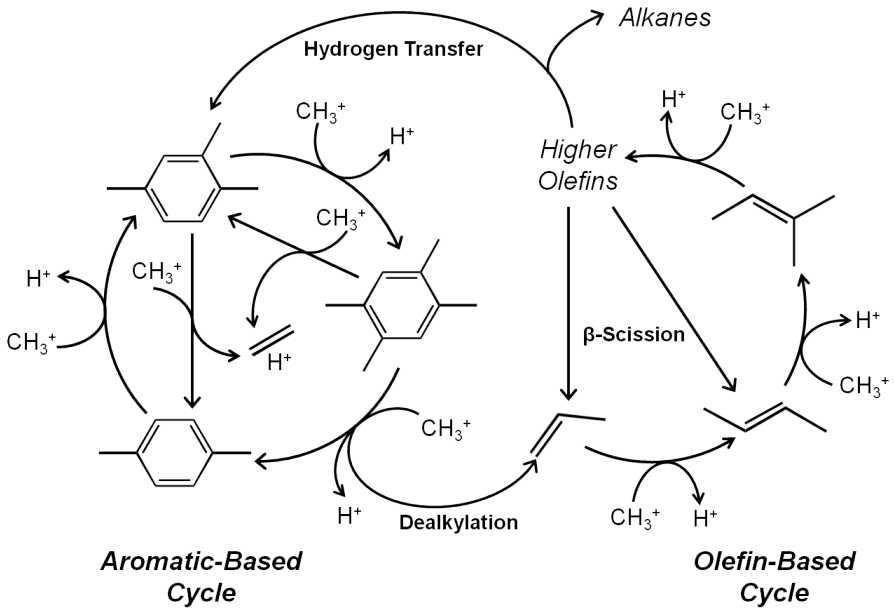

Figure 1.1: Dual olefin and aromatic methylation catalytic cycle for methanol-to-hydrocarbons on H-ZSM-5.

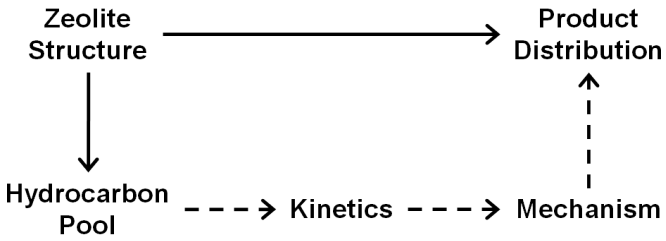

Figure 1.2: The current understanding of MTH has focused on making a direct connection between zeolite structure and product distribution.

species and how the kinetics of these species affects the available mechanistic pathways and selectivity. In this research, we focus specifically on the relationship between the observed product distribution and the mechanism of MTH conversion on acid catalysts.

1.2 Background on the Mechanism of MTH

Six major chemistries occur in MTH and are discussed in Chapter 2: (1) olefin methylation, (2) olefin cracking, (3) hydrogen transfer, (4) cyclization, (5) aromatic methylation, and (6) aromatic dealkylation. The observed product selectivity of MTH conversion is controlled by the relative rates of these reactions

1.3 Tuning the Selectivity of Methanol-to-Hydrocarbons on H-ZSM-5

The catalytic behavior of MTH systems is determined not only by the structural and compositional features of the zeolite catalyst but also by the organic co-catalyst, olefins and aromatics, that comprises the hydrocarbon pool. The relative rates of propagation of the olefin- and aromatic-based cycles control the selectivity of MTH. Olefin and aromatic compounds were co-reacted with DME to systematically seed the hydrocarbon pool and tune the selectivity of MTH catalysis on H-ZSM-5. Systematic changes in the product selectivity of MTH conversion on H-ZSM-5 as a result of co-feeding olefin and aromatic compounds with DME are reported in Chapter 3. By changing the olefin:aromatic ratio of the co-feed, the relative contribution of the olefin- and aromatic- based cycles in MTH can be modulated and the resulting product selectivity can be tuned. Co-processing propene resulted in a monotonic increase in the selectivity to C_4-C_7 acyclic hydrocarbons while co-processing toluene resulted in enhanced selectivity to ethene and aromatics, implying that selectivity on H-ZSM-5 at iso-conversion can be systematically tuned and controlled.

1.4 The Relative Propagation of the Aromatic- and Olefin-Based Cycles

The product distribution of MTH can be rationalized as an effect of the relative propagation of the olefin- and aromatic-based cycles, however, the lack of experimentally measured rates for individual reaction steps has precluded quantitative assessments of the relative propagation of the two cycles. The ratio of ethene to 2-methyl-2-butene + 2-methylbutane (ethene/2MB) yield can be used as descriptor of the relative propagation of the two cycles.

The ethene/2MB yield varies systematically and predictably with changes in the selectivity of MTH conversion on H-ZSM-5 as a result of olefin and aromatic co-feeds, reaction temperature, and conversion and is reported in Chapter 4. Increased propagation of the aromatic-based cycle, evidenced by enhanced selectivity to ethene and methylbenzenes, results in a higher ethene/2MB yield while increased propagation of the olefin-based cycle, evidenced by enhanced selectivity to C_4-C_7 hydrocarbons, results in a lower ethene/2MB yield, showing that the ethene/2MB yield is valid descriptor for the relative propagation of the olefin- and aromatic-based cycles of MTH conversion on H-ZSM-5.

1.5 Tuning the Selectivity of Methanol-to-Hydrocarbons on H-BEA and H-SAPO-34

The ability to tune the selectivity of MTH conversion on H-ZSM-5 and to describe the relative propagation of the aromatic- and olefin-based cycles on H-ZSM-5 using the ethene/2MB ratio are reported in Chapters 3 and 4, respectively. In Chapter 5, these discussions are extended to two large-pore catalysts - H-BEA and H-SAPO-34. Systematic changes in the product selectivity of MTH conversion on H-BEA as a result of co-feeding olefin and aromatic compounds with DME are reported in Chapter 5 and show that the relative propagation of the olefin- and aromatic-based cycles on H-BEA can be controlled. Isotopic switching experiments on H-BEA, however, show that in the absence of an aromatic co-feed, the aromatic-based cycle does not contribute significantly to light olefin production. On H-SAPO-34, a propene co-feed is used to determine if the olefin-based cycle can be activated on this catalyst where the aromatic-based cycle dominates. Aromatics are too large to enter the small 8-MR windows of SAPO-34, therefore, a 2-pentene co-feed is used as an aromatic precursor to determine if the aromatic-based cycle can be propagated more. No changes in the selectivity as a result of olefin co-feeds are observed on H-SAPO-34, showing the structure of the catalyst affects the ability to tune the selectivity.

1.6 The Mechanism of Aromatic Dealkylation on H-ZSM-5

Light olefin formation from aromatics has been postulated to occur through three distinct mechanisms: (1) the paring mechanism, (2) the side-chain mechanism, and (3) the ring expansion mechanism. These mechanisms each differ in how aromatic ring carbons, aromatic methyl carbons, and carbons from DME/methanol are incorporated into the light olefins formed. The isotopologue distribution of olefins and aromatics in the effluent of the co-reactions of DME with toluene, p-xylene, and 4-ethyltoluene with varying $^{12}C/^{13}C$ feed compositions at differential conversions and 523-723 K on H-ZSM-5 are reported and

discussed in Chapter 6. The effluent aromatic isotopologue distributions were used to predict the ^{13}C-content of the ethene and propene based on the three mechanisms for aromatic dealkylation. The predicted ^{13}C-contents of ethene and propene from the paring mechanism most closely matched the experimentally observed ^{13}C-contents of ethene and propene, quantitatively showing for the first time over a 200 K temperature range that aromatic dealkylation on H-ZSM-5 occurs through the paring mechanism.

CHAPTER

TWO

BACKGROUND ON THE MECHANISM OF METHANOL-TO-HYDROCARBONS CATALYSIS*

2.1 Introduction

As global energy demand increases simultaneously with dwindling supplies of conventional petroleum resources, non-traditional carbon-based feedstocks will be essential in supplying the world with fuels and chemicals. The methanol-to-hydrocarbons (MTH) process over acid zeolite catalysts, first discovered by Mobil Research Laboratories in 1976,[12] has seen renewed interest in recent years both for its ability to grow carbon chains and because methanol can be produced via a syngas intermediate from any gasifiable carbon-based feedstock, such as natural gas,[21] coal,[22,23] and biomass.[24,25] Methanol or its dehydration product dimethyl ether (DME) can be used as a feed to produce several different classes of hydrocarbons, including light olefins (methanol-to-olefins, MTO),[16–18] gasoline-range hydrocarbons (methanol-to-gasoline, MTG),[12] branched alkanes,[26,27] and aromatics.[28] The selectivity to any of these classes of compounds is determined both by the zeolite topology and the operating conditions used.

Since the discovery of MTH, there has been much debate regarding two aspects of the chemistry: (1) the origin of the first C-C bond and (2) the mechanism by which MTH proceeds. In the past decade, a broad consensus has emerged on the inability of methanol adsorbed within the zeolite pores to couple directly at rates relevant for steady-state MTH catalysis.[29] Lesthaeghe and co-workers[30,31] used ONIOM methods to calculate activation energies and rate constants for multiple pathways to form C-C bonds starting from two methanol molecules and found activation energy barriers for direct C-C coupling to be prohibitively high ($\sim$200 kJ mol^{-1}). Experiments using fractionally distilled methanol demonstrated that the catalyst induction period for MTH on H-ZSM-5 and H-SAPO-34 is highly sensitive to the impurity concentration in the methanol feed, indicating that if direct

*Reported from Ilias, S. and Bhan, A., *ACS Catalysis* **3**(1), 18-31 (2013)

C_1 coupling does occur, it operates at a rate significantly slower compared to the rate at which trace impurities initiate the reaction.[32] Direct C-C coupling mechanisms also require C-H bond activation, however, Marcus et al. found that feeding d_3-DME over H/D-SAPO-34 (in which 50% of the acid sites were H^+ and the other 50% were D^+) at 623 K resulted in an effluent containing approximately 25% d_0-DME, 50% d_3-DME, and 25% d_6-DME. The binomial distribution of D-atoms in DME showed that C-H activation, and thus direct C-C coupling, does not occur.[33]

Early work in MTH postulated an autocatalytic mechanism, based on the observed catalytic induction period during which increasing the concentration of hydrocarbons greatly increased the rate of methanol/DME conversion.[12] Ono and Mori[34] first showed the co-catalytic effect of co-processing ethene and cis-2-butene with methanol, reducing the catalyst induction period by a factor of 2 and 4, respectively, compared to the reaction of methanol alone over H-ZSM-5 at 512 K. Additionally, Langner et al.[35] noted that by co-feeding methanol with higher alcohols that readily dehydrate to linear olefins under reaction conditions on H-ZSM-5, the kinetic induction period could be substantially reduced, indicating the important catalytic role of olefins in MTH. Dessau and LaPierre[36,37] outlined a reaction mechanism for MTH based on olefins that are sequentially methylated and subsequently crack to form smaller olefins, or participate in hydrogen transfer reactions to form alkanes and aromatics. However, Langner et al.[35] showed that co-feeding cyclohexanol with methanol also significantly reduced the catalyst induction period, indicating that both olefins and cyclic species play a critical role in MTH.

Dahl and Kolboe proposed a hydrocarbon pool mechanism in which methanol forms a pool of $(CH_2)_n$ species within the zeolite pores that produces light olefins, alkanes, and aromatics.[16–18] It is now widely agreed upon that MTH proceeds through this indirect hydrocarbon pool mechanism, though our understanding of the hydrocarbon pool identity has evolved. By reacting a series of two 20-μL pulses of methanol over H-SAPO-34, Haw and co-workers[38] showed that methylbenzenes (MBs) can act as organic co-catalysts for MTO, increasing methanol conversion from 14% to 100% between the first and second pulse. Mole et al.[39] observed the incorporation of ^{12}C-atoms from toluene into ethene when ^{12}C-toluene was co-reacted with ^{13}C-methanol over H-ZSM-5. Similar observations were made by Mikkelsen et al.[40] on H-BEA and H-MOR, providing further evidence that polymethylbenzenes are active hydrocarbon pool species for light olefin formation. Additionally, Davis and co-workers[41] observed that the isotopologue distribution of ethene was distinct from other olefins when ^{14}C-methanol was co-processed with ^{12}C-labeled C_{3+} alcohols on H-ZSM-5, suggesting that the mechanism of ethene formation is different from higher olefin formation. Isotopic switching experiments by Svelle, Bjorgen, and co-workers[19,20] on H-ZSM-5 in which ^{12}C-methanol feed is switched with ^{13}C-methanol feed during steady-state

reaction showed that ^{13}C-incorporation of ethene closely matched that of methylbenzenes, while the ^{13}C-incorporation of C_{3+} olefins matched each other. This result showed that two catalytic cycles are at work in MTH on H-ZSM-5 one that involves methylbenzenes and ethene and another that involves C_{3+} olefins (Figure 1.1). Similar work has since been done on various other zeolites and zeotype materials, though often with the purpose of showing the dominance of one cycle over another.[42–45]

The discovery of the dual aromatic- and olefin-based catalytic cycles in MTH catalysis on acid zeolites has given a new context for rationalizing structure-function relationships for this complex chemistry. The current mechanistic understanding of MTH limits structure-function relationships to the effect of the zeolite framework on the identity of the hydrocarbon pool and the resulting product selectivity. We emphasize the need for assessing the consequences of zeolite structure in MTH in terms of experimentally measured rates and activation barriers for individual reaction steps and in terms of speciation preferences within the dual olefin- and aromatic-catalytic cycles to alter their relative propagation.

2.2 Chemistry of MTH

Six major chemistries occur within the dual cycle mechanism for MTH: (1) olefin methylation, (2) olefin cracking, (3) hydrogen transfer, (4) cyclization, (5) aromatic methylation, and (6) aromatic dealkylation. The rate and role of each of these chemistries in determining the product distribution of MTH is an outstanding question.

2.2.1 Olefin Methylation

Figure 1.1 shows that olefin methylation is one route by which methyls are incorporated into hydrocarbon products. Work by Cui et al.[46,47] on ZSM-22 (TON framework) and subsequent work by Teketel et al.[42,48,49] on ZSM-22 and ZSM-23 (MTT framework) has shown that some unidimensional 10-MR zeolites hinder both the transport of cyclic species out of the zeolite pore and aromatic dealkylation reactions. The olefin methylation pathway dominates in these zeolites, resulting in a product distribution rich in C_{5+} aliphatics at temperatures above 623 K. There are two proposed mechanisms for olefin methylation (Figure 2.1): (1) a co-adsorbed mechanism in which methanol and an olefin are adsorbed on a single acid site and react in a single, concerted step; and (2) a surface-methoxide mechanism in which methanol or DME dehydrates to form a methoxide that desorbs upon reaction with an olefin. While evidence supporting both mechanisms have recently been reviewed,[50] we examine the consequences of methanol dimer formation on these two mechanisms.

The kinetics of C_2-C_4 olefin methylation has been studied on H-ZSM-5 using ^{13}C-methanol by Svelle et al.[1,2] and using DME on H-ZSM-5, H-BEA, H-FER, and H-MOR by

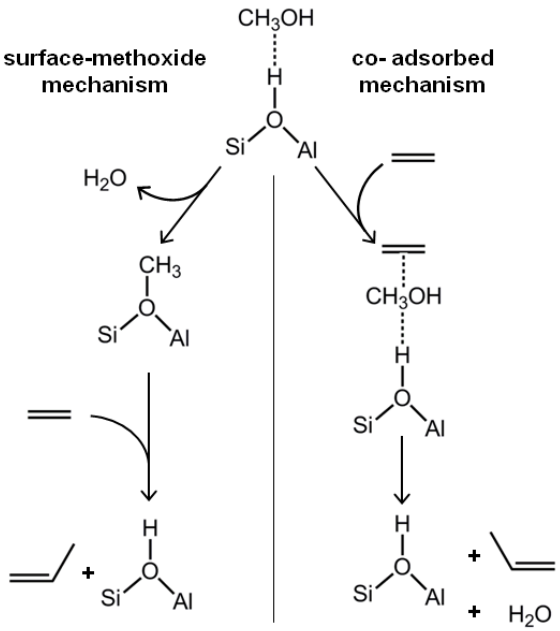

Figure 2.1: A representation of the surface-methoxide mechanism (left) and co-adsorbed mechanism (right) for olefin methylation with methanol.

Hill et al.[3–5] Despite these reactions taking place over a large range of experimental conditions (320-713 K), both studies show that olefin methylation has a first-order dependence on the olefin pressure and a zero-order dependence on the methylating agent (methanol or DME) and that this kinetic behavior is consistent across the zeolite frameworks studied.[1–5] The zero-order dependence on the methylating agent shows that the catalyst surface is saturated with the methylating agent, though the identity of the methylating agent (physisorbed methanol/DME or surface methoxide) is debated. Rate constants for C_2-C_4 olefin methylation on H-ZSM-5 are summarized in Figure 2.2. While all four zeolites investigated by Hill et al. have similar activation barriers for propene and butene methylation, pre-exponential factors and methylation rates are an order of magnitude higher for H-ZSM-5 and H-BEA compared to H-MOR and H-FER, indicating that olefin methylation reactions are propagated to different extents depending on the identity of the zeolite framework.[3–5] Across the four zeolites reported, olefin methylation rate constants increase and activation barriers systematically decrease with increasing olefin size, indicating that the relative stability of reaction intermediates increases with increasing carbon chain length.[1–5] Hill et al. also measured olefin methylation rates for all four butene isomers in the absence of C_4 isomerization reactions on H-ZSM-5 and H-BEA, observing that the rate constant of isobutene methylation was an order of magnitude greater than that of the other butene isomers.[5] These observations are consistent with the conclusion that the reactivity of olefins

is dependent on the degree of substitution about the double bond, which stabilize intermediate carbocations through inductive electron donation. Similarly, Bercaw, Labinger, and co-workers[51–54] show for methanol conversion over ZnI_2 and InI_3 in the liquid phase and Iglesia and co-workers[26,27,55] show for DME conversion over H-BEA that under conditions where skeletal isomerization is suppressed (<500 K), highly branched alkenes and alkanes, particularly triptane and triptene, are the dominant product as a result of methylation reactions favoring the formation of the most substituted carbenium ion as a reaction intermediate.

Computational chemistry studies using DFT on 30-46T cluster sizes to account for dispersion effects have also investigated C_2-C_4 olefin methylation via the co-adsorption mechanism and, in agreement with experimental work, show that activation energy barriers decrease while rate constants increase systematically with olefin size (Figure 2.2).[6,56] Additionally, rate constants and activation energy barriers match reasonably well with experimental work (within a factor of 2 for ethene and propene methylation rates).[6] A recent DFT study by Mazar et al. has investigated the pathway for ethene methylation via a surface-methoxide intermediate on H-ZSM-5, H-FER, H-BEA, H-MOR, and H-CHA.[57] The reaction of a surface methoxide with ethene on all zeolite frameoworks and acid site locations investigated proceeds via two distinct transition states, one in which a cyclopropane-like species is formed and a second which involves ring opening of the cyclopropane-like species. The apparent activation energy barriers for the surface-methoxide mechanism ranged from 97-141 kJ mol^{-1},[57] which compare well to apparent activation energy barriers calculated for the co-adsorption mechanism on H-ZSM-5 (94-104 kJ mol^{-1})[6,56] as well as experimental values (98-109 kJ mol^{-1}).[1,3,4]

The co-adsorbed mechanism requires the simultaneous adsorption of both methanol and an olefin on a single Brønsted acid site. Hybrid MP2/DFT calculations with periodic boundary conditions for a full unit cell of H-ZSM-5 show that the initial adsorption of methanol (-115 kJ mol^{-1}) is stronger than the subsequent co-adsorption of the olefin (-37, and -53 kJ mol^{-1} for ethene and propene, respectively) and the co-adsorption enthalpy for ethene with methanol is only reduced by 2 kJ mol^{-1} if a purely siliceous framework is used instead of H-ZSM-5 which contained one Al/unit cell.[56] This result shows that van der Waals interactions with the zeolite pore walls are the dominant factor in ethylene co-adsorption as opposed to interactions with the Brønsted acid site. In addition to methanol-olefin co-adsorption complexes, methanol dimer co-adsorption complexes may also form at the Brønsted acid site. Lesthaeghe et al. calculated the enthalpy of methanol dimer adsorption to be -117 kJ mol^{-1} using ONIOM calculation on 30T and 46T clusters at 720 K on H-ZSM-5,[30] in agreement with microcalorimetry measurements by Lee and Gorte[58] showing the differential heat of adsorption of methanol on H-ZSM-5 at 400 K to be -115

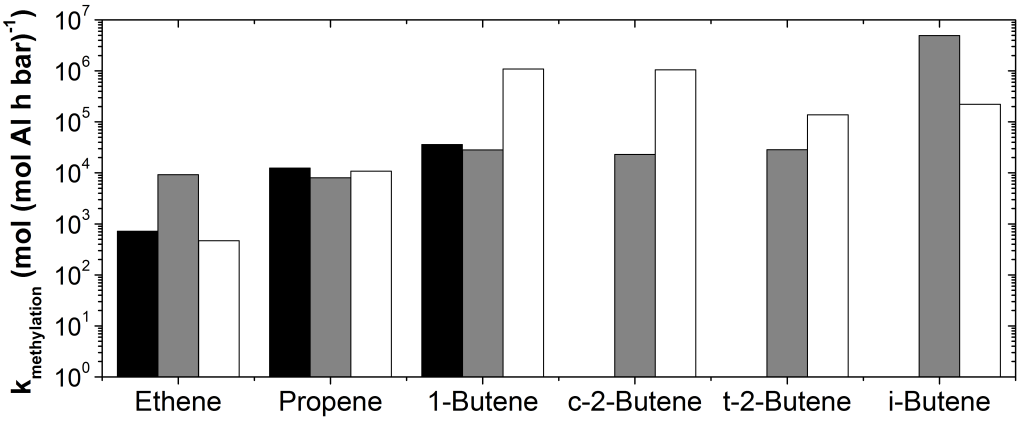

Figure 2.2: Rate constants at 623 K for C_2-C_4 olefin methylation on H-ZSM-5 from ■ Svelle et al.[1,2] (experimental), ■ Hill et al.[3–5] (experimental), and □ Van Speybroek et al.[6] (computational, co-adsorbed mechanism).

kJ mol^{-1} for up to 2 methanol molecules per acid site. The enthalpy of adsorption for methanol dimers is similar to the enthalpy of adsorption for methanol-olefin complexes (-152 kJ mol^{-1} and -168 kJ mol^{-1} for ethene and propene complexes, respectively),[56] hence, methanol dimer formation may compete with the formation of methanol-olefin co-adsorbed complexes. Stich et al.[59] found that the activation of methanol is facile in the absence of hydrogen bonding using first-principle molecular dynamics simulations, suggesting that methanol dimers would be inactive for methylation of olefins. Therefore, the formation of methanol-olefin co-adsorption complexes would be inhibited by the formation of inactive methanol-dimer complexes, and correspondingly, increasing the methanol pressure would result in inhibition of olefin methylation rates.

Unlike larger alkoxide species, surface methoxides lack a β-H and are therefore unable to desorb as olefins. As a result, surface-methoxides are stable intermediates and have been observed on a variety of zeolites via in situ infrared spectroscopy (with bands at 2980 and 2968 cm^{-1} for asymmetric and symmetric stretching, respectively)[34,60–62] and ^{13}C MAS NMR spectroscopy (with a signal at 56 ppm).[38,63–65] Boronat et al.[66] investigated surface-methoxide formation applying DFT-D to 130 atom clusters of the 12-MR channel of H-MOR and found intrinsic activation barriers to be 139 and 150 kJ mol^{-1} for DME and methanol precursors, respectively. In comparison, other DFT studies on 3-4T clusters calculate the barrier for methoxide formation from methanol to be greater than 200 kJ mol^{-1};[67–69] hence, the inclusion of dispersion effects is critical in determining if surface-methoxide species are formed during olefin methylation reactions. Once formed, surface-methoxides have been shown to be reactive with a variety of molecules including, but not

limited to toluene, alkyl halides, and aniline on frameworks such as H-Y, SAPO-34, and H-MOR.[61,64,65,70] Additionally, Marcus et al.[33] fed d_3-DME over SAPO-34 at 573 K and Hill et al.[5] fed a 50:50 mixture of unlabeled DME with d_6-DME over H-ZSM-5 at 393 K and both groups observed a DME effluent dominated by d_0, d_3, and d_6 isotopologues, indicating that methoxide formation is rapid and facile at experimental conditions relevant for MTH. Post-reaction water titration of reactions of DME with butene result in a 1:1 ratio of CH_3OH:Al, providing further evidence of surface-methoxide formation during steady-state olefin methylation reactions.[5]

Olefin methylation has also been investigated on H-SAPO-34 at 673 K by Dahl and Kolboe.[16–18] Co-feed experiments of ^{13}C-methanol with ^{12}C-ethanol (2 methanol:1 ethanol molar ratio), which dehydrates readily to form ethene under reaction conditions, show that at early times-on-stream (<40 minutes) 20% of propene in the effluent came from ethene methylation, containing only one ^{13}C-atom.[17] Similarly, when ^{13}C-methanol was co-reacted with ^{12}C-isopropanol (3 methanol:1 isopropanol molar ratio), which dehydrates to form propene, 24% of trans-2-butene came from propene methylation.[18] The low fraction of propene and trans-2-butene isotopologues containing only one ^{13}C-atom show that olefin methylation is not the dominant route for propene and butene formation on H-SAPO-34; rather aromatic dealkylation reactions are responsible for light olefin formation.[38]

2.2.2 Olefin Cracking

Olefin cracking as a route to light olefin production in MTH was first proposed by Dessau and LaPierre[36,37] and is a route used commercially to increase production of propene in Lurgi's methanol-to-propene (MTP) process, which is based on using H-ZSM-5 formulations. The mechanism of olefin cracking requires protonation of an olefin to form an alkoxide intermediate followed by β-scission of the alkoxide to form a smaller olefin and a smaller alkoxide. The smaller alkoxide subsequently desorbs to form another olefin and leaves behind a proton to regenerate the acid site.

Weitkamp et al.[7] first developed nomenclature to describe the various modes of cracking based on carbenium ion types for products and reactants - a useful method for understanding the difference in cracking rates as a function of olefin size and skeletal structure. Buchanan et al.[8] extended this nomenclature (Figure 2.3) in a study on the relative rates of monomolecular alkene cracking for C_5-C_8 olefins on H-ZSM-5 at 783 K. First order rate constants for cracking were reported, with relative rates of C_5:C_6:C_7:C_8 alkene cracking to be 1:24:192:603. A near equilibrium distribution of hexene isomers was achieved at 26% conversion of 1-hexene feed and the reaction of three different skeletal isomers of heptene resulted in identical product distributions, suggesting that numerous adsorption, isomerization, and

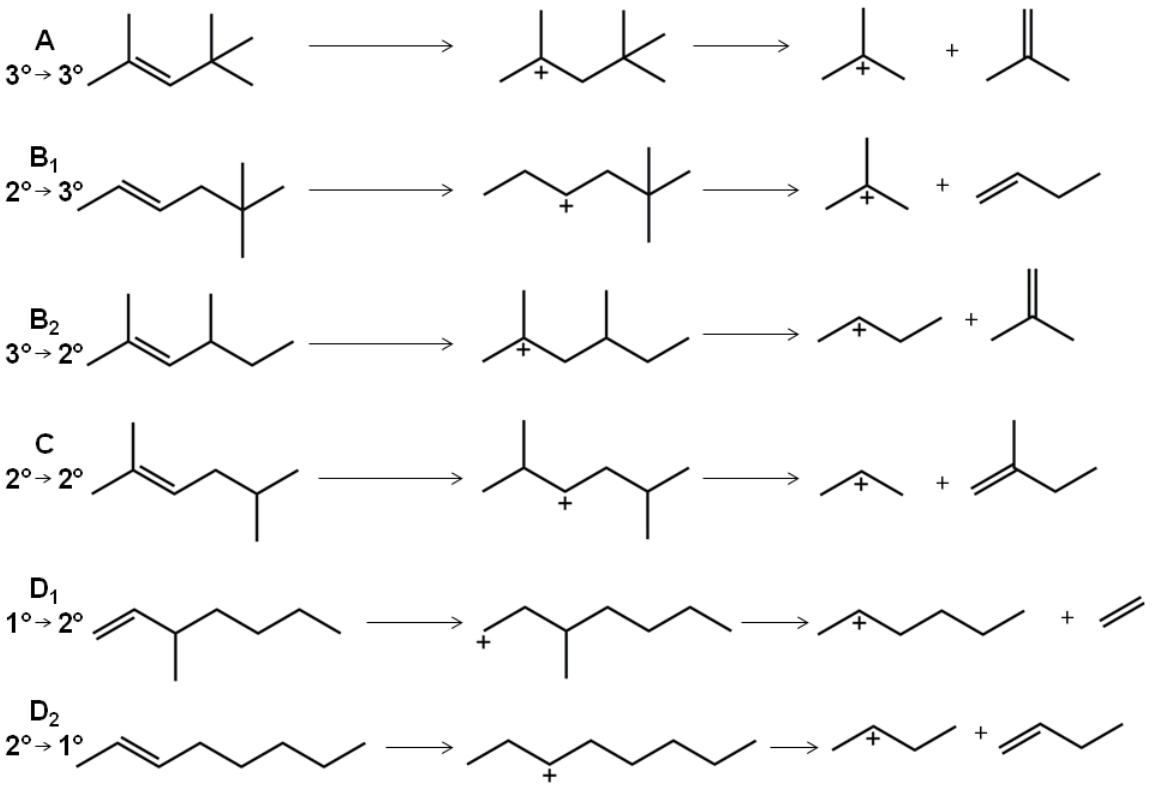

Figure 2.3: Different modes of β-scission for C_8 isomers with nomenclature developed by Weitkamp et al.[7] and Buchanan et al.[8]

desorption events take place prior to and are significantly faster than β-scission.[8] The dominant mode of cracking for hexene was 2°→2°, while for heptenes and 1-octene it was 2°→3° and 3°→2°. In contrast to 1-octene, 2,4,4-trimethyl-2-pentene cracked 50 times slower even though this branched isomer cracked through a more energetically favored 3°→3° cracking mode. The slower reaction rate of 2,4,4-trimethy-2-pentene compared to 1-octene is mostly likely due to diffusion limitations of this molecule in H-ZSM-5.

Speciation of olefin isomers is critical in determining the product selectivity for MTH. For example, if olefin cracking is considerably faster than olefin methylation, then the product distribution should be rich in light olefins. In contrast, if olefin cracking is slower than olefin methylation, then the product distribution may be rich in larger olefins, which may cyclize to eventually form aromatics. Simonetti et al.[27] measured the rates of β-scission for a variety of C_5-C_8 alkene isomers while co-feeding ^{13}C-DME on H-BEA at 473 K and found that in general, the rate of β-scission is at least 40 times slower than olefin methylation and is of the same order of magnitude as skeletal isomerization. The exception was 3,4,4-trimethyl-2-pentene (344T2P); β-scission for this C_8 isomer was almost twice as fast as olefin methylation, most likely because 344T2P is able to form a stable tertiary carbenium ion transition state. As a result of this facile cracking pathway, 344T2P is removed from the product distribution of MTH on H-BEA at these conditions.

Using 3T clusters at the B3LYP/6-31++G** level of theory, van Santen et al.[71–73] found three possible pathways for β-scission of 1-butoxide and 2-pentoxide (1) a one step pathway with a ring-like transition state, (2) a two step pathway involving a hydrogen-bonded transition state with a substituted cyclopropane (pathway HBCP), and (3) a one step pathway with a hydrogen-bonded transition state. Their calculations showed that pathway HBCP had the lowest activation energy barrier. In this pathway, a new C-C bond is formed resulting in the formation of a substituted cyclopropane species that subsequently undergoes cleavage of two different C-C bonds to form an olefin and an alkoxide. Activation energies were found to decrease with increasing carbon number, however, the activation energies reported are overestimated (>230 kJ mol^{-1}) due to the small cluster sizes used.[71,72]

In an independent study using 3T clusters at the HF/6-31G* level of theory, Hay et al.[74] studied the effect of branching on β-scission and found that the activation energy barrier for the β-scission of 2-pentoxide was 20-25 kJ mol^{-1} higher than for the β-scission of 2-methyl-2-pentoxide. At 773 K, this difference in activation energy barriers corresponds to rates for C_6 β-scission being 20-50 times faster compared to C_5 β-scission, assuming that both reactions have similar pre-exponential factors. This ratio of C_6 to C_5 β-scission rates is in agreement with experimental work by Buchanan et al.[8] Elucidating rates of β-scission on various zeolites will be key in determining what fraction of light olefins, particularly propene and butenes, are products of the aromatic- vs. olefin-based carbon pool; however,

the prevalence of secondary reactions such as olefin oligomerization and dehydrocyclization, hinder the measurement of kinetic parameters of β-scission.

2.2.3 Hydrogen Transfer

The dehydrative condensation of CH_3OH ($=CH_2+H_2O$) should lead to the formation of olefins $(CH_2)_n$, however, the observed product distribution for MTG consists predominantly of saturated alkanes and aromatic compounds. The formation of alkanes requires that an equivalent of H_2 be supplied which concurrently results in the formation of hydrogen-deficient species, such as dienes, trienes, and for MTH, polymethylbenzenes. A stoichiometric correlation between the yield of saturated alkanes and the yield of aromatic compounds is noted in both homogeneous and heterogeneous catalyzed C_1 homologation. Hydrogen transfer reactions therefore, alter the relative number of chain carriers available for the olefin- and aromatic-based cycles in MTH.

Hydrogen transfer is a bimolecular reaction in which a hydrogen atom is transferred between an adsorbed surface alkoxide and a cyclic or acyclic alkane or alkene. Because this involves the abstraction of a hydrogen atom and is mediated by carbocationic transition states as inferred from DFT calculations, branched alkanes are facile hydrogen donors compared to linear alkanes because the resulting carbocationic transition states are more stable.[75–78] Alkenes with tertiary allylic C-H bonds are even more reactive hydrogen donors than branched alkanes because they delocalize positive charge more effectively, which leads, in turn, to more stable carbocations. Davis and coworkers[79] co-fed ^{14}C labeled methylcyclohexane and methanol on H-ZSM-5 in a 1:70 molar ratio at 583 K and noted that the toluene formed in MTH was not predominantly ^{14}C labeled suggesting cycloalkanes were poor hydrogen donors under MTH reaction conditions. This observation regarding hydrogen transfer from cyclic molecules under MTH conditions is consistent with our discussion of cyclization mechanisms (Sections 2.2.4 and 3.3.3) where we suggest that ring closure in MTH predominantly occurs for C_{8+} species and also suggests that under low temperature conditions (<548 K) light alkanes and cyclic alkanes may be considered as termination products of MTH.

The hydrogen transfer index (HTI), defined as the ratio of alkanes to alkenes formed has also been used to qualitatively infer the influence of zeolite structure on the rate of hydrogen transfer with the inference being that methanol, $(CH_2)H_2O$, dehydrates to form olefins $(CH_2)_n$ which disproportionate to form alkanes (C_nH_{2n+2}) and aromatics. Hence, the ratio of alkenes to alkanes is a measure of hydrogen transfer characteristics of the zeolite structure. Early work from Mikkelson et al.[28] and more recent work from Teketel et al.[49] for zeolites with one dimensional 10-MR channels have continued to use this description, however, as discussed by Mikkelson, the HTI ratio depends on the time-on-stream and deactivation

characteristics as well as chemical conversion. This method is limited in its description of hydrogen transfer simply because the rate of hydrogen transfer is a bimolecular reaction and the number and identity of species that can undergo hydrogen transfer is changing with conversion and therefore, the rate of hydrogen transfer varies with conversion. The HTI descriptor concept attempts to qualitatively describe an average of the hydrogen transfer rate and cannot be used to infer either coking or deactivation characteristics of the zeolite.

Inferring mechanistic details and kinetic parameters regarding hydrogen transfer from experiments requires the isolation of surface alkoxides on zeolites and experimental conditions such that bimolecular hydrogen transfer steps occur predominantly in absence of competing alkylation, oligomerization/β-scission, and isomerization steps. This challenge has largely precluded experimental studies, however, a significant advancement has resulted from low temperature ($\sim$473 K) methanol homologation studies using ZnI_2 and InI_3 catalysts in the homogeneous phase[51–54,80] and from H-BEA[26,27,55] catalyzed low-temperature (423-473 K) synthesis of branched hydrocarbons.

Bercaw, Labinger, and coworkers[51–54,80] have investigated the mechanism of methanol conversion to branched hydrocarbons on iodide-based homogeneous catalysts to show that the remarkable selectivity to high-octane triptyl compounds can be explained based on (i) methylation and deprotonation preferentially leading to the most highly substituted carbocations; and (ii) the relative rate of hydrogen transfer to methylation being greater for triptene than its precursors. They probed the relative rates of olefin methylation to hydrogen transfer by co-feeding olefins with one equivalent of 1,4-cyclohexadiene (CHD), which is expected to be a particularly good hydrogen donor. A systematic study of olefin substitution comparing behaviors of 2,3-dimethyl-2-pentene, 2,4-dimethyl-2-pentene, 2,4-dimethyl-1-pentene, and triptene - olefins that all contain seven carbon atoms and roughly similar steric properties, but differing degrees of substitution about the double bond - revealed that the addition of CHD resulted in at least a 20-fold reduction in the ratio of C_8 methylation products to that of C_7 alkanes formed via hydrogen transfer, mostly likely from CHD.[80] In the absence of a hydrogen donor like CHD, the source for hydrogen transfer must be the olefin itself; the cyclic diene, CHD, was therefore, 20-times as proficient at hydrogen transfer as the acyclic monoolefins. It was also noted that the ratio of methylation (based on the yield of C_8 products) to hydrogen transfer (based on the yield of C_7 alkanes) was highest for the tetrasubstituted alkene, 2,3-dimethyl-2-pentene, decreasingly markedly for the tri-substituted and again for the di-substituted isomers suggesting that the rate of methylation to hydrogen transfer and therefore, chain growth (methylation) to chain termination (hydrogen transfer) varies systematically with the degree of olefin substitution.[80]

In a series of related studies on zeolite-based heterogeneous catalysts for methanol/ DME

homologation to branched hydrocarbons at low temperature (∼473 K) and high DME pressure such that the olefin-based cycle in MTH dominates over the aromatic-based cycle, Iglesia and coworkers[27,55] have attempted to quantify the rate of methylation versus the rate of hydrogen transfer reactions in experiments involving a co-feed of ^{13}C-DME with various ^{12}C-labeled C_4-C_7 olefins. The rate of hydrogen transfer for DME homologation intermediates of a given chain length and carbon backbone structure was determined from the rate of formation of the unlabeled alkane corresponding to the added unlabeled alkene. The rate of methylation of each alkene co-feed was assessed from the rate of formation of all molecules containing at least one ^{12}C atom, except those containing only ^{12}C atoms. The authors further define the ratio of the rate of hydrogen transfer to the sum of the rates of methylation and hydrogen transfer as β, and attempt to rationalize the variation in β depending on the carbon chain length and branching of the olefin. High β values therefore, represent fast hydrogen transfer and slow methylation. The authors observe that β values involved in acid catalyzed C_1 homologation can be rationalized on the basis of carbocation stability of the transition state complexes, with hydrogen transfer to tertiary alkoxides being favored and low termination probabilities of alkenes with alkyl substituents at both C-atoms resulting from stable transition states for methylation.[27] Intraparticle concentration gradients and high reactivity of olefins make accurate measurements of hydrogen transfer rates difficult, however, the definition of β precludes the need to measure these concentrations since it contains a ratio of methylation and hydrogen transfer rates, which are both proportional to alkene concentrations.

The addition of adamantane as a hydrogen transfer co-catalyst has been shown for both homogeneous[54] and heterogeneous[55] catalyzed low temperature methanol/DME homologation to result in co-homologation of alkanes with a marked increase (>10 fold) in the incorporation of C atoms from the alkane in presence of adamantane. Because dehydrogenation of adamantane is not possible, it acts as a reversible hydrogen shuttle and facilitates dehydrogenation of alkanes to alkenes and terminates chains formed in methylation via alkoxide desorption as alkanes instead of as alkenes. The addition of such hydrogen transfer co-catalysts and the co-processing of alkanes provide distinct strategies to change the number of olefin and alkane chain carriers in MTH and to satisfy the stoichiometric requirements of forming thermodynamically favored alkanes without the formation of hydrogen-deficient aromatics, which act as coke precursors. Although these recent studies clearly represent an advancement in our understanding of hydrogen transfer reactions involved in MTH, only relative rates of hydrogen transfer under specific reaction conditions that do not include a description of the identity or reactivity of the co-reactant in hydrogen transfer elementary steps has been described. For instance, the β parameter described by Iglesia and coworkers,[55] is noted to increase with increasing olefin pressure (β increases by

a factor of ∼2-3 depending on the identity of the olefin when olefin pressure is increased from 0.5 to 3.7 kPa). These effects of olefin pressure on β indicate that olefins influence hydrogen transfer rates more strongly than methylation rates, even though both rates are expected to depend linearly on olefin pressure. Olefins upon dehydrogenation by hydrogen transfer form multiply-unsaturated olefins and cyclic compounds that are presumably even more efficient at hydrogen transfer, however, the identity and reactivity of such molecules eludes experimental probes prior to their subsequent dehydrogenation to form aromatics.

Computational density functional theory (DFT) and ab initio studies have played a seminal role in elucidating the mechanism of elementary hydrogen transfer steps on zeolitic acids. Early work from Kazansky and coworkers[71,75,76,81] examined hydrogen transfer reactions for systems involving surface alkoxides and alkanes with reactant and product states comprising alkoxides (1°→1°, 2°→2°, 3°→2°, 3°→3°) adsorbed on the surface on 1T clusters at the MP2(fc)//6-31++G*//HF/6-31G** level of theory. The geometry and charge of the carbocationic transition state in these studies closely resembled a non-classical penta-coordinated carbonium ion species. At the transition state the alkoxide and alkane are connected by a central hydrogen atom with a small positive or even negative charge, hence, the hydridic character of the reaction. Corma and coworkers[77,78,82,83] extended the scope of these studies by proposing a common intermediate for hydride transfer, disproportionation, and alkylation reactions between adsorbed alkoxides and alkanes based on DFT calculations (B3PW91/6-31G*) done on 3T clusters. Periodic DFT calculations from Neurock and coworkers[84] postulated a relatively flat potential energy surface, however, predicted carbenium-ion-like transition states and shared hydride species as lower energy intermediates. On this basis, the authors postulate that carbenium ion stability is expected to correlate with selectivity to hydrogen transfer versus alkylation and oligomerization. A recent study from Mullen and Janik[85] employing DFT-D methods to account for dispersion interactions in zeolites shows, in agreement with experimental studies from Bercaw and coworkers[51–54] and Iglesia and coworkers,[26,27,55] that activation energies decrease as the substitution of the hydride donor or acceptor species increases. The identity and reactivity of the specific co-reactant involved in hydrogen transfer and the dependence of catalytic rates (or relative rates) on spatial constraints remain as outstanding questions for MTH and more generally, acid catalysis by zeolites.

2.2.4 Cyclization

Shown in Figure 1.1, the olefin- and aromatic-based cycles are not independent of one another and communicate through cyclization and aromatic dealkylation steps. Cyclization is related to aromatization in that cycloalkanes and cyclo-olefins are not stable products of MTH and are quickly dehydrogenated to form aromatics.

There are two possible generalized routes to olefin cyclization and aromatization. One involves dehydrogenation of olefins to form dienes and trienes that undergo cyclization to aromatics. In the second route, olefins first form cycloalkanes and are subsequently dehydrogenated to form aromatics. In both of these routes, dehydrogenation occurs through hydrogen transfer reactions in which olefins or cycloalkanes donate hydrogen to other hydrocarbons that act as hydrogen acceptors. Temperature programmed surface reaction studies of C_6-C_9 olefins on HY using mass spectroscopy show the presence of dehydrogenated intermediates of aromatics, however, it was not determined if the intermediates were dienes/trienes or their cyclic analogues.[86] Studies in which n-hexane and n-heptane were converted over H-ZSM-5 at 683 K resulted in the production of C_1-C_5 aliphatics as well as a significant yield of C_7 and C_8 aromatics (over 25 wt% for both reactants).[87] The presence of aliphatics smaller than the reactant indicates that alkane cracking is occurring simultaneously with cyclization reactions. The formation of aromatics larger than the reactant show that side reactions of cyclization, such as olefin oligomerization and alkylation of aromatics also occur. The prevalence of secondary reactions such as these prevents experimental evidence from revealing if olefin dehydrogenation occurs prior to cyclization or vice versa.

Computational studies have investigated olefin and diene cyclization through 1,5-cyclization and 1,6-cyclization pathways on H-ZSM-5 using both embedded cluster calculations at the DFT/MM level for a 138T cluster and 2-layered ONIOM(B3LYP/6-31+g(d):HF/6-31+g(d)).[9,10] The results of these studies are summarized in Figure 2.4. The cyclization of physisorbed hexene to methylcyclopentane (Figure 2.4, Path I) has the lowest activation energy of the cyclization pathways shown in Figure 2.4. However, because the ring expansion mechanism for the formation of cyclohexane was not studied, it is unclear if methylcyclopentane is a favorable precursor to benzene. The results in Figure 2.4 also show that for 1,5-hexadiene, the pathway for 1,5-cyclization (Path II) is more highly activated than that for 1,6-cyclization (Path III), most likely due to the higher total charge of the transition state (0.848 au vs. 0.770 au) and the longer distance between the transition state and alkoxide oxygen (3.05 $\AA$ vs. 2.36 $\AA$) for 1,5-cyclization compared to the analogue for 1,6 cyclization.[9] Based on the high activation energy barrier for 1,5-cyclization of hexadiene as well as for ring expansion from methylcyclopentene to cyclohexene, Joshi and Thomson concluded that 1,6-cyclization occurs for C_6 aliphatic precursors.[9]

Joshi and Thomson[88] also studied 1,6-cyclization reactions using DFT/MM for C_7 and C_8 dienes in which a secondary alkoxide intermediate is formed prior to cyclization. Their findings show that increased stability of secondary carbenium ion transition states over primary carbenium ion transitions states results in the activation energy of C_7 and C_8 diene cyclization to be 29 kJ mol^{-1} lower than C_6 diene cyclization.[88] These computational results

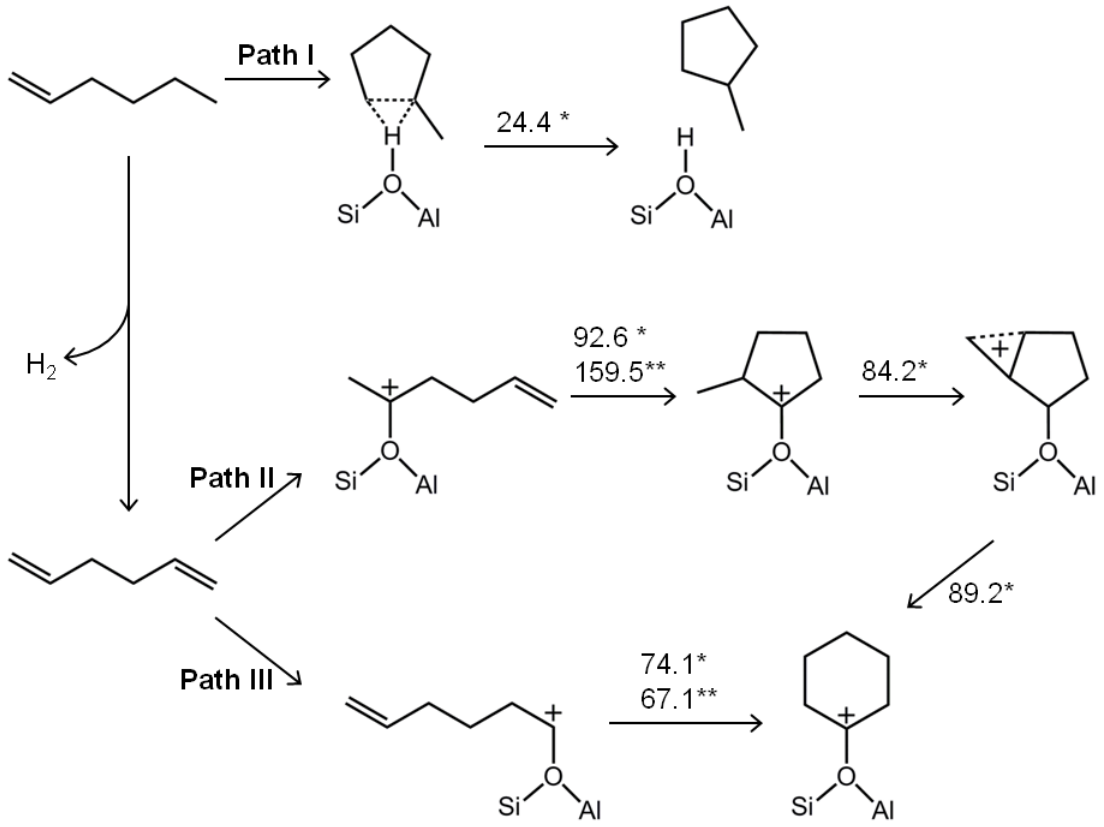

Figure 2.4: Possible pathways for 1-hexene and 1,5-hexadiene cyclization on acid zeolites with activation energy barriers (kJ mol^{-1}) based on DFT/MM level calculations on 138 T sites (*, by Joshi et al.[9]) and 2-layered ONIOM(B3LYP/6-31+g(d):HF/6-31+g(d) calculations (**, by Vandichel et al.[10]).

are in agreement with our recent experimental work, discussed further in Section 3.3.3, which shows that C_{8+} aliphatics are precursors to aromatics based on the significant fraction of completely ^{12}C-labeled isotopologues formed for p-xylene, 1,2,4-triMB, and 1,2,4,5-tetraMB when ^{13}C-toluene was co-reacted with ^{12}C-DME at 548 K on H-ZSM-5.

2.2.5 Aromatic Methylation

Aromatics, specifically polymethylbenzenes, play a crucial role in MTH catalysis in that these species, along with olefins, act as scaffolds for methylation. Isotopic labeling studies of methanol co-fed with an aromatic show that aromatic methylation reactions involve sequential methylation steps, however, varying incorporation of ^{13}C-atoms into methylbenzenes, also shows that aromatic methylation is not the only route by which methylbenzenes are formed.[40,89–91]

Similar to olefin methylation, there are two proposed mechanisms for aromatic methylation – a step-wise mechanism and a co-adsorbed mechanism. In the step-wise mechanism, methanol or dimethyl ether first dehydrate at the Brønsted acid site to form a surface methoxide which then methylates aromatics in a Rideal-type mechanism. In the co-adsorbed mechanism, methanol or dimethyl ether and the aromatic form a co-adsorption complex at the acid site and form the methylated product in a single concerted step. A discussion on the surface-methoxide mechanism and co-adsorption mechanism has already been presented in Section 2.2.1 on olefin methylation and is also applicable to aromatic methylation. To extend the discussion in Section 2.2.1 to aromatics, Mirth and Lercher[92] showed that at 473 K on H-ZSM-5, toluene/methanol co-adsorbed complexes decompose under 10-6 mbar vacuum first by toluene desorption followed by incomplete methanol desorption monitored with infrared spectroscopy and mass spectrometry. The incomplete desorption of methanol under vacuum is consistent with the formation of surface-methoxide species. In contrast, Saepurahman et al.[93] observed using infrared spectroscopy that during steady-state benzene methylation on H-ZSM-5 the band for Brønsted acid sites (3595 cm^{-1}) remained unchanged while methoxides on Brønsted acid sites were not observed after the first few minutes of reaction, which would be consistent with the co-adsorbed mechanism.

Much of the previous work on aromatic methylation has focused on toluene methylation and we briefly summarize some of these results with a focus on H-ZSM-5. DFT calculations for 4T clusters estimate the intrinsic activation energy of toluene methylation to be 180-195 kJ mol^{-1}, with methylation proceeding through a co-adsorption complex.[94–97] ONIOM calculations on 46T clusters of H-ZSM-5 estimate a lower barrier of ∼162.5 kJ mol^{-1}.[98] In comparison, most experimental work on H-ZSM-5 shows that the apparent activation energy of toluene methylation is between 50-80 kJ mol^{-1}.[99–101] Estimating the enthalpy of adsorption to be ∼80 kJ mol^{-1} for low loadings of toluene on H-ZSM-5,[102,103] the intrinsic

activation energy for toluene methylation on H-ZSM-5 based on experimental work is in the range of 130-160 kJ mol^{-1}.

A recent kinetics and DFT study[91,93] has shown that the kinetics of benzene methylation on both H-ZSM-5 and H-BEA vary little with topology. Benzene methylation on both zeolites exhibits a zero-order dependence on methanol partial pressure, activation energies between 56-58 kJ mol^{-1}, and rate constants within a factor of 3.7 at 623 K.[91,93] Activation energy barriers of gem-methylation of hexamethylbenzene on H-ZSM-5 (126 kJ mol^{-1}), H-BEA (144 kJ mol^{-1}), and H-CHA (60.8 kJ mol^{-1}) have been calculated using ONIOM methods[104] and imply that the similarity in benzene methylation kinetics and rate constants for H-ZSM-5 and H-BEA does not necessarily indicate that aromatic methylation in general is similar for both catalysts. It is probable that aromatic methylation kinetics differ significantly for larger methylbenzenes as their kinetic diameters approach the zeolite pore diameter. While the elucidation of benzene methylation kinetics is an important step in understanding aromatic methylation, we surmise that barriers to methylation will vary as the aromatic species size approaches the size of the zeolite pore and a systematic study of reactions kinetics in absence of intraparticle mass transfer and secondary reactions will be critical in understanding the crossover for aromatics from active hydrocarbon pool species to coke precursors. Obtaining kinetic behavior of methylbenezenes in the absence of intraparticle mass transfer will in turn require an assessment of methylbenzene diffusion in zeolite pores.

2.2.6 Aromatic Dealkylation

SAPO-34, a catalyst that is used commercially in UOP/Norsk Hydros MTO process,[105] forms light olefins almost exclusively through aromatic dealkylation, showing the importance of this chemistry as a route to olefin production. In a series of experiments using methanol as a reactant on SAPO-34, Song et al.[106] stopped methanol flow after a duration of time and observed the gas phase effluent with GC and the aromatics entrained within the catalyst with ^{13}C CP/MAS NMR. For these experiments, a low number of average methyl groups per benzene ring (Me_{avg}) was correlated to higher ethene selectivity compared to propene selectivity and this trend was consistent with space velocities varying by 4 orders of magnitude and temperatures from 673-823 K. While this correlation of low Me_{avg} to high ethene selectivity on SAPO-34 provides insight into the precursors for ethene formation from methylbenzenes, the mechanism of olefin formation on SAPO-34, as well as on other zeolites, is unclear. Two different mechanisms have been proposed for aromatic dealkylation and are shown in Figure 2.5: (1) the side-chain methylation mechanism and (2) the paring mechanism. A recent review[13] has provided a comprehensive summary of the computational literature regarding these two mechanisms; therefore, we will focus primarily on

experimental evidence supporting these mechanisms. Briefly summarizing the two proposed mechanisms, in the side-chain methylation mechanism, gem-methylation of a methylbenzene species results in elimination of a methyl hydrogen, thus forming an exocyclic double bond, which can undergo side chain methylation. This side-chain can then crack to form ethene or propene. The paring mechanism is also initiated by the gem-methylation of a methylbenzene, which in this mechanism, results in ring-contraction. An alkyl substituent is formed which in turn cracks to produce light olefins.

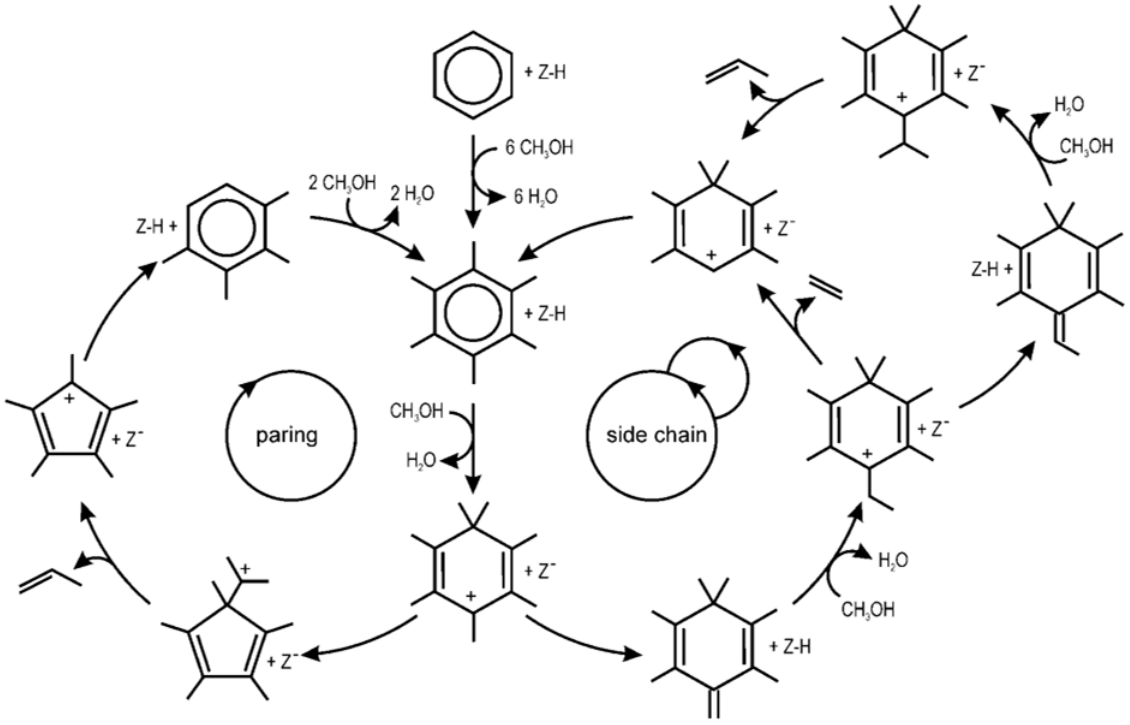

Figure 2.5: A representation of the paring and side-chain methylation mechanism for olefin elimination from hexamethylbenzene with the zeolite represented as Z-H or Z- in its protonated or deprotonated form, respectively. Reproduced with permission from Lesthaeghe et al.[11]

The starting point for both the paring mechanism and the side chain methylation is a gem-methylation step in which an aromatic ring carbon is doubly methylated, thus breaking aromaticity and forming a charged species. Using hexamethylbenzene as an example, gem-methylation of this species would result in the formation of a heptamethylbenzenium ion. GC-MS and NMR spectroscopy studies have shown that heptamethylbenzium ions are easily formed by co-feeding benzene with methanol on H-BEA at low temperatures (<623 K) and are easily methylated further to eventually form naphthalenes that behave as coke precursors.[90,107–110] Additionally, ONIOM calculations on 5T clusters have shown that the activation energy for gem-methylation decreases as the number of methyl groups on the

benzene ring increases.[104] This trend, however, does not hold in the presence of a zeolite framework due to effects of confinement. Calculations on 46T clusters of H-ZSM-5 show that the barrier height for gem-methylation decreases monotonically with increasing number of methyl groups for toluene, p-xylene, and 1,2,4-trimethylbenzene.[104] The activation energies of gem-methylation for durene, pentamethylbenzene, and hexamethylbenzene on H-ZSM-5, however, are all higher than that for 1,2,4-trimethylbenzene. The common route explored by DFT is for exo-cyclic methylation to occur at the para position to the gem-methyl group.[11,111] Lesthaeghe et al.,[112] however, assert that because aromatic cations are rigid and tend to stay close to the aluminum defect, it is more likely that exo-cyclic methylation occurs ortho to the gem-methyl group.

The paring mechanism was first hypothesized by Sullivan et al.[113] to explain the high selectivity of hexamethylbenzene conversion to isobutane on nickel sulfide on silica-alumina. The formation of a cyclopentenyl cation is a key step in this reaction mechanism. Xu and Haw[114] first provided NMR evidence for the existence of these species on zeolites in significant amounts when feeding cyclopentene over H-ZSM-5. Additional IR and NMR spectroscopic studies have also shown that cyclopentenyl cations form over various acid zeolites and are persistent cations.[115–118] In later pulse experiments, Haw et al.[119] showed that the 1,3-dimethylcyclopentyl carbenium ion forms in less than 0.5 s after one pulse of ethene (1.9 mol ethene per acid site) is reacted on H-ZSM-5 at 623 K. The presence of this cation in the zeolite completely eliminated the induction period of dimethyl ether conversion in a subsequent pulse to the same catalyst (0.46 mol DME per acid site). This result shows the high reactivity and co-catalytic nature of cyclopentenyl species for MTH, however, this alone does not confirm that light olefins are eliminated from these species.

One consequence of the paring mechanism that distinguishes it from the side-chain methylation mechanism is that ring contraction and subsequent olefin elimination steps result in a ring carbon from the methylbenzene being incorporated into the olefin formed. Isotopic studies in which an aromatic is co-fed with methanol/DME (with only one ^{13}C-labeled reactant) have shown that aromatic ring carbons are indeed incorporated into light olefins for multiple acid zeolites.[38–40,89,90,109,120] and Bjørgen et al. observed that a majority of propene and isobutane molecules (approximately 60%) contained only one ^{12}C-atom when ^{13}C-methanol was co-fed with ^{12}C-benzene at low temperatures (523 K-543 K) on H-BEA.[90] Only one aromatic ring carbon was incorporated into these products, which supports the paring mechanism for olefin formation.

Another consequence of the paring mechanism is that it provides a mechanism for methyl group carbons on aromatics to become incorporated into the benzene ring. For isotopic experiments by Bjørgen et al. described above, this would result in aromatics with mixed

isotopologue distributions for the benzene ring in methylbenzenes and has also been observed experimentally by various researchers on multiple acid zeolites.[36,40,89,90,120] Scrambling, however, maybe be an event independent of the paring mechanism if repeated ring contractions and ring expansions occur without the elimination of alkyl groups. This could also lead carbons that were originally ring carbons being incorporated into olefins through the side-chain methylation mechanism.

The key intermediate of the side-chain methylation mechanism that distinguishes it from the paring mechanism is the formation of methylbenzenes that also have ethyl, propyl, or other alkyl groups. Co-reactions of ^{13}C-methanol with ^{12}C-ethylbenzene and ^{12}C-cumene at 623 K on H-BEA have shown that these species react to form significant amounts of ethene and propene, respectively.[120] Additionally, ethylbenzene alone over H-BEA was essentially unreactive, while cumene alone did eliminate propene, and both ethylbenzene and cumene were more reactive for olefin elimination in the presence of methanol,[120] implying that methylation of the aromatic facilitates olefin elimination. Reactions of butylbenzene isomers over H-BEA at 623 K in the absence of methanol show that reactivity of these molecules to eliminate butenes follows what would be expected for carbocation chemistry - butylbenzene isomers with tertiary and quaternary alkyl carbons neighboring the aromatic ring carbons were significantly more reactive with conversions of 87-96% compared to isomers with secondary alkyl carbons neighboring the aromatic ring carbon, which had conversions of 10-13% under identical conditions.[121] When these butylbenzene isomers were co-reacted with ^{13}C-methanol, the isotopic distribution of C_4 alkenes and alkanes was consistent with what would be expected to be eliminated from the butylbenzene co-feed.[121] These results provide evidence that the side-chain methylation mechanism is a possible route for olefin formation from methylbenzenes.

Lesthaeghe et al.[11] investigated the activation energy required for various gem-methylated methylbenzium ions (with the positive charge located para to the gem-methyl group) to form gem-methylated aromatics with an exocyclic double bond located at the para position to the gem-methyl group using 5T cluster calculations at the B3LYP/6-31+G(d) level of theory. In general, larger methylbenzenes form more stable carbocations and are thus more difficult to deprotonate, however, the location of the methyl group relative to the gem-methyl group primarily determines the barrier to exocyclic double bond formation. Activation barriers increase by approximately 5 kJ mol^{-1} for each additional methyl group that is para or ortho to the gem-methyl group.[11] ^{13}C-NMR studies of methanol conversion on H-ZSM-5 by Anderson and Klinowski[122] show that although trimethylbenzene isomers are not equilibrated in the effluent, isomers adsorbed within the zeolite pores are in equilibrium with one another. In contrast, tetramethylbenzene isomers are not equilibrated within

the zeolite pores or the effluent, most likely due to the narrow zeolite pores restricting isomerization reactions. Restriction of isomerization reactions within the pores of some zeolites will thus determine the relative abundance of particular methylbenzene isomers compared to others, affecting the rate at which aromatic dealkylation occurs.

Isotopic switching experiments in which a ^{12}C-methanol feed is switched with a ^{13}C-methanol feed during steady-state reaction show that the isotopic distribution of ethene matches that of di-, tri-, and tetramethylbenzenes on medium-pore zeolite H-ZSM-5[19,20] and penta- and hexamethylbenzene on larger pore zeolites H-BEA,[44,45] and H-SAPO-34.[43] A quantitative model of ^{13}C-atom incorporation into the olefin and aromatic products at short times-on-stream after the switch could provide a valuable method for distinguishing which of these two aromatic dealkylation mechanisms occurs in MTH, as well as determining the identity of the immediate aromatic precursor to ethene and propene. Additionally, experimental rates of olefin elimination from aromatics have not been determined and would be key in understanding what fraction of light olefins formed come from the aromatic- or olefin-based cycles.

2.3 Conclusion

The conversion of MTH is a complex chemistry in which aromatics and olefins act as co-catalysts that undergo repeated methylation and cracking reactions. The six chemistries discussed in this work - olefin methylation, olefin cracking, hydrogen transfer, cyclization, aromatic methylation, and aromatic dealkylation are the major chemistries in MTH in which the dual catalytic cycle operates. For olefin methylation, olefin cracking, hydrogen transfer, and cyclization, chemistries involving olefins (or dienes in the case of cyclization), the rate of reaction and activation energy barriers strongly depended on the degree of substitution about the double bond. Longer chain lengths and more branching generally result in higher reaction rates due to the formation of more stable carbocationic transition states compared to linear alkenes. Chemistries involving aromatics are in general more space-demanding than those involving olefins, hence, steric effects of confinement within the zeolite pores can result in larger, more substituted aromatic transition states corresponding to lower reactions rates compared to smaller aromatics.

Product distributions of MTH can be understood to be the effect of zeolite topology and operating conditions causing either the aromatic- or olefin-based cycle to propagate more relative to the other cycle. Referring back to Figure 1.2, the goal in understanding MTH should be developing structure-function relationships for the zeolite catalysts used in this chemistry. With the emergence of the dual cycle mechanism, the relationship between

zeolite structure and product selectivity has been elucidated for a few catalysts (H-SAPO-34 and H-ZSM-22), and isotopic experiments have established the relationship between zeolite structure and the identity of aromatic hydrocarbon pool species. An understanding of the interplay between the mechanism and the observed product distribution is key in understanding how the product selectivity can be controlled and how product selectivity can be used to provide insight on the mechanisms occurring in MTH.

Acknowledgments

This work was supported The Dow Chemical Company, the National Science Foundation (CBET 1055846), and the Abu Dhabi-Minnesota Institute for Research Excellence, and the donors of the American Chemical Society Petroleum Research Fund. The authors acknowledge Mr. Ian Hill and Mr. Mark N. Mazar for helpful technical discussions.

CHAPTER

THREE

TUNING THE SELECTIVITY OF METHANOL-TO-HYDROCARBONS CONVERSION ON H-ZSM-5*

3.1 Introduction

Discussed in Section 2.1, both aromatics and olefins play a critical role in the hydrocarbon pool mechanism of MTH. Carbon chain growth in this chemistry occurs through methylation of olefins and aromatics, and both olefins and aromatics can undergo cracking reactions to form light olefins, resulting in a dual catalytic cycle (Figure 1.1). Understanding the role these two different cycles play within the zeolite pores is key to understanding how selectivity for MTH can be controlled. In this work, we demonstrate that on H-ZSM-5, we can control the composition of the organic hydrocarbon pool by co-processing small amounts of propene and toluene (total 4 kPa) with dimethyl ether (70 kPa) on at 548 K,and thereby modulate the relative contribution of olefin and aromatic methylation cycles in MTH resulting in a systematic variation in the selectivity of ethene (14.5-18 C%), C_4-C_7 aliphatics (42.8-16.9 C%) and aromatics (xylenes, triMBs, and tetraMBs: 7.1-33.7 C%) at iso-conversion (20.8-22.7 C%).

3.2 Materials and Methods

3.2.1 Catalyst Preparation

The catalyst, H-ZSM-5, Si/Al=42.6, was obtained in the ammonium form from Zeolyst International. Structural and chemical characterization of the H-ZSM-5 sample used in this study is reported in Section 3.5.1. The silicon to aluminum ratio was determined by ICP-OES elemental analysis (performed by Galbraith Laboratories). The ammonium-form zeolite was sieved to obtain aggregate particle sizes between 180 and 425 μm (40-80 mesh)

*Reported from Ilias, S. and Bhan, A., *Journal of Catalsis* **290**, 186-192 (2012)

and treated in 1.67 cm^3 s^{-1} of dry air (20-21% O_2, <10 ppm H_2O, Minneapolis Oxygen), heated at a rate of 0.0167 K s^{-1} to 773 K, and holding for 4 hours to convert it to the proton-form zeolite. The catalyst was pre-treated in-situ in 1.67 cm^3 s^{-1} of helium flow (99.995% purity, Minneapolis Oxygen) at 773 K overnight using a heating rate of 0.0167 K s^{-1} prior to reaction.

3.2.2 Catalytic reactions of DME with and without co-feeds over H-ZSM-5

A stainless steel packed bed reactor (0.25 in o.d.; 0.215 in i.d.) equipped with a concentric thermal well (0.0625 in o.d.; 0.0485 in i.d.) aligned along the tube center was used for the conversion of dimethyl ether (DME). The catalyst bed was supported between quartz wool plugs and operated at isothermal conditions using an ARI heating coil regulated by a Watlow Temperature Controller (96 Series). Reactions were run at 548 K using 50 mg of catalyst and at 623 K using 5 mg of catalyst. At these conditions, a flow rate of 0.45 cm^3 s^{-1} DME (Matheson Tri-Gas, 99.5% purity) was used. Propene (50% propene, 50% argon, Praxair) and toluene (99.9% purity, Sigma-Aldrich) co-reactants were fed so that the total co-feed gas flow rate was 0.025 cm^3 s^{-1}. Toluene was fed as a liquid using a Cole Parmer EW-74900-00 syringe pump. Methane (10% methane, 90% argon, Airgas), fed at 0.16 cm^3 s^{-1}, was used as an internal standard. A balance of helium was used to achieve a total flow rate of 0.83 cm^3 s^{-1}. The total pressure of the reactor was 130 kPa. The resulting partial pressure of DME was 70 kPa and the total co-feed pressure was 4 kPa. All results shown are for data recorded at 10 minutes time-on-stream. Heat traced lines (423 K) were used to transfer toluene to the reactor and the reactor effluent to a gas chromatograph (Agilent 7890) equipped with a methyl-siloxane capillary column (HP-1, 50.0 m $\times$ 320 μm $\times$ 0.52 μm) connected to a flame ionization detector.

3.2.3 Reactions using ^{13}C-labeled co-feeds with DME over H-ZSM-5

For experiments using ^{13}C-labeled co-feeds, reactions were run using 100 mg of catalyst at 548 K. The following flow rates were used using the same procedure as above unless otherwise noted: 0.23 cm^3 s^{-1} DME, 0.013 cm^3 s^{-1} co-feed, and 0.18 cm^3 s^{-1} methane/argon with no additional helium. ^{13}C-propene (99% purity) and ^{13}C-toluene (99% purity) were obtained from Isotec. ^{13}C-toluene was fed using a saturator immersed in a water bath heated by a Cole Parmer heating jacket regulated by a Watlow Temperature Controller (96 Series). The methane/argon gas stream was used as a carrier gas for the toluene and the water bath temperature was adjusted to achieve the desired toluene partial pressure (1.2-4.1 kPa). Isotopologue distributions were determined from mass fragmentation patterns using the

method outlined by Price and Iglesia.[123]

3.3 Results and Discussion

3.3.1 Selectivity of DME conversion with varying feed compositions, temperatures, and space velocities

At 548 K and a DME WHSV of 15.5 g (g catalyst h)$^{-1}$, five different feed compositions were tested: (1) DME only, (2) DME + propene, (3) DME + toluene, (4) DME + 1:1 molar ratio of propene:toluene, and (5) DME + 1:1 C ratio of propene:toluene. Co-feeds were labeled with ^{13}C to determine the fractional conversion of the co-feed and how much of the co-fed species was formed during the reaction. A high ratio of DME to co-feed was used (35:2) to ensure that changes in the product selectivity were not a result of stoichiometric reactions of methyls with the co-feed and that the dominant surface species was DME or a DME-derivative. The chemical conversion, catalytic conversion rates, and product selectivity for the different feed compositions tested are shown in Table 3.1. The results reported in Table 3.1 are all shown at iso-conversion (20.8-22.7 C%) and 548 K, where methanol is considered to be unreacted feed. The unconverted olefin and aromatic co-feeds (determined by the amount of entirely ^{13}C-labeled co-feed in the effluent) are not included in the assessment of product selectivity. Previous work by Schulz[124] has shown that at 543 K on H-ZSM-5, methanol conversion at short times-on-stream (<50 minutes) results in a higher yield to products retained within the zeolite pores than to gaseous products in the reactor effluent. Products retained within the zeolite pores in this work, however, are not included in the assessment of product selectivity as carbon balances for all results reported in this work close within 10% when only considering products in the reactor effluent. The conversion of DME on a carbon basis is consistently at least two-fold higher than that of either of the co-feeds, indicating that DME is not stoichiometrically reacting with the co-feed.

Independent reaction studies done with propene and toluene in absence of DME confirm that changes in product selectivity were not a result of the co-reaction of propene and toluene. Additionally, the observed product selectivity in the absence of DME differed significantly from the product selectivity at similar conditions, but using DME as co-reactant. Ethene selectivity increased 37-fold and xylenes were the most abundant aromatic product in the presence of DME, whereas propyl methyl benzenes were the major aromatic product for the co-reaction of propene and toluene in the absence of DME (see Section 3.5.2 in the Supplemental Information for data and discussion).

Shown in Table 3.1 and depicted graphically in Figure 3.1, the product selectivity of

Table 3.1: Conversion and product selectivity for the reaction of 70 kPa DME in the absence and in the presence of a co-feed at 548 K over H-ZSM-5, DME WHSV=15.5 g (g catalyst h)$^{-1}$.

Co-feed	**None**	**Propene**	**Mixed 1:1 mol**	**Mixed 1:1 C**	**Toluene**
Co-feed partial pressures (kPa)					
Propene	–	4.1	3.0	2.1	–
Toluene	–	–	1.2	1.9	4.1
Conversion (%)					
Total C	21.1	22.7	21.9	22.7	20.8
DME	21.1	17.9	17.8	19.1	18.1
Propene[a]	–	52.3	57.3	36.5	–
Toluene[b]	–	–	44.9	33.4	40.3
Conversion Rate(mol C (mol Al s)$^{-1}$)					
DME	0.15	0.13	0.13	0.14	0.13
Propene[a]	–	0.03	0.03	0.01	–
Toluene[b]	–	–	0.02	0.02	0.06
Product Selectivity (C%)					
C_2	16.8	14.5	16.5	17.3	18.0
C_3	19.8	16.3	23.2	19.6	22.4
C_4	10.8	14.0	11.8	11.4	8.0
C_5	7.9	9.6	6.2	6.6	3.7
C_6	8.5	9.5	5.2	5.3	2.6
C_7	8.8	9.7	5.3	4.9	2.6
C_8 (total)	9.2	10.1	14.0	15.4	25.6
Xylenes	2.8	2.7	9.9	11.7	23.6
C_{9+} (total)	18.4	16.3	17.7	19.5	17.0
TriMBs	4.8	3.3	4.9	6.0	7.8
TetraMBs	0.1	1.1	1.8	2.4	2.3

[a] Based on the conversion of ^{13}C-propene.
[b] Based on the conversion of ^{13}C-toluene.

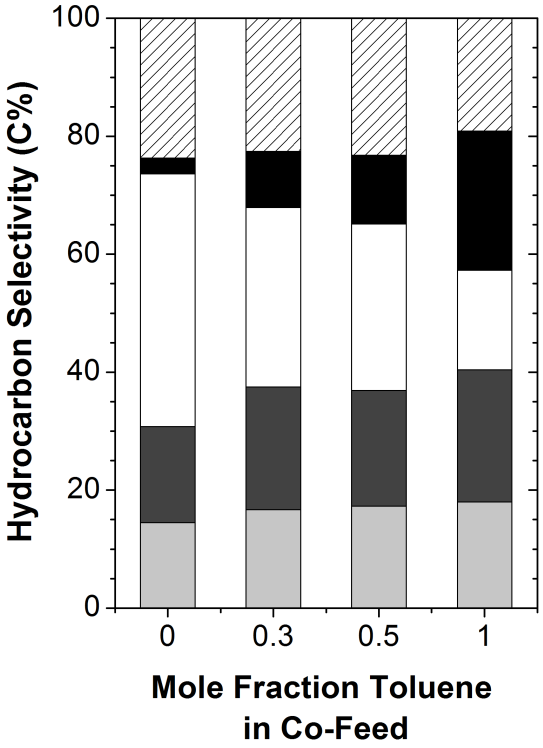

Figure 3.1: Product selectivity for the reaction of 70 kPa DME in the absence and in the presence of a co-feed at 548 K over H-ZSM-5, DME WHSV=15.5 g (g catalyst h)$^{-1}$; ■ C_2, ■ C_3, □ C_4-C_7, ■ xylenes, ▨ other hydrocarbon products.

C_4-C_7 aliphatics increased monotonically with increasing amounts of propene in the co-feed. For the co-reaction of DME and propene, selectivity to C_4-C_7 aliphatics (16.9-42.8 C%) increased by a factor of 2.5 compared to the co-reaction of DME and toluene. Increasing the amount of toluene in the co-feed resulted in a higher selectivity to aromatics (xylenes, triMBs, and tetraMBs: 7.1-33.7 C%) and ethene (14.5-18 C%) (Table 3.1). A more detailed description of the aliphatic products is given in Table 3.4 in the Supplemental Information. The results shown in Table 3.1 contrast to previous work by Svelle et al.[2] which showed that increasing the partial pressure of propene (0.5-10 kPa) decreased selectivity to n-butenes, which is the expected product of propene methylation,[2,95,96,125] at 623 K and 5 kPa methanol and work by Mikkelsen et al.[40] which showed that increasing the toluene partial pressure (1.2-9.5 kPa) decreased selectivity to ethene at 623 K and 8.9 kPa methanol. In both these cases, the methyl:co-feed ratio is much lower than that being used in this study, most likely resulting in competitive adsorbtion between methanol and the co-feed. As a result, Svelle et al. observed an increased selectivity to C_6s, but no change in C_5 selectivity, indicating increased propene dimerization reactions. Mikkelsen et al. also observed that when increasing the pressure of an aromatic co-feed with methanol, the conversion of methanol to DME decreased, indicating the inhibitory effect of aromatics on methanol dehydration when the pressures of the methylating agent and the aromatic are comparable. The trends observed in this work show that the selectivity of DME to hydrocarbons at high surface coverages of DME can be controlled systematically through the use of an olefin and aromatic co-feed.

The selectivity of DME conversion on H-ZSM-5 can also be tuned at lower conversions (4.6-5.1 C%) at 548 K (Figure 3.2). At these conditions, the selectivity to C_4-C_7 hydrocarbons decreased while selectivity to xylenes and other aromatics increased with increasing amounts of toluene in the co-feed. This trend is also observed for higher temperatures (623 K) and iso-conversion conditions (7.4-9.7 C%) by varying the olefin:aromatic ratio in the co-feed (Figure 3.2b). In Figure 3.2, hydrocarbon selectivity is used instead of product selectivity as ^{13}C-labeled co-feeds were not used in these reactions. The identity and partial pressure of the co-feed likely affects the degree to which the aromatic-based carbon pool is methylated relative to the olefin-based carbon pool and thereby enables us to control selectivity in MTH (Figure 1.1) at a variety of temperatures and conversions.

3.3.2 Propagation of the olefin- and aromatic-based methylation cycles

A propene co-feed was used to propagate the olefin-based catalytic cycle, in which olefins are successively methylated and then cracked to form light olefins[36,37], at a higher rate relative to the aromatic-based cycle, and resulted in a systematic increase in selectivity to C_4-C_7 aliphatics with increasing amounts of propene in the co-feed (16.9 - 42.8 C%,

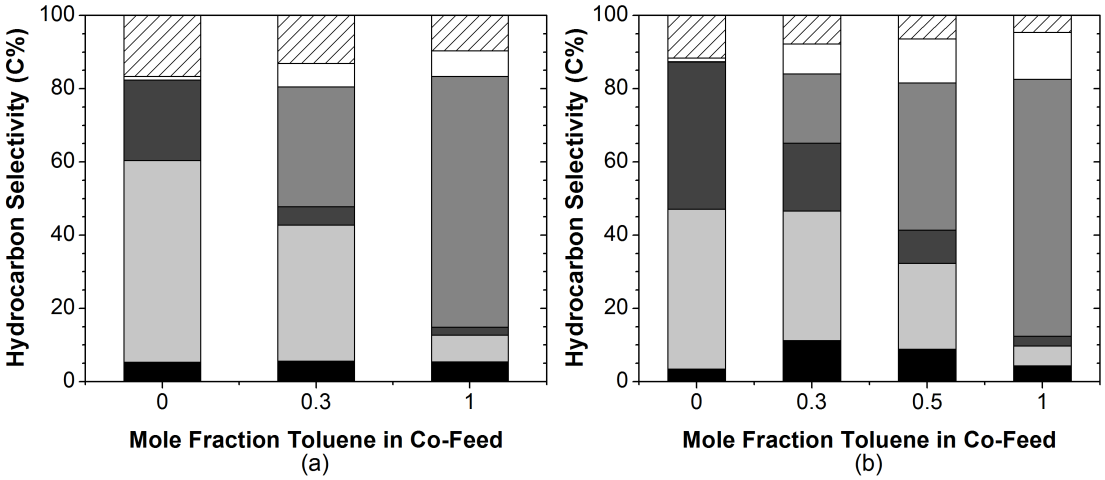

Figure 3.2: Hydrocarbon selectivity for the reaction of 70 kPa ^{12}C-DME with 4 kPa co-feed (^{12}C-propene and/or ^{12}C-toluene) over H-ZSM-5 at (a) 548 K DME WHSV=62 g (g catalyst h)$^{-1}$ and (b) 623 K, DME WHSV=516 g (g catalyst h)$^{-1}$; ■ C_2, ■ C_3, ■ C_4-C_7 aliphatics, ■ toluene, □ xylenes, ▨ other hydrocarbon products.

Table 3.1). Successive methylation of olefins was tracked using ^{13}C-labeled co-feeds. For all feed compositions in which ^{13}C-propene was used as a co-feed (see panel (a) in Figure 3.9 - Figure 3.12 in the Supplemental Information), C_5-C_7 olefins all had very similar fractions of isotopologues containing three ^{13}C-atoms (Figure 3.3). Irrespective of whether ^{13}C-propene or ^{13}C-toluene was used as a co-feed, the total ^{13}C content of these olefins closely matched the expected content based on methylation of the $(n-1)$ olefin (panel (b), Figure 3.9-Figure 3.14 in the Supplemental Information). For example, in Figure 3.9b, the ^{13}C-content of pentene is 23.8%, which is close to the expected value based on methylation of 2-butene with 32.1% ^{13}C-content (25.7%). C_4s, both linear and branched, however, do not follow this trend and have a lower ^{13}C-content than what is expected based on methylation of propene, indicating that they are formed in both methylation and cracking reactions.[27] The high fraction of propene isotopologues with at least one ^{12}C-atom (55.1%) and butene isotopologues containing two or more ^{12}C-atoms (71.4%) shows that cracking reactions are prevalent (Figure 3.3). A low fraction of olefin isotopologues with more than three ^{13}C-atoms (less than 4% for C_4-C_7 olefins) was observed, confirming that olefin oligomerization is not a major reaction pathway at the conditions used in this work. The low selectivity to polyMBs (xylenes, triMBs, and tetraMBs: 7.1 C%; Table 3.1) shows that propagation of the aromatic based cycle can be suppressed with the introduction of propene as a co-feed.

The propagation of the aromatic-based cycle relative to the olefin-based cycle was enhanced by increasing toluene pressure in the co-feed. Selectivity to C_8 and higher aromatics

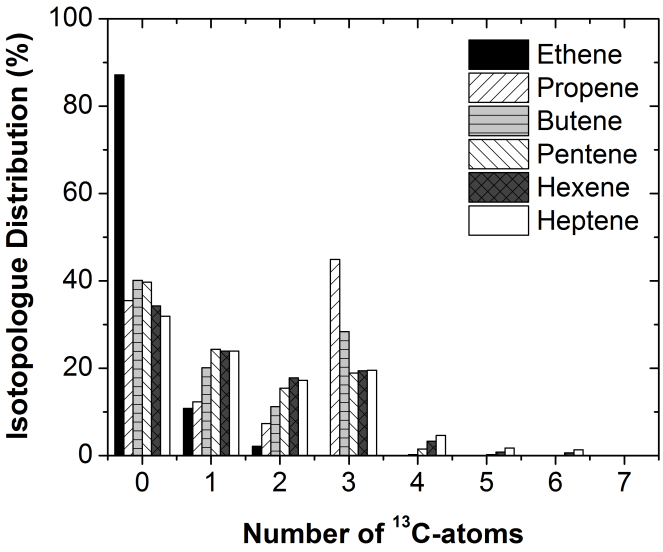

Figure 3.3: $^{12}C/^{13}C$ Isotopologue distribution for 70 kPa ^{12}C-DME co-reacted with 4.1 kPa ^{13}C-propene at 548 K over H-ZSM-5, DME WHSV=15.5 g (g catalyst h)$^{-1}$.

and ethene increased with increasing amounts of toluene in the co-feed (Table 3.1). The isotopic distribution of ethene is distinct for almost all feed compositions tested (see panels (a) and (b) in Figure 3.9 - Figure 3.12 in the Supplemental Information), indicating that ethene formation is mechanistically distinct from higher olefins and ethene is not involved in olefin methylation/cracking cycles, in agreement with previous findings in the literature.[8] Kinetic studies of olefin methylation on H-ZSM-5 have also shown that the rate constant of ethene methylation is at least an order of magnitude lower than that for propene methylation,[1–4,6] providing further evidence that ethene does not play a significant role in the olefin-based catalytic cycle. The isotopic distribution of ethene closely matches that of propene in the case where DME is co-reacted with only ^{13}C-toluene (Figure 3.4a). At this condition, the total ^{13}C-content of propene (9.9% ^{13}C-atom) is higher than the expected ^{13}C-content if propene originated from ethene methylation (6.8% ^{13}C-atom), as shown in Figure 3.14b in the Supplemental Information. At the conditions studied here, propene is not formed from ethene methylation; instead both ethene and propene are most likely being formed from dealkylation reactions of polyMBs. By seeding the hydrocarbon pool with toluene, the olefin methylation and cracking route was suppressed, evidenced by the low selectivity to C_4-C_7 aliphatics (16.9 C%), while rates of aromatic methylation and olefin elimination increased as evidenced by the higher selectivity to ethene (18.5 C%) and aromatics (xylenes, triMBs, and tetraMBs: 33.7 C%; Table 3.1).

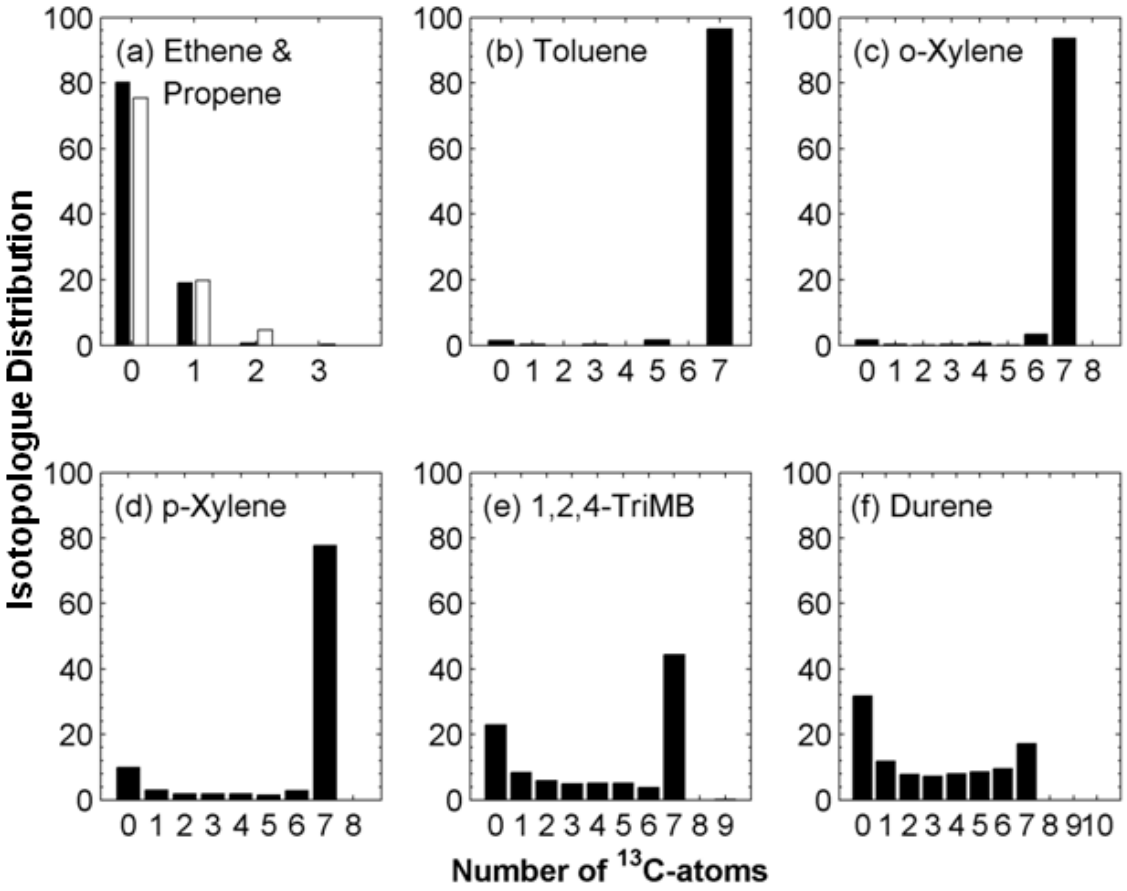

Figure 3.4: $^{12}C/^{13}C$ isotopologue distributions for (a) ■ ethene and □ propene (b) toluene, (c) o-xylene, (d) p-xylene, (e) 1,2,4-triMB, and (f) 1,2,4,5-tetraMB for the co-reaction of 70 kPa ^{12}C-DME (WHSV=15.5 g (g catalyst h)$^{-1}$) with 4.1 kPa of $^{13}C_7$-toluene at 548 K over H-ZSM-5.

3.3.3 Cyclization Reactions

Figure 3.4 also shows the ^{13}C-isotopologue distribution for toluene, o-xylene, p-xylene, 1,2,4-triMB, and 1,2,4,5-tetraMB for the co-reaction of ^{13}C-toluene and ^{12}C-DME. The isotopologue distribution of toluene in the reactor effluent is virtually unchanged from that of the ^{13}C-toluene feed (Figure 3.5), showing that toluene is not formed as a significant product. From the isotopologue distribution of o-xylene and p-xylene (Figure 3.4c-d), it is clear that both these species are formed from toluene methylation, with 93.6% of o-xylene and 77.6% of p-xylene containing seven ^{13}C-atoms. In Figure 3.6, the total ^{13}C-content of polyMBs are shown for varying feed compositions using ^{13}C-toluene with ^{12}C-DME and ^{12}C-propene. The observed ^{13}C-contents are compared to the expected ^{13}C-content based on methylation of the $(n-1)$ methylbenzene. Figure 3.6 shows that the observed isotopic distribution of o-xylene closely matches the expected isotopic distribution, indicating that if toluene is present in the feed, o-xylene comes almost entirely from toluene methylation, whereas the observed ^{13}C-contents for p-xylene and larger polyMBs differ from the expected ^{13}C content by methylation of the $(n-1)$ methylbenzene, indicating that these aromatics are not exclusively formed from methylation reactions.

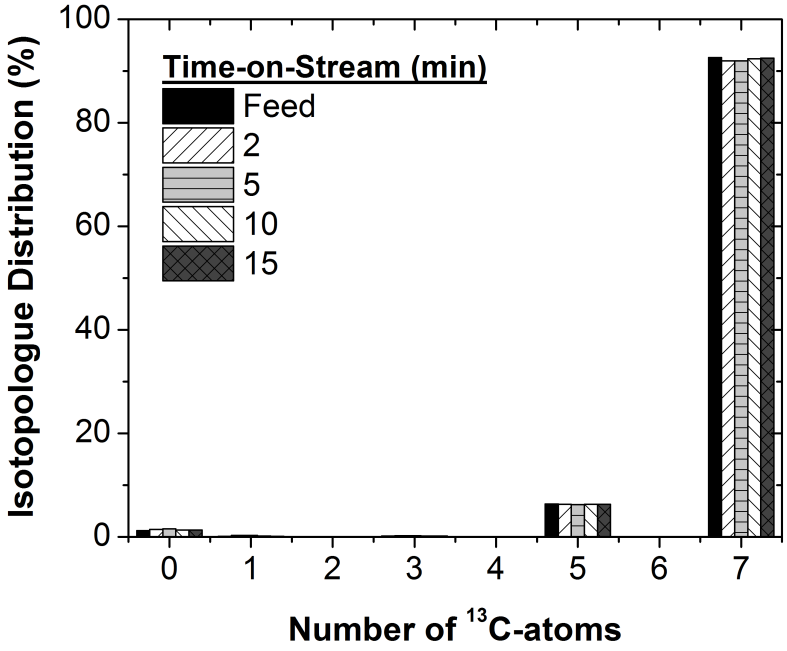

Figure 3.5: Isotopic distribution of ^{13}C-toluene feed and toluene effluent at 2, 5, 10, and 15 minutes time-on-steam for the co-reaction of 70 kPa ^{12}C-DME (WHSV=15.5 g (g catalyst h)$^{-1}$) with 4.1 kPa of $^{13}C_7$-toluene at 548 K over H-ZSM-5.

Figure 3.7 shows the total ^{13}C-content of aromatics for reactions in which ^{13}C-propene is

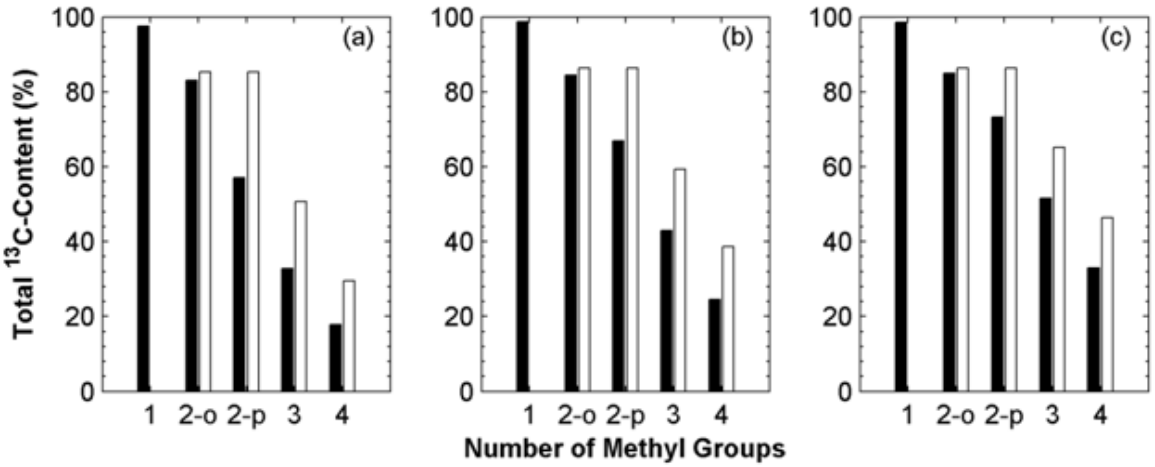

Figure 3.6: Total ^{13}C content of C_7-C_{10} methylbenzenes for the co-reaction of 70 kPa ^{12}C-DME (WHSV=15.5 g (g catalyst h)-1) and (a) 3 kPa ^{12}C-propene and 1.2 kPa ^{13}C-toluene (b) 2.1 kPa ^{12}C-propene and 1.9 kPa ^{13}C-toluene and (c) 4.1 kPa ^{13}C-toluene at 548 K over H-ZSM-5; ■ observed distribution and □ expected distribution based on methylation of the $(n-1)$ methylbenzene.

co-reacted with ^{12}C-DME and ^{12}C-toluene. Because the ^{13}C-atoms in these reactions originate from propene, these results provide insight into which aromatic species are products of aliphatics cyclization. In cases where a mixed propene and toluene co-feed is used, the total ^{12}C-content for aromatics shown Figure 3.7b-c increases monotonically with carbon number, indicating that cyclization occurs more readily for larger aliphatics, which is in agreement with hybrid QM/MM studies on H-ZSM-5 showing that for 1,6-cyclization of dienes, C_7 and C_8 diene cyclization is much more facile than C_6 diene cyclization.[9,88] The total ^{13}C-content for MB products of the co-reaction of ^{13}C-propene and ^{12}C-DME in the absence of toluene in the co-feed (Figure 3.7a) however, does not follow any discernable trend with aromatic size.

Toluene and o-xylene are distinct from the other MBs in that these species have very little ^{12}C/^{13}C scrambling with greater than 90% of these species containing seven ^{13}C-atoms (Figure 3.7). The ^{13}C benzene ring is almost entirely intact for these species while p-xylene, triMB, and tetraMB show considerably more ^{12}C/^{13}C scrambling (Figure 3.4). For these MBs, the fraction of isotopologues containing no ^{13}C-labels increases monotonically with the size of the aromatic, from 9.8% for p-xylene to 31.8% for tetraMB, showing that a significant fraction of these MBs are built up entirely from carbons originating from unlabeled DME. The high fraction of C_{8+} aromatics with no ^{13}C labels suggests that cyclization occurs predominantly for C_{8+} aliphatics rather than for C_6 and C_7 aliphatics. Additionally, the selectivity to benzene and toluene was low (<0.5 C%) for all the feed compositions tested.

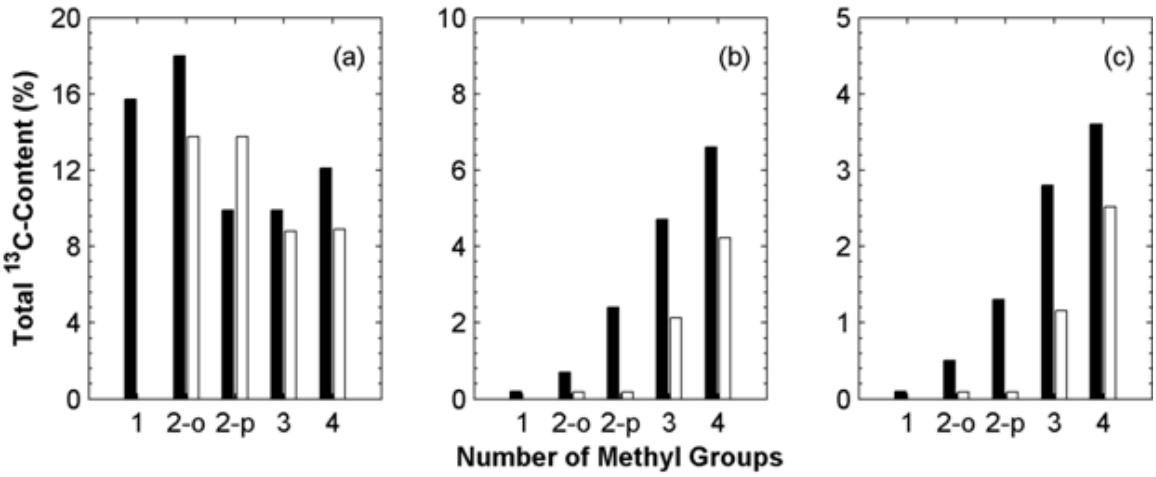

Figure 3.7: Total ^{13}C content of C_7-C_{10} methylbenzenes for the co-reaction of 70 kPa ^{12}C-DME (WHSV=15.5 g (g catalyst h)$^{-1}$) and (a) 4.1 kPa ^{13}C-propene (b) 3 kPa ^{13}C-propene and 1.2 kPa ^{12}C-toluene and (c) 2.1 kPa ^{13}C-propene and 1.9 kPa ^{12}C-toluene at 548 K over H-ZSM-5; ■ observed distribution and □ expected distribution based on methylation of the $(n-1)$ methylbenzene.

It is unlikely that benzene and toluene are highly reactive unobserved intermediates, as ONIOM studies have estimated that toluene methylation is an order-of-magnitude slower than p-xylene methylation.[98] Therefore, it is improbable that benzene and toluene are the predominant products of aliphatic cyclization.

The results in this work provide the basis for an alternative to changing the inorganic zeolite catalyst to control the selectivity for MTH at multiple temperatures and conversions. Rather than changing the inorganic catalyst, the identity and reactivity of the organic co-catalyst can be manipulated to tune the selectivity of MTH on H-ZSM-5 at iso-conversion conditions in a way that can be both predicted and controlled. Furthermore, based on the varying extents of incorporation of ^{13}C-atoms into aromatic products when using ^{13}C-labeled propene and toluene as co-reactants with DME, it is evident that at the reaction conditions studied in this work, benzene and toluene are not the major products of cyclization; instead, cyclization reactions occur predominantly for C_{8+} aliphatics to form p-xylene and larger aromatics.

3.4 Conclusion

In summary, the organic hydrocarbon pool co-catalyst can be used as a parameter to develop selective MTH catalysts. At the conditions studied in this work, we show that by co-processing olefins or aromatics with DME, we can control the composition of the organic

hydrocarbon pool and therefore its catalytic consequences on MTH selectivity on H-ZSM-5. The addition of propene resulted in a 2.5-fold increase in selectivity for C_4-C_7 aliphatics compared to the addition of toluene at 548 K. By changing the ratio of olefin:aromatic in the co-feed, the selectivity of MTH over H-ZSM-5 can be systematically tuned at iso-conversion (Table 3.1 and Figure 3.1).

For all feed compositions tested using ^{13}C-labeled co-feeds, the total ^{13}C-content of C_5-C_7 olefins matched the expected ^{13}C-content based on methylation of the $(n-1)$ olefin, indicating that these olefins are formed primarily from methylation reactions. In contrast, the expected ^{13}C-content of propene based on ethene methylation did not match the observed ^{13}C-distibution of propene for any of the feed compositions tested, showing that ethene methylation is not a significant route for propene formation. Rather, there is a high fraction of ^{12}C-atoms in propene when 4 kPa of ^{13}C-propene is co-reacted with 70 kPa ^{12}C-DME, indicating that propene is formed by cracking reactions of larger olefins. Additionally, the ^{13}C-content of propene closely matches that of ethene when 4 kPa of ^{13}C-toluene is co-reacted with ^{12}C-DME, suggesting that under conditions where the olefin-based cycle is suppressed, both ethene and propene originate from similar precursors.

The ^{13}C-content of toluene in the effluent was unchanged compared to the ^{13}C-toluene feed, showing that toluene is not formed as a significant product of MTH at the conditions studied in this work. The ^{12}C/^{13}C isotopologue distribution of aromatics shows that p-xylene, 1,2,4-trimethylbenzene, and 1,2,4,5-tetramethylbenzene have a significant fraction of completely ^{12}C-labeled isotopologues (greater than 9.8%) compared to toluene and o-xylene (less than 2%). Therefore, cyclization in MTH at the conditions studied in this work occurs predominantly for C_{8+} aliphatics to form p-xylene and larger aromatics.

3.5 Supplemental Information

3.5.1 Catalyst Characterization

Determination of the number of Brønsted Acid Sites

Chemical titration using dimethyl ether (DME) over the H-ZSM-5 sample used in this study was performed previously by Chiang et al.[126] in a tubular packed-bed quartz reactor (10 mm inner diameter) under atmospheric pressure. A mixture of DME/Ar/He (0.17 cm^3 s^{-1}; 24.9% DME, 25.1% Ar and 50% He; Praxair) was introduced by He (0.67 cm^3 s^{-1}, ultrapure, Minneapolis oxygen) during each pulse with 90s intervals. The physisorbed DME and water formed were subsequently removed by He (1.67 cm^3 s^{-1}) for 1.5 to 2.5 hours.

The DME uptake ratio per Al site for the sample of H-ZSM-5 used in this study was found to be 0.49.[126] Cheung et al.[61] showed that each Brønsted acid site in zeolites can

adsorb 0.5 DME molecules because DME reacts with surface hydroxyl groups to form persistent methyl groups. Therefore, the concentration of Brønsted acid sites in the zeolite used in this study is nearly identical to that inferred from the framework aluminum content in this material.

Nitrogen adsorption experiments

Nitrogen adsorption/desorption measurements for the H-ZSM-5 sample used in this work were previously carried out by Liu et al.[127] at 77 K on an Autosorb-1 analyzer (Quantachrome Instruments). Prior to the measurement, the sample was evacuated overnight at 573 K and 1 mm Hg. The specific surface area and the pore size distribution were calculated using the Brunauer Emmett Teller (BET) and BJH method, respectively. Conventional t-plot methods were also used for extracting micropore volume and external surface area from the nitrogen adsorption data over t ranges from 3 to 5 Å. The BET equation was used to calculate the BET specific surface area from the adsorption data obtained at P/P_0 between 0.1 and 0.3. Derived values from Liu et al.[127] are reproduced in Table 3.2.

Table 3.2: Characterization information for the catalyst sample used in this study. Si/Al was determined from ICP-OES elemental analysis as performed my Galbraith Laboratories.

	Si/Al	BET surface DME/Al	BET micropore Area (m^2g^{-1})	volume (cc g^{-1})
H-ZSM-5	42.6	0.49[126]	406[127]	0.13[127]

X-ray diffraction pattern

The powder X-ray diffraction (XRD) pattern for the sample of H-ZSM-5 used in this work was previously collected by collected by Liu et al.[127] on a Bruker AXS D5005 diffractometer using Cu- Kα radiation. Data were collected with a step size of 0.04° and a step time of 3 s. This diffraction pattern confirms the crystallinity and identity of the H-ZSM-5 sample used in this work. The diffraction pattern from Liu et al.[127] is reproduced in Figure 3.8.

3.5.2 Co-reaction of propene and toluene in the absence of DME

To ensure that changes in product selectivity were not an effect of propene and toluene reacting with each other when a mixed olefin and aromatic co-feed was reacted with DME, 2 kPa of propene and 2 kPa of toluene were co-reacted in the absence of DME over H-ZSM-5 at 548 K. The hydrocarbon selectivity and net chemical conversions for the co-reaction of

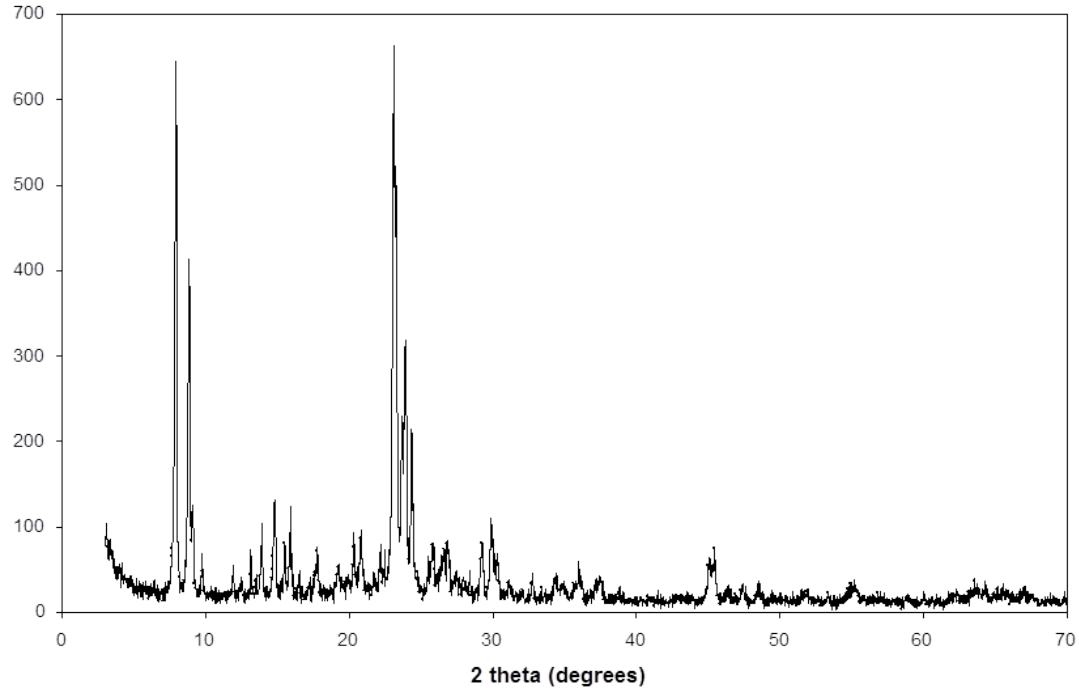

Figure 3.8: XRD pattern for H-ZSM-5.

propene and toluene in the absence of and in the presence of DME are shown in Table 3.3. Because isotopically-labeled reactants were not used for the reaction in the absence of DME, any propene and toluene in the effluent was included in the assessment of selectivity while unreacted DME and methanol were not. In the absence of DME, there is a net conversion of propene, whereas when DME is present in the feed, there is more propene produced than is consumed during the reactions (Table 3.3). Additionally, the conversion of toluene doubles when DME is co-reacted with propene and toluene, indicating that the reaction of toluene with propene is slower than the reaction of toluene with DME.

The hydrocarbon selectivity of the co-reaction of propene and toluene in the absence of DME differs significantly compared to the co-reaction propene and toluene with DME. In the absence of DME, the most abundant aromatic products formed are propyl methyl benzenes, whereas xylenes are the dominant aromatic species in the presence of DME. Most strikingly, there is a 32-fold increase in ethene selectivity when DME is present in the feed, indicating that DME is required for ethene formation under the reactions conditions used here. The co-reaction of propene and toluene in the absence of DME confirms that the while these hydrocarbons can react with each other, the introduction of DME into the feed increases the reactivity of toluene and changes the product distribution so that it is more representative of a typical MTH product selectivity.

Table 3.3: Hydrocarbon selectivity and net conversion for the co-reaction of propene and toluene (approximately 2 kPa each) in the absence of and the presence of 70 kPa DME at 548 K over 100 mg H-ZSM-5, 0.42 cm^3 s^{-1} total flow.

	Absence of DME	**Presence of DME**
Net Conversion (C%)		
Propene	75.1	-74.3
Toluene	16.0	33.4
Hydrocarbon Selectivity (C%)		
C_2	0.4	12.9
C_3	9.5	21.7
C_4	12.4	8.5
C_5	5.4	4.9
C_6	1.8	4.0
C_7 (Total)	63.4	22.0
Toluene	62.0	18.4
C_8 (Total)	1.5	11.5
Xylenes	0.5	8.7
C_{9+}	5.7	14.6

3.5.3 Selectivity at 548 K

Further details of C_3-C_5 aliphatic products are given in Table 3.4 for the co-reaction of 70 kPa DME with 4 kPa co-feed at iso-conversion (20.8-22. C%) and 548 K.

Table 3.4: Ratios of alkane/olefin products and branched C_4/linear C_4 products for the conversion of DME (70 kPa) in the absence and presence of a co-feed (4 kPa) at 548 K over H-ZSM-5, DME WHSV=15.5 g (g catalyst h)$^{-1}$.

Co-Feed:	None	Propene	Mixed 1:1C	Mixed 1:1 mol	Toluene
Alkane/Olefin					
C3	0.09	0.21	0.12	0.18	0.11
C4	0.78	0.46	0.29	0.39	0.34
C5	3.38	1.89	1.13	1.19	0.80
Branched C_4/Linear C_4					
Upper Bound[a]	1.12	0.72	0.60	0.57	0.57
Lower Bound[a]	0.58	0.29	0.18	0.19	0.16

[a] Peaks in FID chromatograms for isobutene and 1-butene were not fully resolved.

3.5.4 Isotopic Distribution of Products for Varying Feed Compositions

In Figure 3.9 - Figure 3.14, the $^{12}C/^{13}C$ isotopic distributions of olefins and methylbenzenes are shown for different feed compositions where either ^{13}C-propene or ^{13}C-toluene was used as a co-feed.

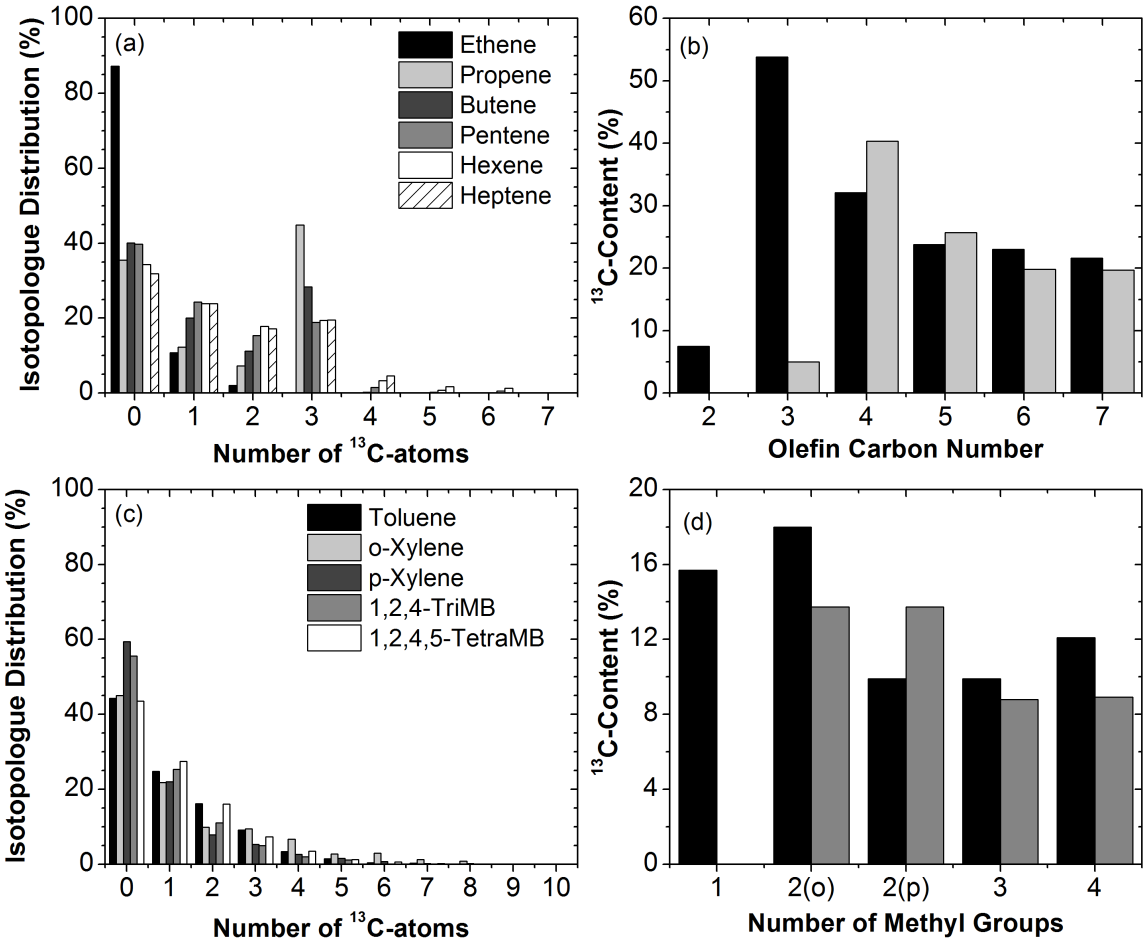

Figure 3.9: Co-reaction of 70 kPa ^{12}C-DME (WHSV=15.5 g (g catalyst h)$^{-1}$) with 4.1 kPa of ^{13}C-propene at 548 K over H-ZSM-5 (a) isotopologue distribution of C_2-C_7 olefins (b) Total ^{13}C-atom content of C_2-C_7 olefins (c) isotopologue distribution of C_7-C_{10} methylbenzenes (d) Total ^{13}C-atom content of C_7-C_{10} methylbenzenes; ■ observed distribution, ■ expected distribution based on methylation of $(n-1)$ olefin or methylbenzene.

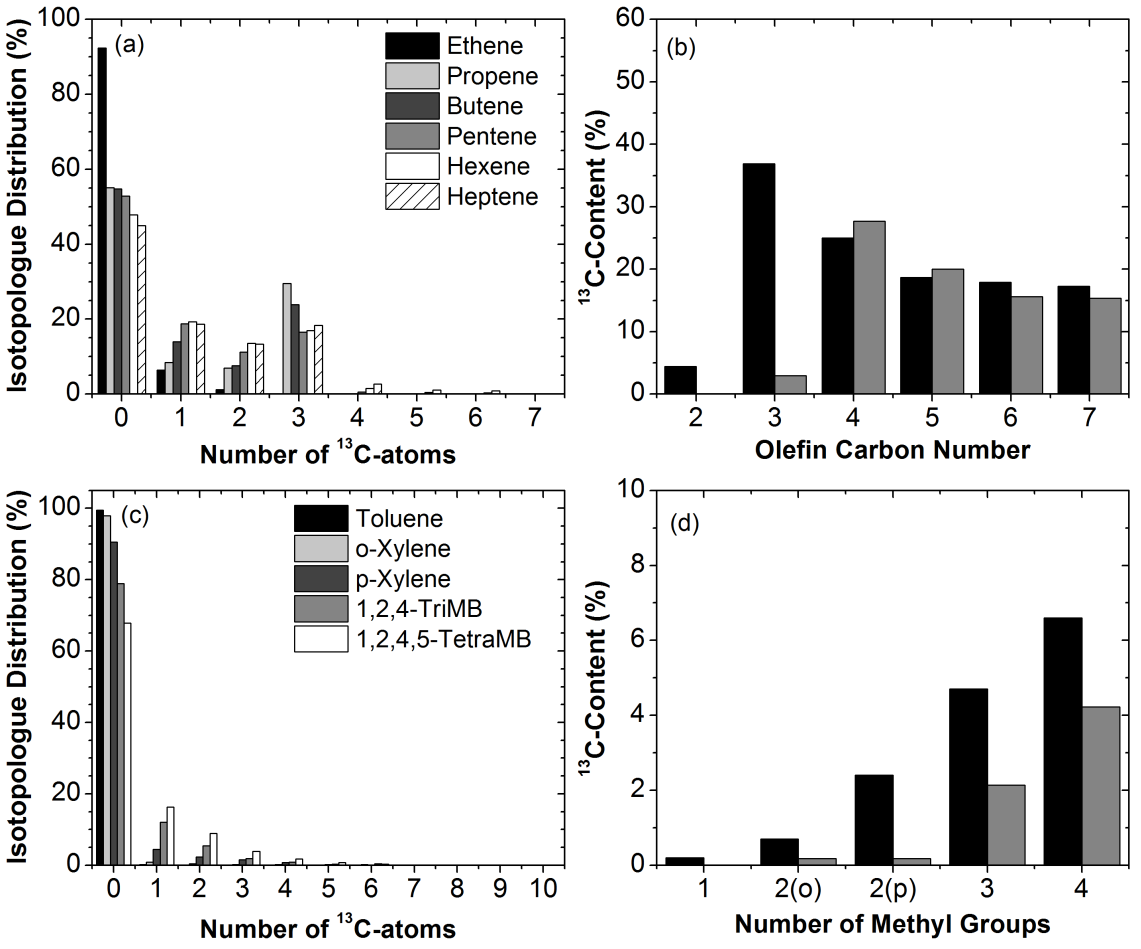

Figure 3.10: Co-reaction of 70 kPa ^{12}C-DME (WHSV=15.5 g (g catalyst h)$^{-1}$) with 3.0 kPa of ^{13}C-propene and 1.0 kPa of ^{12}C-toluene at 548 K over H-ZSM-5 (a) isotopologue distribution of C_2-C_7 olefins (b) Total ^{13}C-atom content of C_2-C_7 olefins (c) isotopologue distribution of C_7-C_{10} methylbenzenes (d) Total ^{13}C-atom content of C_7-C_{10} methylbenzenes; ■ observed distribution, ■ expected distribution based on methylation of $(n-1)$ olefin or methylbenzene.

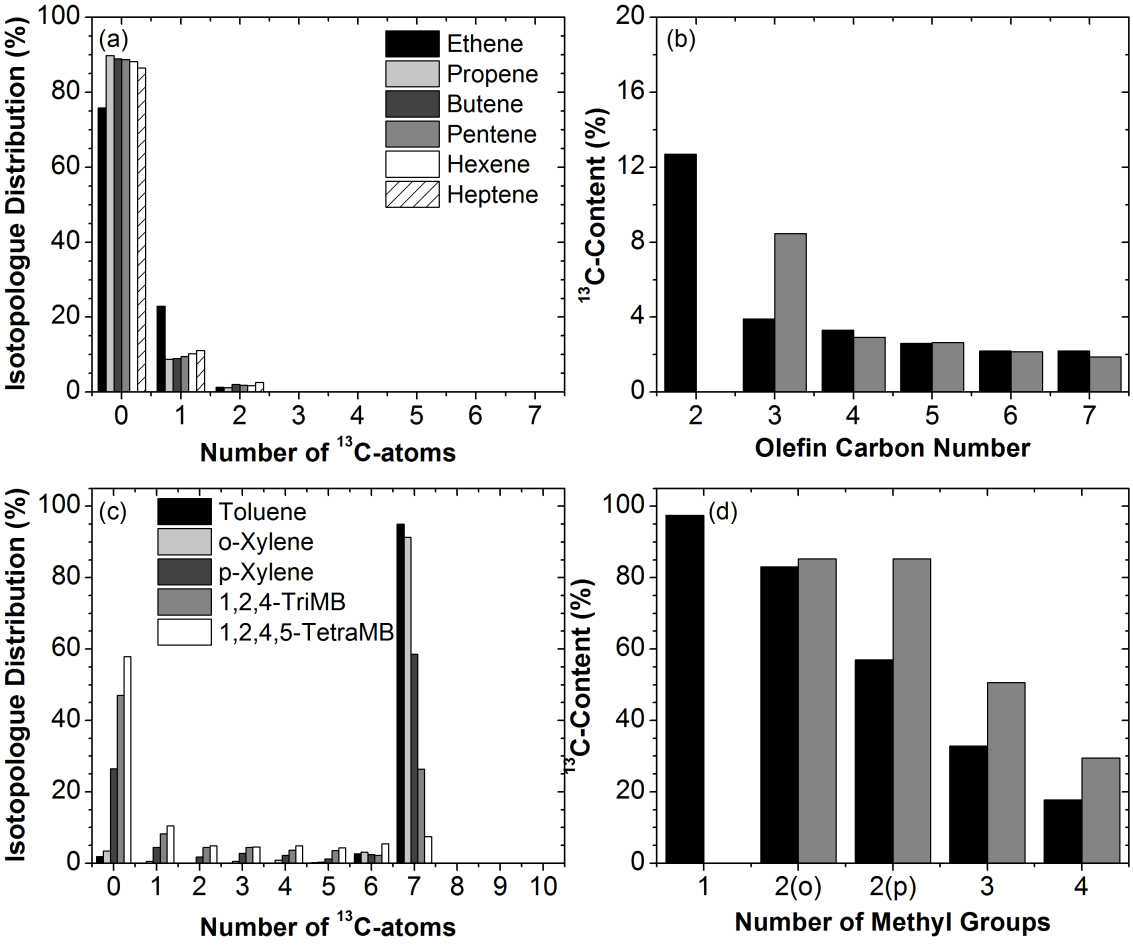

Figure 3.11: Co-reaction of 70 kPa ^{12}C-DME (WHSV=15.5 g (g catalyst h)$^{-1}$) with 3.0 kPa of ^{12}C-propene and 1.0 kPa of ^{13}C-toluene at 548 K over H-ZSM-5 (a) isotopologue distribution of C_2-C_7 olefins (b) Total ^{13}C-atom content of C_2-C_7 olefins (c) isotopologue distribution of C_7-C_{10} methylbenzenes (d) Total ^{13}C-atom content of C_7-C_{10} methylbenzenes; ■ observed distribution, ■ expected distribution based on methylation of $(n-1)$ olefin or methylbenzene.

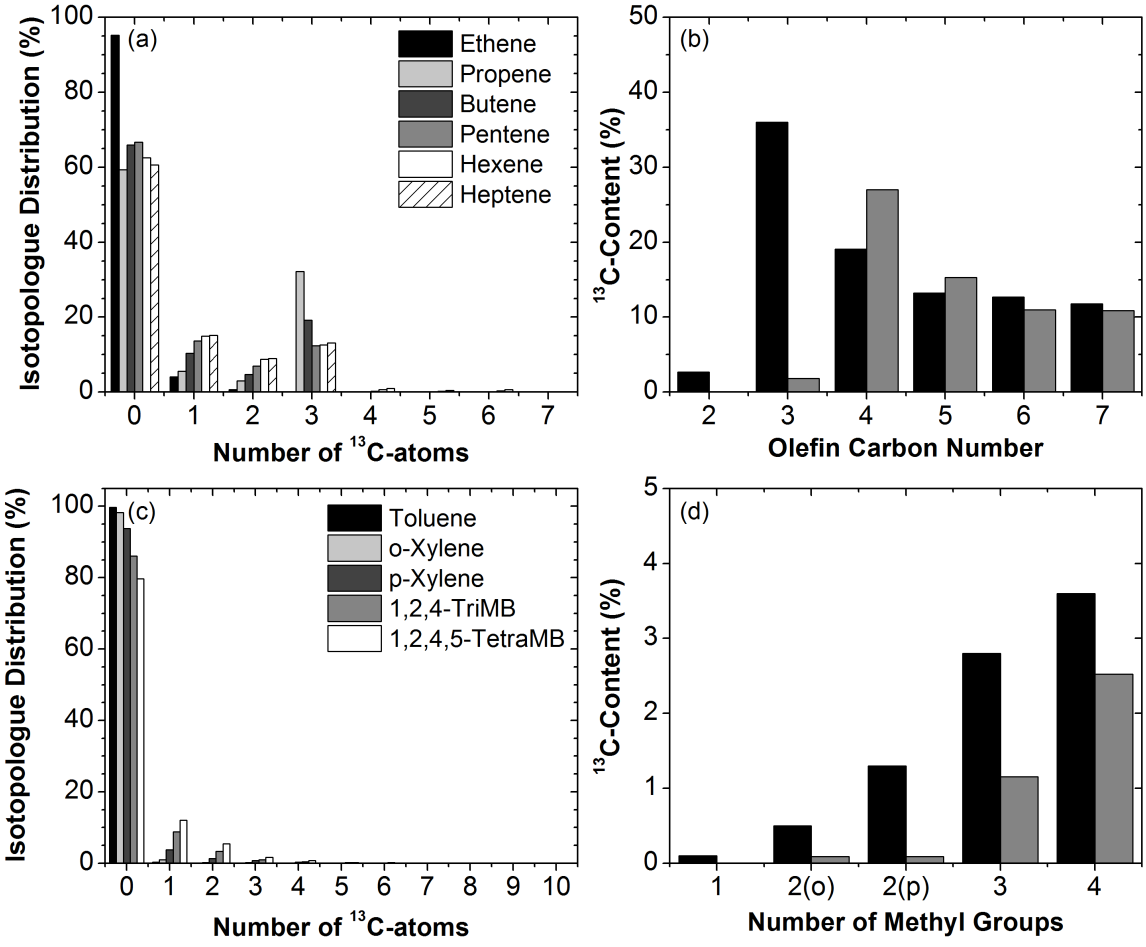

Figure 3.12: Co-reaction of 70 kPa ^{12}C-DME (WHSV=15.5 g (g catalyst h)$^{-1}$) with 2.1 kPa of ^{13}C-propene and 1.9 kPa of ^{12}C-toluene at 548 K over H-ZSM-5 (a) isotopologue distribution of C_2-C_7 olefins (b) Total ^{13}C-atom content of C_2-C_7 olefins (c) isotopologue distribution of C_7-C_{10} methylbenzenes (d) Total ^{13}C-atom content of C_7-C_{10} methylbenzenes; ■ observed distribution, ■ expected distribution based on methylation of $(n-1)$ olefin or methylbenzene.

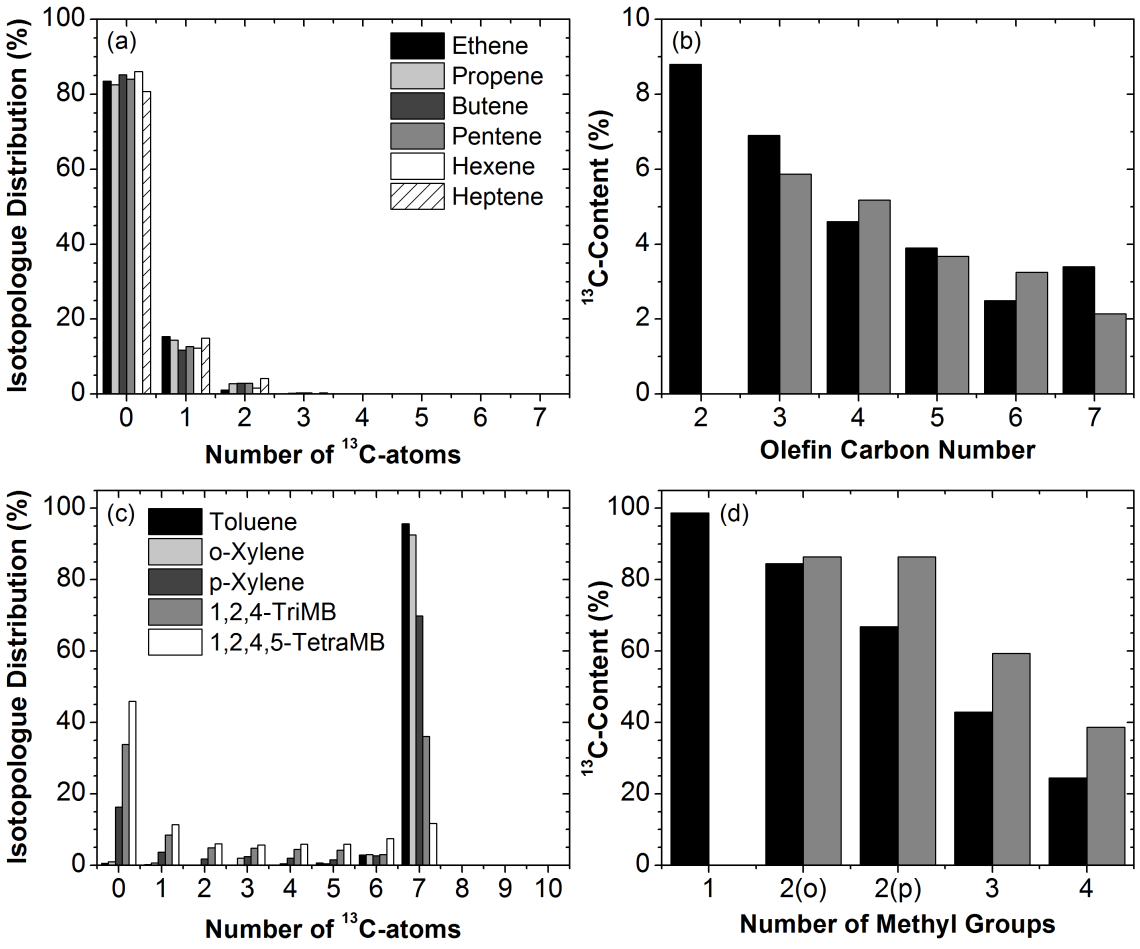

Figure 3.13: Co-reaction of 70 kPa ^{12}C-DME (WHSV=15.5 g (g catalyst h)$^{-1}$) with 2.1 kPa of ^{12}C-propene and 1.9 kPa of ^{13}C-toluene at 548 K over H-ZSM-5 (a) isotopologue distribution of C_2-C_7 olefins (b) Total ^{13}C-atom content of C_2-C_7 olefins (c) isotopologue distribution of C_7-C_{10} methylbenzenes (d) Total ^{13}C-atom content of C_7-C_{10} methylbenzenes; ■ observed distribution, ■ expected distribution based on methylation of $(n-1)$ olefin or methylbenzene.

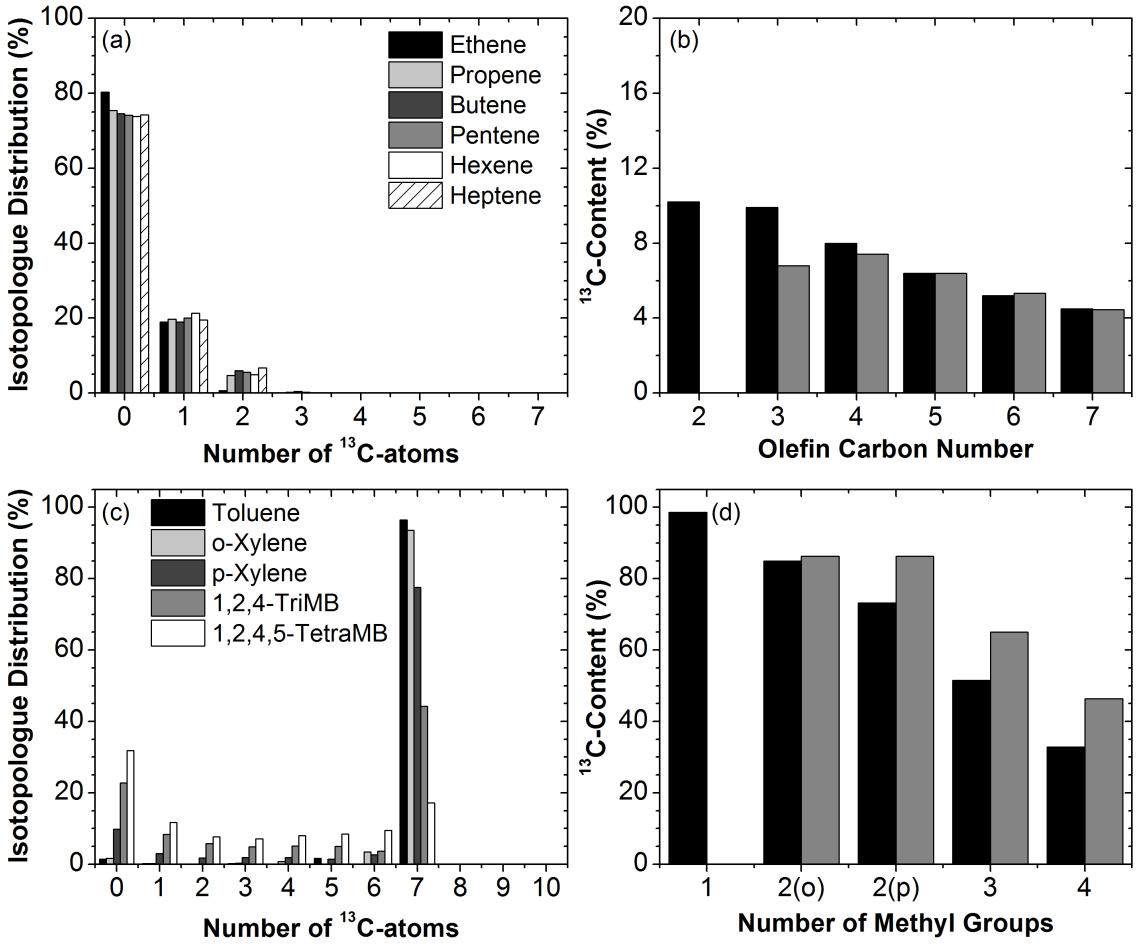

Figure 3.14: Co-reaction of 70 kPa ^{12}C-DME (WHSV=15.5 g (g catalyst h)$^{-1}$) with 4.1 kPa of ^{13}C-toluene at 548 K over H-ZSM-5 (a) isotopologue distribution of C_2-C_7 olefins (b) Total ^{13}C-atom content of C_2-C_7 olefins (c) isotopologue distribution of C_7-C_{10} methylbenzenes (d) Total ^{13}C-atom content of C_7-C_{10} methylbenzenes; ■ observed distribution, ■ expected distribution based on methylation of $(n-1)$ olefin or methylbenzene.

Acknowledgments

This work was supported by The Dow Chemical Company, the National Science Foundation (CBET 1055846), and the National Science Foundation graduate research fellowship. The authors acknowledge Connor OBrien for his assistance with reaction experiments.

CHAPTER

FOUR

A DESCRIPTOR FOR THE RELATIVE PROPAGATION OF THE AROMATIC AND OLEFIN-BASED CYCLES IN METHANOL-TO-HYDROCARBONS CONVERSION ON H-ZSM-5

4.1 Introduction

Methanol-to-hydrocarbons conversion on acid zeolites proceeds through an indirect mechanism known as the hydrocarbon pool mechanism in which olefins and aromatics act as scaffolds for carbon-carbon bond formation.[16–18,29] As a result, two catalytic cycles are at work: one in which olefins are repeatedly methylated to form branched species which are susceptible to cracking and another in which aromatics are repeatedly methylated and dealkylated to form light olefins (Figure 1.1).[19,20] The observed product distribution of MTH can be rationalized as an effect of the relative propagation of these two cycles. For some zeolites, such as SAPO-34 and ZSM-22, the product distribution can easily be understood in this manner. The observed product selectivity of SAPO-34 is rich in light olefins because small 8-MR windows hinder C_{5+} hydrocarbons from escaping the larger 12-MR cavities, resulting in the aromatic-based cycle dominating over the olefin-based cycle.[16–18,43] In contrast, the olefin-based cycle dominates in the one-dimensional 10-MR pores of H-ZSM-22, which are too small for aromatics to be reactive for olefin elimination.[42,46,48,49] In these two zeolites, one cycle predominantly propagates over another, however, in other zeolites, such as H-ZSM-5, both cycles contribute to the observed product distribution and the product distribution is tunable, showing that the aromatic- and olefin-based cycles can be propagated to different extents depending on the reaction conditions.(Chapter 3)

Kinetic studies for the different reactions depicted in Figure 1.1 are sparse, thus far, available only for C_2-C_4 olefin methylation and benzene methylation.[1–5,91,93] Global kinetic models have also been used to determine activation energies for aromatic methylation, but are

limited in that they do not always account for secondary reactions and diffusion.[99,100,128–132] Other than computational studies, there have been few experimental studies on the kinetics of aromatic dealkylation, olefin cracking, cyclization, and hydrogen transfer. Understanding how these steps contribute to the overall product distribution and which cycle is dominant on the zeolite is critical for developing structure-function relationships for MTH catalysts. In the absence of experimental studies detailing kinetic parameters for the various elementary steps in MTH, we propose that the ratio of ethene to 2-methylbutane + 2-methylbutene (ethene/2MB) yield can be used as a descriptor to assess the relative propagation of the aromatic- and olefin-based cycles and we show that this ratio varies systematically and predictably with olefin and aromatic co-feeds at iso-conversion. The selectivity of MTH was systematically tuned at iso-conversion using aromatic and olefin co-feeds over H-ZSM-5 and was reported in Chapter 3. Co-processing propene with DME resulted in increased propagation of the olefin-based cycle relative to the aromatic-based cycle, whereas toluene co-fed with DME resulted in increased propagation of the aromatic-based cycle. In this work, we show that the ethene/2MB yield is a valid descriptor for the relative propagation of these two cycles as a function of co-feed composition, reaction temperature, and DME conversion.

4.2 Materials and Methods

4.2.1 Catalyst Preparation

The catalyst, H-ZSM-5 (CBV8014), Si/Al=42.6, was obtained in the ammonium form from Zeolyst International. Structural and chemical characterization of the commercial H-ZSM-5 sample used in this study is reported in section 3.5.1 of the Supplemental Information section. H-ZSM-5 with 17 μm crystals (Si/Al=28) was also used in this work. This material was synthesized according to the procedure in Ref.[133] and the characterization of the material is shown in the Supplementary Material section of Ref.[134]. The silicon to aluminum ratio of the commercial H-ZSM-5 sample was determined by ICP-OES elemental analysis (performed by Galbraith Laboratories). The ammonium-form zeolite was sieved to obtain aggregate particle sizes between 180 and 425 μm (40-80 mesh) and treated in 1.67 cm^3 s^{-1} of dry air (20-21% O_2, <10 ppm H_2O, Minneapolis Oxygen) at 773 K for 4 hours (heating rate of 0.0167 K s^{-1}) to convert it to the proton-form zeolite. The catalyst was pre-treated in-situ in 1.67 cm^3 s^{-1} of helium flow (99.995% purity, Minneapolis Oxygen) at 773 K overnight using a heating rate of 0.0167 K s^{-1} prior to reaction.

4.2.2 Catalytic reactions of DME with and without co-feeds over H-ZSM-5

A stainless steel packed bed reactor (0.25 in o.d.; 0.215 in i.d.) equipped with a concentric thermal well (0.0625 in o.d.; 0.0485 in i.d.) aligned along the tube center was used for the conversion of DME. The catalyst bed was supported between quartz wool plugs and operated at isothermal conditions using an ARI heating coil regulated by a Watlow Temperature Controller (96 Series). Reactions were run at 548 K, 623 K, and 723 K. To achieve the desired chemical conversions, reactions were performed using 4-100 mg catalyst with DME at 70 kPa (Matheson Tri-Gas, 99.5% purity; 0.033-0.448 $cm^3\ s^{-1}$) with a mixture of CH_4 and argon as an internal standard (10% methane, 90% argon, Airgas; 0.031-0.175 $cm^3\ s^{-1}$) and a balance of helium (0-0.195 $cm^3\ s^{-1}$) was used if necessary to keep the concentration of internal standard comparable to the concentration of the effluent products. In some reactions, propene (50% propene, 50% argon, Praxair) and toluene (99.9% purity, Sigma-Aldrich) co-reactants were fed so that the olefin or aromatic co-feed partial pressure was 4 kPa (0.013-0.026 $cm^3\ s^{-1}$). Toluene was fed as a liquid using a Cole Parmer EW-74900-00 syringe pump. The resulting DME space velocity varied from 2.7 to 833 g DME (g catalyst h)$^{-1}$. The total pressure of the reactor was 130 kPa. Heat traced lines (423 K) were used to transfer toluene to the reactor and the reactor effluent to a gas chromatograph (Agilent 7890) equipped with a methyl-siloxane capillary column (HP-1, 50.0 m $\times$ 320 μm $\times$ 0.52 μm) connected to a flame ionization detector. Product distributions shown in Section 4.3 include C_{8+} hydrocarbons that were not identified and are grouped as others. The H/C stoichiometry listed for these species in figure captions are determined based on the weighted difference of the stoichiometry of converted feed and stoichiometry of known C_2-C_7 hydrocarbon products.

4.2.3 Reactions using ^{13}C-labeled DME with ethene over H-ZSM-5

For the experiment using ^{13}C-DME with ^{12}C-ethene, the reaction was run using 10 mg of catalyst at 623 K with 0.153 $cm^3\ s^{-1}$ of DME (99% ^{13}C-atom purity) and 0.017 $cm^3\ s^{-1}$ of ethene (Matheson Tri-Gas, chemical purity grade) with a balance of CH_4/Ar to achieve a total flow rate of 0.278 $cm^3\ s^{-1}$. Isotopologue distributions were determined from mass fragmentation patterns using the method outlined by Price and Iglesia.[123]

4.3 Results and Discussion

4.3.1 Reactivity of ethene, 2-methylbutane, and 2-methyl-2-butene in MTH catalysis

Isotopic switching experiments at 598-623 K on H-ZSM-5, H-BEA, and H-SAPO-34 show that the ^{13}C-incorporation of ethene closely matches that of methylbenzenes, indicating that ethene is a product of the aromatic-based carbon pool.[19,20,43–45] Additionally, kinetic studies show that the rate of ethene methylation is at least an order of magnitude slower than propene or butene methylation, suggesting that ethene can be considered to be a termination product of the aromatic-based cycle.[1–5] To confirm that ethene can be considered a termination product of DME conversion to hydrocarbons on H-ZSM-5, ^{13}C-DME (70.2 kPa) was co-processed with 7.7 kPa of ^{12}C-ethene. These results, summarized in Table 4.1, show that although some ethene is converted when co-processed with DME, ethene reacts ∼20 times slower than DME, hence, it can be considered termination product of the aromatic-based cycle of MTH on H-ZSM-5.

Table 4.1: Feed rate, fractional conversion, and conversion rate for co-reaction of 70 kPa DME with 7.7 kPa of ethene 623 K.

	Feed Rate/ mol C (mol Al s)$^{-1}$		**Conversion/ %**		**Conversion Rate/ mol C (mol Al s)$^{-1}$**	
Co-feed	*DME*	*Co-Feed*	*DME*	*Co-Feed*	*DME*	*Co-Feed*
Ethene	4.09	0.44	39.6	19.1	1.62	0.08

Alkanes may be considered as termination products for the olefin-based cycles. Olefins can form alkanes through hydrogen transfer reactions, and in general, alkanes are less reactive than either olefins or aromatics. The selectivity to both alkanes and olefins in MTH is, however, dependent on the extent of hydrogen transfer. Figure 4.1 shows the extent of hydrogen transfer, measured by the ratio of alkanes to alkenes, with a higher ratio indicating a greater extent of hydrogen transfer, occurring for different MTH reaction conditions used in this work. The extent of hydrogen transfer in MTH is dependent on the conversion of DME, the reaction temperature, and the identity of the aromatic or olefin co-feed. Therefore, an individual alkane or olefin cannot be used as a representative of the olefin-based cycle because the relative amount of olefins and alkanes is dependent on hydrogen transfer, which is necessary for the formation of aromatics. To eliminate the effect of hydrogen transfer on a descriptor for the relative propagation of the aromatic-based cycle compared to the olefin-based cycle, we use the sum of the yields of 2-methylbutane and 2-methyl-2-butene to represent the propagation of the olefin-based cycle.

The alkane to alkene ratio increases with increasing chemical conversion for the reaction

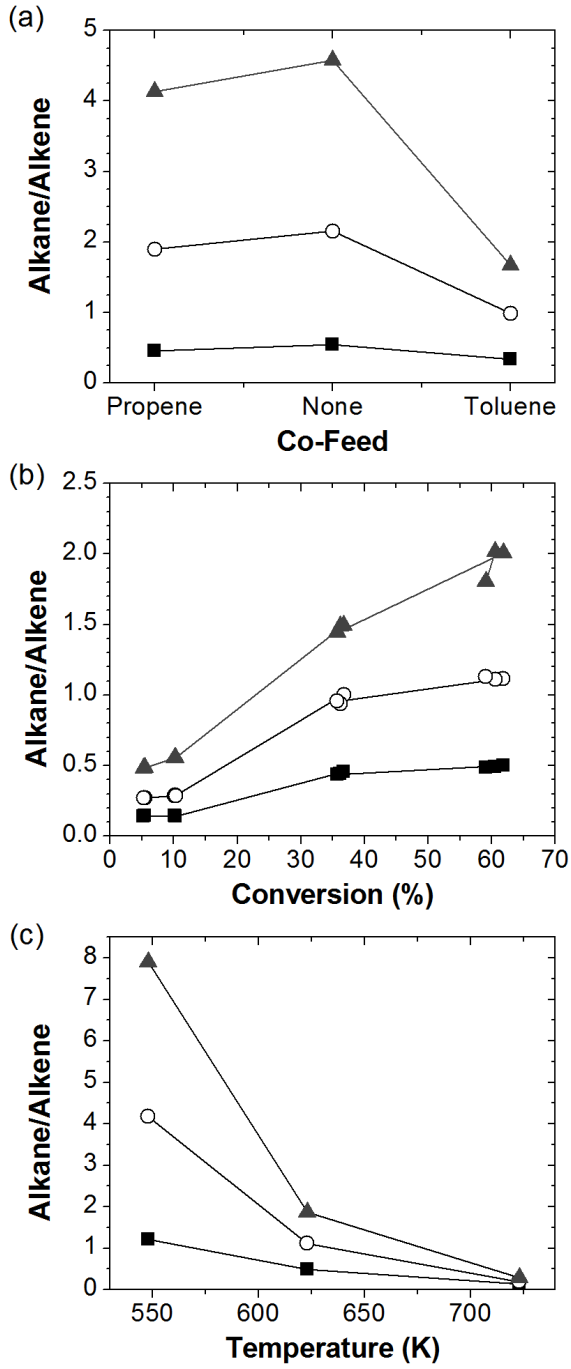

Figure 4.1: The ratio of alkane to alkene ■ C_4 , ○ C_5, and ▲C_6 products on H-ZSM-5 (Si/Al=42.5) for the reaction of 70 kPa DME (a) with and without 4 kPa of co-feed at 548 K and 17.9-18.6% DME conversion, (b) at 623 K and 5-62% conversion, and (c) at 548-723 K and 59.4-60.7% DME conversion.

of DME at 623 K showing that hydrogen transfer increases with increasing conversion (Figure 4.1b). As a result, the selectivity to 2-methylbutane increases by a factor of 2.6 while the selectivity to 2-methyl-2-butene decreases a factor of 2.6, however, the sum of the two remains relatively constant as conversion increases from 5 to 62% (Supplemental Information Figure 4.6a). Similar trends are also seen with the effect of temperature on the alkane to alkene ratio for the reaction of DME on H-ZSM-5 between 548 K and 723 K. As temperature increases, the alkane to alkene ratio decreases. The selectivity to 2-methyl butane decreases by a factor of 3.1 while the selectivity to 2-methyl-2-butene increases a factor of 8.9 as temperature increases and the alkane to alkane ratio decreases (Supplemental Information Figure 4.6b). The carbon selectivity to total 2MB however, remains relatively constant with the alkane to alkene ratio. The differing trends observed for 2-methylbutane and 2-methyl-2-butene and the relatively invariant selectivity to 2MB with varying temperature and chemical conversion further support our claim that both an alkane and an olefin must be used to represent the propagation of the olefin-based cycle.

The ratio of the yield of ethene to other C_3-C_5 hydrocarbons and a detailed description of the composition of the C_5 fraction for the various reaction conditions used in this work is shown in Section 4.5.2 of the Supplemental Information. Although other ratios, such as ethene/(i-C_4+1-butene) and ethene/propene also follow the same trends as ethene/2MB, branched C_5 hydrocarbons were chosen specifically because isotopic experiments in which methanol/DME is co-processed with aromatics on H-ZSM-5 have shown that propene in the effluent contains a significant fraction (10-42%) of carbons originating from aromatics showing that the aromatic-based cycle is one route for propene formation.[40,89] Additionally, similar isotopic experiments on H-BEA show that isobutane also contains aromatic carbons, suggesting that the aromatic-based cycle is a route to i-C_4 formation on H-BEA.[90] Although there is no direct experimental evidence linking isobutene to the aromatic-based cycle on H-ZSM-5, branched C_5 hydrocarbons are used in this work to represent the propagation of the olefin-based cycle because methanol conversion on H-ZSM-22, a catalyst in which the olefin-based cycle dominates over the aromatic-based cycle, has a much higher selectivity to branched C_5 hydrocarbons compared to branched C_4 hydrocarbons.[48]

4.3.2 Effect of olefin and aromatic co-feeds on ethene/2MB yield

In Chapter 3, we reported that at iso-conversion conditions at 548 K on H-ZSM-5, co-feeding 4 kPa propene with 70 kPa DME propagates the olefin-based cycle evidenced by selectivity to C_4-C_7 increasing 2.5-fold compared to when 4 kPa toluene is co-fed with 70 kPa DME. Co-feeding toluene increased the relative propagation of the aromatic-based cycle and a corresponding increase in ethene and methylbenzene selectivity was observed. Figure 4.2 shows the effect of feed composition on the product selectivity and the ethene/2MB yield

(on a carbon basis) at iso-conversion conditions at 548 K (17.9-18.6% DME). For these experiments, propene and toluene feeds were completely labeled with ^{13}C-atoms and any $^{13}C_3$-propene or $^{13}C_7$-toluene in the reaction effluent is not included in the assessment of product selectivity. Additionally, the isotopic distribution of propene and toluene in the reaction effluent was used to determine chemical conversions of the $^{13}C_3$-propene and $^{13}C_7$-toluene co-feed, which were 52.3% and 40.3%, respectively (Table 3.1). The ethene/2MB yield decreases by a factor of 1.9 when propene is co-processed with DME compared to the conversion of DME alone as a result of increased propagation of the olefin-based cycle (Figure 4.2b). In contrast, the ratio increases by a factor of 2.1 when toluene is co-processed with DME due to increased propagation of the aromatic-based cycle (Figure 4.2b). These results showing systematic trends in the ethene/2MB yield support our hypothesis that ethene/2MB yield can be used a descriptor for the propagation of the aromatic-based cycle relative to the propagation of the olefin based cycle.

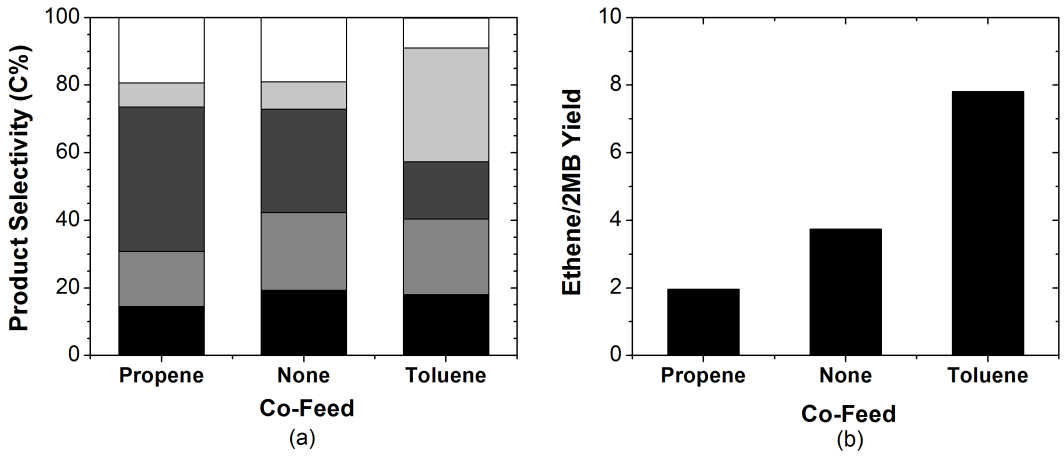

Figure 4.2: The effect of feed composition on (a) the product selectivity and (b) the ethene/2MB yield on a carbon basis for the reaction of 70 kPa DME (+4 kPa co-feed) at 548 K and 17.9-18.6% DME conversion over H-ZSM-5 (Si/Al=42.5); for (a) ■ C_2, ■ C_3, ■ C_4-C_7, ■ methylbenzenes, □ others. The H/C stoichiometry for the fraction labeled others is the following: 2.03 for DME+propene, 1.85 for DME, and 1.29 for DME+toluene.

Figure 4.3 shows the effect of co-processing propene, toluene, and p-xylene with DME at 623 K on selectivity and the ethene/2MB yield at iso-conversion conditions (33.3-36.7% DME). The product distributions for the results shown in Figure 3 are shown in Figure S.6 of the Supplemental Information. The effect of co-processing propene with DME on the ethene/2MB yield compared to DME alone was relatively small, only a 26% decrease in the ratio was observed. We postulate that this small change in ethene/2MB yield is a result of the large fraction of olefins already produced when DME alone is reacted at 623 K,

with olefin pressure increasing by less than 50% with the addition of a propene co-feed. In contrast, the addition of toluene as a co-feed increases the amount of aromatics in the system by 580%. The co-reaction of DME with toluene increases the ethene/2MB yield by a factor of 3.2 compared to the reaction of DME alone as a result of increased propagation of the aromatic-based cycle relative to the olefin-based cycle, which is similar to the observation at 548 K shown in Figure 2b. Similar trends in selectivity and ethene/2MB yield for propene, toluene, and ethylbenzene co-feeds with DME are also observed at 723 K (Section 4.5.3 of the Supplemental Information).

Co-feeding p-xylene with DME has similar effects on both the product distribution (shown in Figure 4.11 of the Supplemental Information) and the ethene/2MB yield as co-feeding toluene with DME, with the ethene/2MB yield increasing by a factor of 3.2 compared to the reaction of DME alone (Figure 4.3). The similarity in ethene/2MB yield and product distribution for the co-reaction of p-xylene and toluene with DME shows that both aromatic co-feeds influence the propagation of the aromatic based cycle in a similar manner increasing the overall partial pressure of aromatics in the system increases the propagation of the aromatic-based cycle relative to the olefin-based cycle.

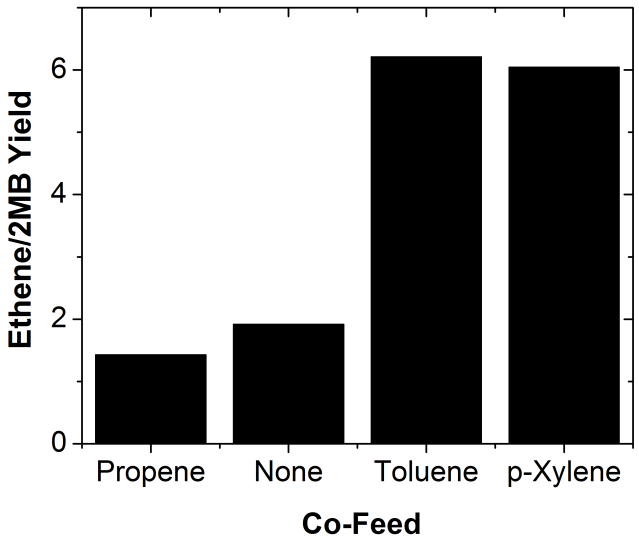

Figure 4.3: The effect of feed composition on the ethene/2MB yield on a carbon basis for the reaction of 70 kPa DME (+4 kPa co-feed) at 623 K over H-ZSM-5 (Si/Al=42.5).

4.3.3 Effect of conversion on ethene/2MB yield

At 623 K, the product selectivity for reaction of DME alone over H-ZSM-5 varied slightly for DME chemical conversions between 5% and 62% (Figure 4.4a). Correspondingly, the

ethene/2MB yield on a carbon basis varied slightly, between 0.9 and 2.1 (Figure 4.4b). The small increase in the ethene/2MB yield at 623 K as DME conversion increases from 5 to 62% suggests that the rate of propagation for the aromatic-based cycle increases slightly compared to the propagation of the olefin-based cycle as conversion increases. The effect of conversion was also examined for the reaction of DME on 17 μm crystals of H-ZSM-5 at 623 K between 8.7-32.3% conversion. Product selectivity for the large crystal H-ZSM-5 sample was nearly invariant for the range of conversions studied (Figure S.8a of the Supplemental Information) and correspondingly, the ethene/2MB yield (∼4.1) was also relatively invariant (Figure 4.12b of the Supplemental Information).

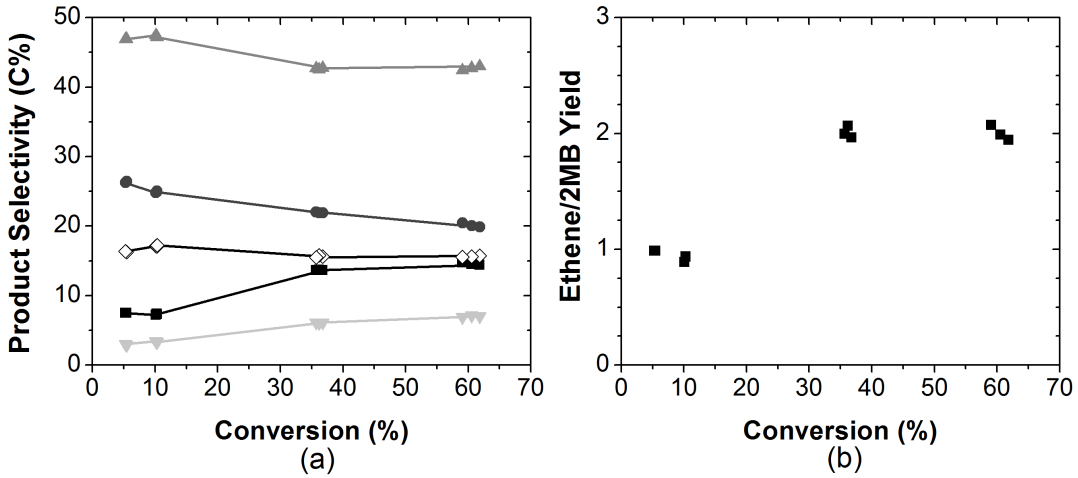

Figure 4.4: The effect of fractional conversion of DME on (a) product selectivity and (b) ethene/2MB yield for the reaction of 70 kPa DME at 623 K over H-ZSM-5 (Si/Al=42.5); for (a) ■ C_2, ● C_3, ▲ C_4-C_7, ▼ methylbenzenes, ◇ others (H/C stoichiometry of 1.87-1.96).

4.3.4 Effect of temperature on ethene/2MB yield

Figure 4.5a shows the selectivity of the reaction of DME only over H-ZSM-5 at 548 K, 623 K, and 723 K at iso-conversion conditions (59.4-60.7% DME conversion). At these conditions, the selectivity to C_2 hydrocarbons (>99% of which is ethene), methylbenzenes, and others systematically decreases with increasing temperature. With increasing temperature, an increase in selectivity to C_3-C_7 hydrocarbons is also seen. These trends in selectivity show that as temperature increases, the rate of propagation of the olefin-based cycle increases more than the rate of propagation of the aromatic-based cycle. The selectivity of MTH systematically varies with reaction temperatures at iso-conversion conditions which results in a monotonic decrease in the ethene/2MB yield as shown in Figure 4.5b.

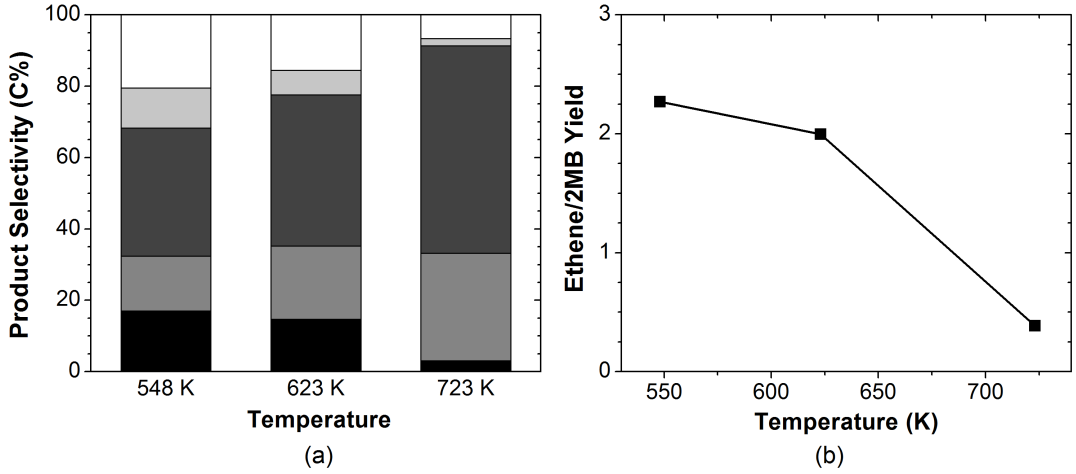

Figure 4.5: The effect of temperature on (a) product selectivity and (b) ethene/2MB yield on a carbon basis for the reaction of 70 kPa DME over H-ZSM-5 (Si/Al=42.5); for (a) ■ C_2, ■ C_3, ■ C_4-C_7, ■ methylbenzenes, □ others. The H/C stoichiometry for the fraction labeled others is the following: 1.85 at 548 K, 1.88 at 623 K, and 1.77 at 723 K.

At 723 K, the selectivity to ethene and methylbenzenes is low compared to that at lower temperatures (Figure 4.5b). To further understand if ethene selectivity is lower at higher temperatures at least in part because of the lower concentration of methylbenzenes, toluene was co-fed with DME at 723 K. At 72.6% DME conversion and 73.9% net toluene conversion, ethene selectivity increased to 14.7 C% and correspondingly, the ethene/2MB yield increased to 3.2, compared to the reaction of DME alone at 723 K and 60% conversion which results in 3.0% selectivity to ethene and an ethene/2MB yield of 0.4. This increase in ethene selectivity shows that one reason that selectivity of DME conversion to ethene is low at high temperatures (∼723 K) is due to the low concentration of methylbenzenes, not necessarily because the rate of aromatic dealkylation is slower relative to olefin methylation and cracking rates. The selectivity to methylbenzenes is low for the reaction of DME alone at 723 K because methylbenzene formation, which requires olefins to undergo both cyclization and dehydrogenation reactions, occurs to a lesser extent at higher temperatures, suggesting that at higher temperatures, olefins prefer other pathways, such as methylation and cracking.

4.4 Conclusions

The ethene/2MB yield is used to describe the relative propagation of the aromatic- and olefin-based cycles in MTH catalysis on H-ZSM-5, where a high ethene/2MB yield indicates increased propagation of the aromatic-based cycle and low ethene/2MB yield indicates

increased propagation of the olefin-based cycle. Isotopic experiments of ^{13}C-DME with ^{12}C-ethene show that the reaction rate of DME conversion is ∼20 times faster than ethene. At iso-conversion conditions at 548 K, propene and toluene are co-fed with DME to increase propagation of the olefin- and aromatic-based cycles, respectively. The ethene/2MB yield correspondingly decreases by a factor of 1.9 with the addition of propene and increases by a factor of 2.1 with the addition of toluene. The ethene/2MB yield increases slightly (0.9-2.1) with increasing conversion of DME (5-62%) at 623 K on commercial H-ZSM-5, showing that aromatic-based cycle propagates more relative to the olefin-based at higher conversions. For the reaction of DME alone, a monotonic increase in selectivity to C_3-C_7 hydrocarbons and monotonic decrease in selectivity to methylbenzenes and ethene with increasing reaction temperature from 548 K to 723 K is observed, showing that selectivity can be tuned at iso-conversion conditions and that at higher temperatures the olefin-based cycle dominates over the aromatic-based cycle resulting in lower ethene/2MB yield. The ethene/2MB yield varies systematically with varying feed composition and temperature, showing that the relative rates of propagation of the aromatic- and olefin-based cycles in MTH catalysis on H-ZSM-5 can be described by this ratio.

4.5 Supplemental Information

4.5.1 Trends in Product Selectivity with Hydrogen Transfer

The change in selectivity to 2-methylbutane, 2-methyl-2-butene, 2MB, and C_5 alkane to alkene ratio are shown for the reaction of DME alone over H-ZSM-5 between 5-62% DME conversions at 623 K (Figure 4.6a) and 548-623 K at 60% DME conversion (Figure 4.6b).

4.5.2 Other Descriptors for the Relative Propagation of the Aromatic- and Olefin-Based Cycles

Figure 4.7 - Figure 4.9 show the ratio of yields for ethene to other C_3-C_5 hydrocarbon products for the reaction conditions used in this work. Table 4.2 - Table 4.7 also show a detailed product distribution for the C_5 products for the reaction conditions used in this work.

4.5.3 Effect of Feed Composition on Ethene/2MB Yield at 623 K and 723 K

Figure 4.10 shows the effect of co-processing approximately 4 kPa of propene, toluene, and p-xylene with 70 kPa of DME at iso-conversion conditions (33.3-36.7% DME) at 623 K

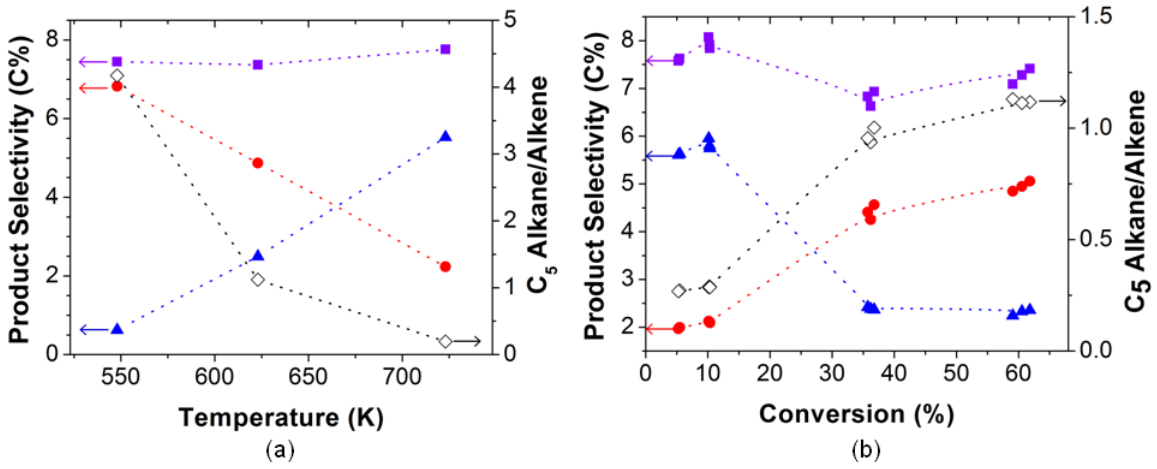

Figure 4.6: Changes in selectivity to ● 2-methylbutane, ▲ 2-methyl-2-butene, ■ 2MB, and ◇ C_5 alkane to alkene ratio for the reaction of 70 kPa DME over H-ZSM-5 (Si/Al=42.5) at (a) 623 K and 5-62% DME conversion and (b) 60% DME conversion and 548-723 K.

Table 4.2: Product selectivity to C_5 hydrocarbons for the reaction of 70 kPa DME (+4 kPa co-feed) on H-ZSM-5 (Si/Al=42.5) at 548 K and 17.9-18.6% DME conversion.

	Co-Feed		
Product Selectivity	*Propene*	*None*	*Toluene*
total C_5 hydrocarbons (C%)	9.6	7.0	3.7
2-methylbutane (C%)	5.9	4.2	1.4
2-methyl-2-butene (C%)	1.5	1.0	0.9

Table 4.3: Product selectivity to C_5 hydrocarbons for the reaction of 70 kPa DME (+4 kPa co-feed) on H-ZSM-5 (Si/Al=42.5) at 623 K and 33.3-36.8% DME conversion.

	Co-Feed			
Product Selectivity	*Propene*	*None*	*Toluene*	*p-Xylene*
total C_5 hydrocarbons (C%)	9.7	9.3	4.4	4.3
2-methylbutane (C%)	3.9	4.4	1.5	1.5
2-methyl-2-butene (C%)	3.1	2.7	1.2	1.2

Table 4.4: Product selectivity to C_5 hydrocarbons for the reaction of 70 kPa DME (+4 kPa co-feed) on H-ZSM-5 (Si/Al=42.5) at 723 K and 60.2-70.6% DME conversion.

	Co-Feed			
Product Selectivity	*Propene*	*None*	*Toluene*	*Ethylbenzene*
total C_5 hydrocarbons (C%)	17.3	14.7	8.9	8.8
2-methylbutane (C%)	2.1	2.2	1.1	0.6
2-methyl-2-butene (C%)	7.0	5.5	3.4	0.9

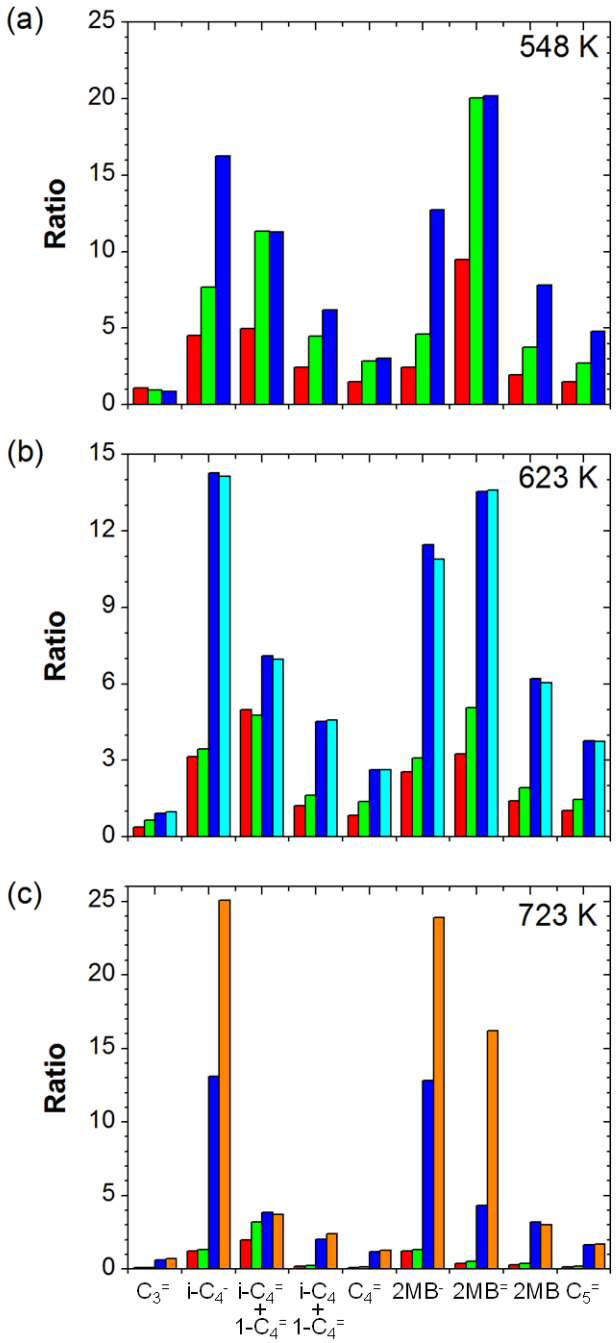

Figure 4.7: The ratio of yields of ethene to various C_3-C_5 alkanes and olefins for the reaction of 70 kPa DME with ■ 4 kPa propene, ■ no co-feed, ■ 4 kPa toluene, ■ 4 kPa p-xylene, and ■ 4 kPa ethylbenzene on H-ZSM-5 (Si/Al=42.5) at (a) 548 K and 17.9-18.6% DME conversion, (b) 623 K and 33.3-36.8% DME conversion, and (c) 723 K and 60.2-70.6% DME conversion.

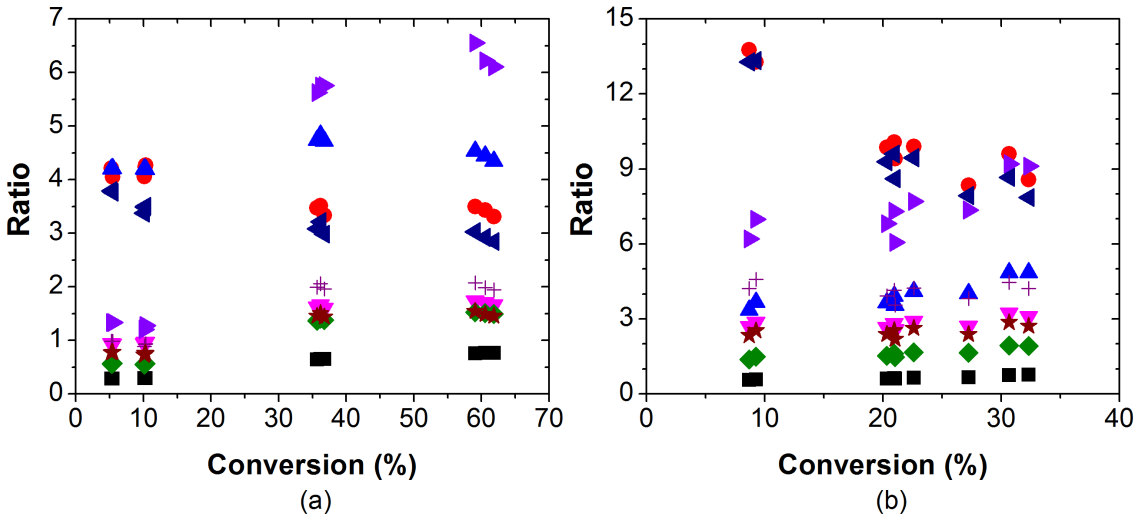

Figure 4.8: The ratio of yields of ethene to ■ propene, ● isobutane, ▲ isobutene and 1-butene, ▼ isobutane, isobutene, and 1-butene, ◆ C_4 olefins, ◀ 2-methylbutane, ▶ 2-methyl-2-butene, + 2MB, and ★ C_5 hydrocarbons for the reaction of DME at varying conversions at 623 K on (a) a commercial sample of H-ZSM-5 (Si/Al=42.5) and (b) a sample of H-ZSM-5 with 17 μm crystals (Si/Al=28).

Table 4.5: Product selectivity to C_5 hydrocarbons for the reaction of 70 kPa DME on commercial H-ZSM-5 (Si/Al=42.5) at 623 K with varying fractional DME conversion.

DME	**Product Selectivity (C%)**		
Conversion (%)	*total C_5 hydrocarbons*	*2-methylbutane*	*2-methyl-2-butene*
5.5	9.6	2.0	5.6
5.3	9.6	2.0	5.6
10.1	9.9	2.1	6.0
10.3	9.7	2.1	5.8
10.3	9.7	2.1	5.7
36.8	9.5	4.6	2.4
36.2	9.1	4.3	2.4
35.7	9.4	4.4	2.4
61.8	9.9	5.1	2.4
60.5	9.7	5.0	2.3
59.1	9.5	4.8	2.2

Table 4.6: Product selectivity to C_5 hydrocarbons for the reaction of 70 kPa DME on H-ZSM-5 (17 μm crystallite size) at 623 K with varying fractional DME conversion.

DME	**Product Selectivity (C%)**		
Conversion (%)	*total C_5 hydrocarbons*	*2-methylbutane*	*2-methyl-2-butene*
8.7	8.0	1.4	3.0
9.3	7.8	1.5	2.8
20.3	8.0	2.1	2.8
21.0	8.4	2.1	3.1
20.9	7.9	2.1	2.7
22.6	7.8	2.2	2.7
27.2	8.3	2.5	2.7
30.7	7.7	2.5	2.4
32.3	8.0	2.8	2.4

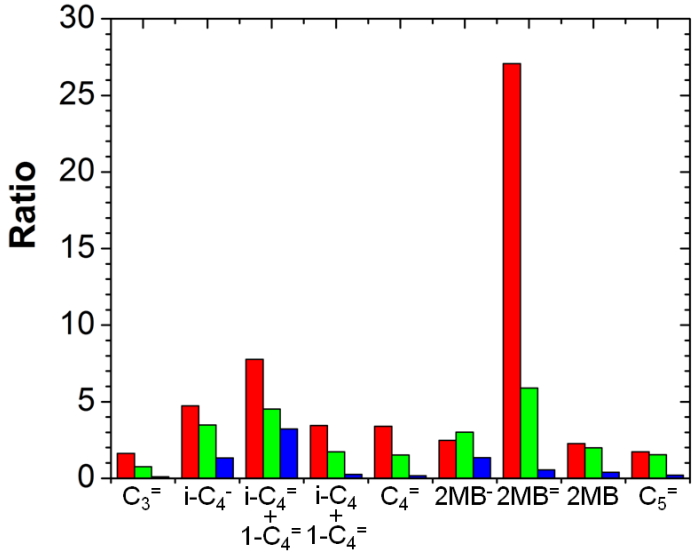

Figure 4.9: The ratio of yields of ethene to various C_3-C_5 alkanes and olefins for the reaction of 70 kPa DME at 59.4-60.8% conversion on H-ZSM-5 (Si/Al=42.5) at ■ 548 K, ■ 623 K, and ■ 723 K.

Table 4.7: Product selectivity to C_5 hydrocarbons for the reaction of 70 kPa DME on H-ZSM-5 (Si/Al=42.5) at 59.4-60.8% DME conversion and varying temperatures.

	Temperature (K)		
Product Selectivity	*548*	*623*	*723*
total C_5 hydrocarbons (C%)	9.6	7.0	3.7
2-methylbutane (C%)	5.9	4.2	1.4
2-methyl-2-butene (C%)	1.5	1.0	0.9

on H-ZSM-5. Because isotopically-labeled reactants were not used for these reactions, all hydrocarbons in the reaction effluent are included in the assesment of product selectivity.

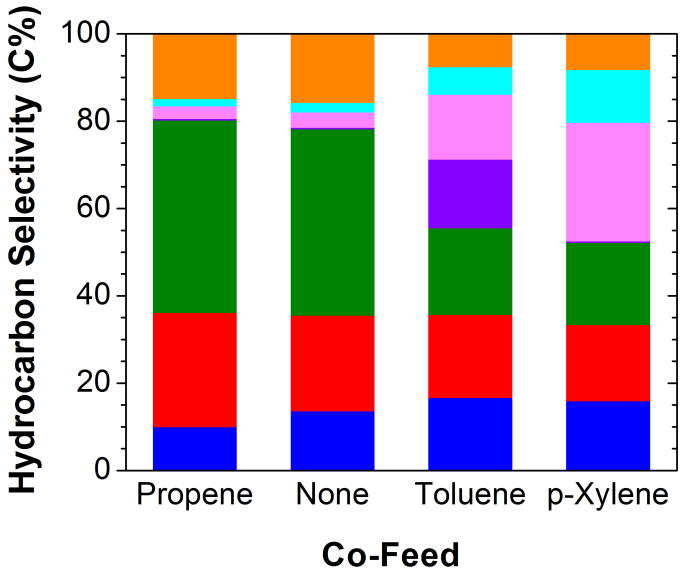

Figure 4.10: . The effect of feed composition on the hydrocarbon selectivity for the reaction of 70 kPa DME (+4 kPa co-feed) at 623 K over H-ZSM-5 (Si/Al=42.5); C_2, C_3, C_4-C_7, toluene, xylenes, C_{9+} methylbenzenes, and others. The H/C stoichiometry for the fraction labeled others is the following: 1.85 for DME+propene, 1.89 for DME, 1.65 for DME+toluene, and 1.57 for DME+p-xylene.

Figure 4.11 shows the effect of co-processing approximately 4 kPa or propene, toluene, and ethylbenzene with 70 kPa of DME at similar DME conversions (60-73%) on product selectivity and the ethene/2MB yield. ^{13}C-labeled co-feeds were used for the reactions with propene and toluene, and completely ^{13}C-labeled propene and toluene in the effluent were not included in the assessment of product selectivity. For the reaction of DME with ethylbenzene, the ethylbenzene in the effluent was not included in the assessment of product selectivity because of the negligible amount of ethylbenzene (<0.5% selectivity) formed during the reaction of DME alone at similar conditions.

4.5.4 Ethene/2MB Yield for MTH on Large Crystal H-ZSM-5 at 623 K

Figure 4.12 shows the effect of conversion on the product selectivity and ethene/2MB yield for the reaction DME alone at 623 K on 17 μm crystals of H-ZSM-5. Between 8.7 and 32.3% DME conversion, the fractional conversion of DME has little effect on both the product selectivity and ethene/2MB yield, which is around 4.1.

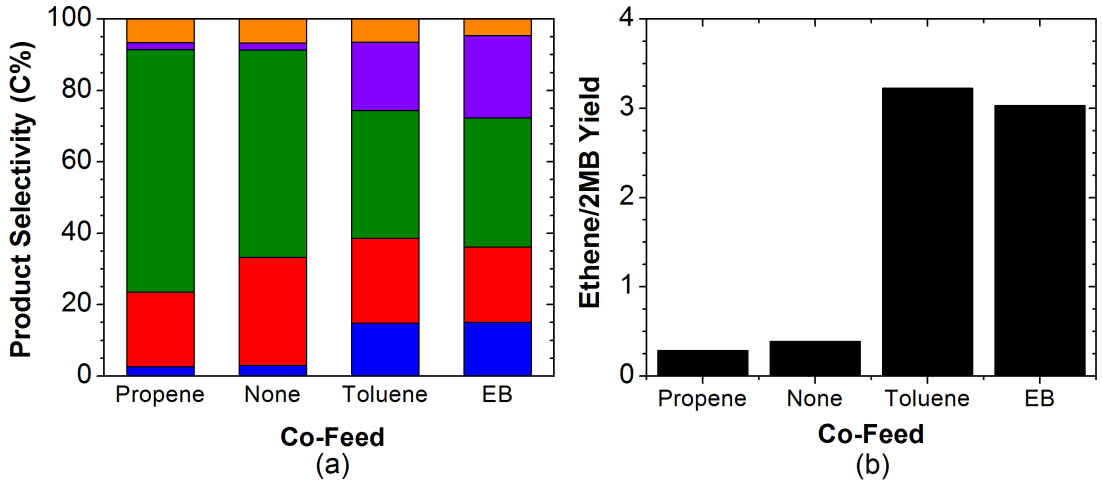

Figure 4.11: The effect of feed composition on (a) the hydrocarbon selectivity and (b) ethene/2MB yield for the reaction of 70 kPa DME (+4 kPa co-feed) at 723 K over H-ZSM-5 (Si/Al=42.5); for (a) ■ C_2, ■ C_3, ■ C_4-C_7, ■ methyl/ethylbenzenes, and ■ others.

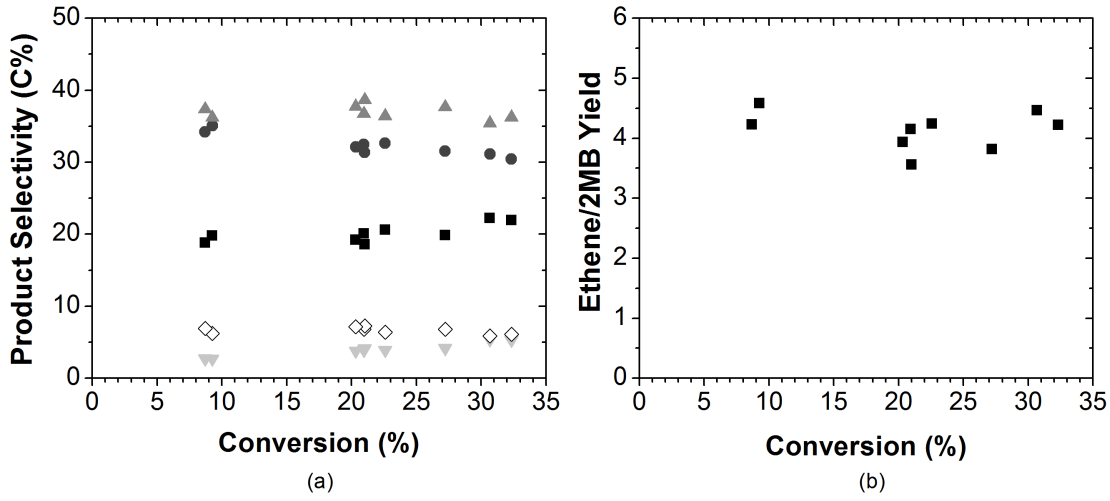

Figure 4.12: The effect of fractional conversion of DME on (a) product selectivity and (b) ethene/2MB yield for the reaction of 70 kPa DME at 623 K over 17 μm crystals of H-ZSM-5 (Si/Al=28); for (a) ■ C_2, ● C_3, ▲ C_4-C_7, ▼ methylbenzenes, ◇ others.

Acknowledgments

This work was supported by The Dow Chemical Company and the National Science Foundation (CBET 1055846). The authors also acknowledge Professor Dongxia Liu, University of Maryland, for synthesis and characterization of H-ZSM-5 with 17 μm crystals.

CHAPTER

FIVE

TUNING THE SELECTIVITY OF METHANOL-TO-HYDROCARBONS CONVERSION ON H-BEA AND H-SAPO-34

5.1 Introduction

The emergence of the dual-catalytic cycle for methanol-to-hydrocarbons (MTH) was an important step in understanding the identity of reactive intermediates that comprise the hydrocarbon pool and in understanding how these hydrocarbon pool species contribute to the selectivity towards certain products of MTH.[13,15] In this context, the effect of different zeolite or zeotype frameworks on observed product selectivity can be understood. H-SAPO-34 and H-ZSM-22 are two frameworks that can essentially be viewed as two different extremes of the dual-catalytic cycle. In H-SAPO-34, the aromatic-based cycle dominates due to product shape selectivity in which the small 8-MR windows hinders C_{5+} hydrocarbons from escaping the larger 12-MR cavities, resulting in a product selectivity rich in light olefins.[16–18,135] In contrast, the unidimensional 10-MR pores of H-ZSM-22 are too small for aromatics to be reactive for olefin formation and the olefin-based cycle dominates, resulting in a selectivity rich in C_{5+} aliphatics.[42,46–48]

The ability to relate the product selectivity of H-SAPO-34 and H-ZSM-22 to the catalyst topology is unique to these two zeolites. For these two catalysts, the relationship between structure, hydrocarbon pool composition, and product selectivity is easier to understand. For other zeolite structures, however, the relationship is less clear. For example, H-ZSM-5 can propagate both the aromatic- and olefin-based cycle and the propagation of these two cycles is tunable. The ability to systematically tune the product selectivity of MTH through the use of an aromatic and olefin co-feed on H-ZSM-5 at different temperatures

and space velocities was investigated and is discussed in Chapter 3. By using an olefin co-feed, the propagation of the olefin-based cycle increased relative to the propagation of the aromatic-based cycle. Similarly, the use of an aromatic co-feed increased propagation of the aromatic-based cycle relative to the olefin-based cycle. In Chapter 4 we show that the ratio of ethene/2MB yield is a valid descriptor for the relative propagation of the two cycles on H-ZSM-5. On H-BEA, the effect of zeolite framework on the the relative propagation of the two cycles is also unclear. Isotopic switching experiments on H-BEA at 623 K have shown that after switching from ^{12}C-methanol to ^{13}C-methanol, the ^{13}C-content of C_{2+} olefins, penta-, and hexaMB are similar.[44,45] Co-reactions of methanol/DME with aromatics and olefins both show that light olefins can come from both olefin cracking and aromatic dealkylation, suggesting that both cycles propagate on H-BEA.[26,27,40,90]

In this work, ability to tune selectivity of two different large-pore catalysts, H-BEA and H-SAPO-34, through the use of olefin and aromatic co-feeds and reaction temperature was investigated. On H-BEA, the ethene/2MB yield was determined and isotopic switching experiments at low DME conversion were also performed to determine the relative propagation of the olefin- and aromatic-based cycle in the presence of co-feeds and in the absence of co-feeds. On H-SAPO-34, a propene co-feed was used to determine if the olefin-based cycle can be activated on this catalyst where the aromatic-based cycle dominates. Aromatics are too large to enter the small 8-MR windows of SAPO-34, therefore, a 2-pentene co-feed was used as an aromatic precursor to determine if the aromatic-based cycle can be propagated more.

5.2 Materials and Methods

5.2.1 Catalyst Preparation

H-BEA (CP814), Si/Al=12, was obtained in the ammonium form from Zeolyst International. Structural and chemical characterization of the catalyst sample is reported in Section 5.5.1 of the Supplemental Information. The silicon to aluminum ratio of the H-BEA sample used in this work was determined by ICP-OES elemental analysis (performed by Galbraith Laboratories). The ammonium-form zeolite was sieved to obtain aggregate particle sizes between 180 and 425 μm (40-80 mesh) and treated in 1.67 cm^3 s^{-1} of dry air (20-21% O_2, <10 ppm H_2O, Minneapolis Oxygen) at 773 K for 4 hours (heating rate of 0.0167 K s^{-1}) to convert it to the proton-form zeolite. The catalyst was pre-treated *in situ* in 1.67 cm^3 s^{-1} of helium flow (99.995% purity, Minneapolis Oxygen) at 773 K overnight using a heating rate of 0.0167 K s^{-1} prior to reaction.

SAPO-34 (0.15 Si:1.00 Al:0.80 P:3.90 O) was obtained from The Dow Chemical Company with the catalyst sample still containing the synthesis template. The sample was

sieved to obtain aggregate particle sizes between 180 and 425 μm (40-80 mesh) and treated *in situ* immediately prior to reaction with with 1.67 cm^3 s^{-1} of dry air (20-21% O_2, <10 ppm H_2O, Minneapolis Oxygen) at 773 K for 4 hours (heating rate of 0.0167 K s^{-1}) to remove the template and convert it to the proton-form catalyst.

5.2.2 Catalytic reactions of DME in the absence and in the presence of olefin and aromatic co-feeds over H-BEA

A stainless steel packed bed reactor (0.25 in o.d.; 0.215 in i.d.) equipped with a concentric thermal well (0.0625 in o.d.; 0.0485 in i.d.) aligned along the tube center was used for the conversion of dimethyl ether (DME). The catalyst bed was supported between quartz wool plugs and operated at isothermal conditions using an ARI heating coil regulated by a Watlow Temperature Controller (96 Series). Reactions were run at 623 K using 17 mg of catalyst and at 723 K using 8 mg of catalyst. At these conditions, a flow rate of 0.23 cm^3 s^{-1} DME (Matheson Tri-Gas, 99.5% purity) was used. Propene (50% propene, 50% argon, Praxair), toluene (99.9% purity, Sigma-Aldrich), and 1,2,4-triMB (98% purity, Sigma-Aldrich) co-reactants were fed so that the total co-feed gas flow rate was 0.013 cm^3 s^{-1}. Toluene and 1,2,4-triMB were fed as a liquid using a Cole Parmer EW-74900-00 syringe pump. A balance of methane and argon (10% methane, 90% argon, Airgas), used as an internal standard, was fed so that the total flow rate was 0.417 cm^3 s^{-1}. The total pressure of the reactor was 130 kPa. The resulting partial pressure of DME was 70 kPa and the total co-feed pressure was 4 kPa. Heat traced lines (423 K) were used to transfer the aromatic to the reactor and the reactor effluent to a gas chromatograph-mass spectrometer (Agilent 7890-5975C) equipped with a methyl-siloxane capillary column (HP-1, 50.0 m $\times$ 320 μm $\times$ 0.52 μm) connected to a flame ionization detector and a 5% diphenyl, 95% methyl-siloxane capillary column (HP-5, 50.0 m $\times$ 320 μm $\times$ 0.52 μm) connected to a mass spectrometer.

For these reactions, the product selectivity on an aromatic-free basis ($S_{AF,i}$) was also determined for species i to be

$$S_{AF,i} = \frac{S_i}{S_{C_{2-7}}}, \tag{5.1}$$

where S_i and $S_{C_{2-7}}$ are the product selectivity of species i and of all C_2-C_7 hydrocarbons, respectively, calculated on a carbon basis of all the product hydrocarbons.

5.2.3 Reactions using ^{13}C-labeled co-feeds with DME over H-BEA

For experiments using ^{13}C-labeled co-feeds, reaction conditions were the same as those used above in Section 5.2.2. ^{13}C-propene (99% purity, Aldrich) and ^{13}C-toluene (99% purity, Aldrich) were co-reacted with DME. ^{13}C-toluene was fed using a saturator immersed in a water bath heated by a Cole Parmer heating jacket regulated by a Watlow Temperature

Controller (96 Series). The methane/argon gas stream was used as a carrier gas for the toluene and the water bath temperature was adjusted to achieve the desired toluene partial pressure (1.3-4.1 kPa). Isotopologue distributions were determined from mass fragmentation patterns using the method outlined by Price and Iglesia [55].

5.2.4 Isotopic switching experiment for the conversion of DME over H-BEA

The isotopic switching experiment for the conversion of DME over H-BEA was performed at 623 K using 16.5 mg of catalyst, DME flow rate of 0.224 $cm^3\ s^{-1}$, and a methane/argon flow rate of 17.8 $cm^3\ s^{-1}$. Two identical and separate feed lines, one with flowing ^{12}C-DME and the other with flowing ^{13}C-DME (99% ^{13}C-atom purity, Isotec) were connected to a VICI Valco 4-way valve, where one outlet was a vent line and the other outlet went to the reactor. A separate feed line of methane/argon was connected directly to the reactor. For the first 10 minutes of reaction, ^{12}C-DME was reacted over H-BEA, followed by a switch to ^{13}C-DME (at the same flow rate as the ^{12}C-DME), with all other reaction conditions remaining constant. The reactor effluent was analyzed using GC-MS.

5.2.5 Catalytic reactions of DME in the absence and in the presence of olefin and aromatic co-feeds over H-SAPO-34

Reactions on H-SAPO-34 were performed using a similar procedure as those used in Section 5.2.2. Reactions at 548 and 723 K were performed using 49.5 and 19 mg of catalyst, respectively, and flow rates of 0.226 $cm^3\ s^{-1}$ DME and 0.192 $cm^3\ s^{-1}$ methane/argon. Reactions at 623 K were performed using 49.5 mg of catalyst and a flow rate of 0.114 $cm^3\ s^{-1}$ DME (70 kPa). Propene fed at 0.013 $cm^3\ s^{-1}$ of the propene/argon gas mixture and 2-pentene fed using a syringe pump at a liquid flow rate of 3.89×10^{-5} $cm^3\ s^{-1}$ were used as co-feeds at these conditions so that the co-feed partial pressure was 4.1 and 5.3 kPa, respectively. A balance of methane/argon was used so that the total flow rate for reactions performed at 623 K was 0.208 $cm^3\ s^{-1}$.

5.3 Results and Discussion

5.3.1 Selectivity of DME conversion with varying feed compositions and temperatures on H-BEA

At 623 K and a DME WHSV of 96 g (g catalyst h)$^{-1}$, five different feed compositions were tested: (1) DME only, (2) DME + propene, (3) DME + toluene, (4) DME + 1:1 C ratio of propene:toluene, and (5) DME + 1,2,4-triMB. The chemical conversion, and product

selectivity for the different feed compositions tested are shown in Table 5.1 and Figure 5.1. The results reported where a co-feed was used with DME are shown at iso-conversion of DME (17.0-22.9%), where methanol is considered to be unreacted feed. Because propene is a major product for the reaction of DME alone over H-BEA, ^{13}C-propene was used to determine the propene co-feed conversion. Any completely ^{13}C-labeled propene in the effluent was considered unreacted feed. For the reaction of DME alone on H-BEA at 623 K, selectivity to toluene and 1,2,4-triMB is negligible and so in reactions using an aromatic co-feed, any of the aromatic co-feed in the reaction effluent was considered unreacted feed. The product selectivity of the reaction of DME alone and DME co-fed with 1,2,4-triMB is also shown at 723 K at 80-90 C% in Figure 5.2.

Table 5.1 and Figure 5.1 show that the addition of propene as a co-feed results in the highest selectivity to C_3-C_7 hydrocarbons (78.5%) and the lowest selectivity to C_{8+} (18.5%). The high selectivity to the C_3-C_7 hydrocarbon fraction shows that there is increased propagation of the olefin-based cycle, as these hydrocarbons are most likely the result of repeated olefin methylation and cracking cycles. In contrast, the addition of 1,2,4-triMB as a co-feed results in the lowest selectivity to C_3-C_7 hydrocarbons (25.4%) and the highest selectivity to C_{8+} hydrocarbons (72.5%), a four-fold decrease in C_3-C_7 hydrocarbon selectivity and a corresponding four-fold increase in selectivity to C_{8+}. The high selectivity to C_{8+} hydrocarbons with the addition of 1,2,4-triMB as a co-feed is a result of increased aromatic methylation, evidenced by the high selectivity to penta- (10.8 C%) and hexaMB (30.8 C%). For the reactions in which toluene and a 1:1 C mixture of propene and toluene were used as co-feeds, the the observed selectivity was in between the two extreme product distributions of the co-reaction of DME with propene and 1,2,4-triMB. Although toluene and 1,2,4-triMB co-feeds both propagate the aromatic-based cycle more than the propene or 1:1 C mixed co-feed based on the enhanced selectivity to polyMBs when aromatic are used as co-feeds (Table 5.1), 1,2,4-triMB has a higher selectivity polyMBs and therefore propagates the aromatic-based cycle more that toluene, indicating that 1,2,4-triMB undergoes methylation faster than toluene. Similar to the results presented in Chapter 3 on tuning the selectivity of MTH on H-ZSM-5, systematic changes in product selectivity shown in Figure 5.1 show that the selectivity of MTH can be systematically tuned on BEA through the use of an olefin and/or aromatic co-feed.

On H-ZSM-5, rates of both aromatic methylation and dealkylation were increased with the addition of an aromatic co-feed with DME, evidenced by increased selectivity to both methylbenzenes and ethene, a product of aromatic dealkylation but not a significant product of olefin cracking (Table 3.1). On H-BEA, co-reactions of ^{12}C-benzene with ^{13}C-methanol at 523 K at 6 C% conversion by Bjørgen et al.[90] have shown that propene and isobutane (coming from isobutene), incorporate aromatic carbons. Similar work from Mikkelsen et

Table 5.1: Conversion, conversion rate, and product selectivity for the reaction of 70 kPa DME in the absence and in the presence of a co-feed at 623 K over H-BEA, DME WHSV = 96 g (g catalyst h)$^{-1}$.

Co-feed	**None**	**Propene**	**1:1 C**	**Toluene**	**1,2,4-triMB**
Co-feed partial pressures (kPa)					
Propene	–	4.2	2.8	–	–
Aromatic	–	–	1.3	4.1	4.0
Conversion (%)					
Total C	19.5	20.7	21.1	17.4	25.9
DME	19.5	17.5	17.0	22.9	18.3
Propene[a]	–	24.0	21.5	–	–
Aromatic tnoteb	–	–	64.9	51.4	74.4
Product Selectivity (C%)					
C_2	1.9	3.1	2.7	3.8	2.1
C_3	7.6	10.9	8.6	7.6	4.5
C_4 (total)	30.4	32.7	29.2	16.5	9.5
i-butane	30.3	29.9	28.2	22.4	5.7
C_5	12.2	13.8	12.2	7.2	4.5
C_6	7.3	8.8	7.7	4.6	3.0
C_7	12.6	12.1	11.7	6.0	3.9
C_8+ (total)	28.0	18.5	27.8	54.4	72.5
PentaMB	0.2	0.7	2.5	4.9	10.8
HexaMB	10.0	0.9	1.5	5.2	30.8

[a] Based on the conversion of ^{13}C-propene.
[b] Aromatic co-feed in the effluent is considered to be unreacted feed.

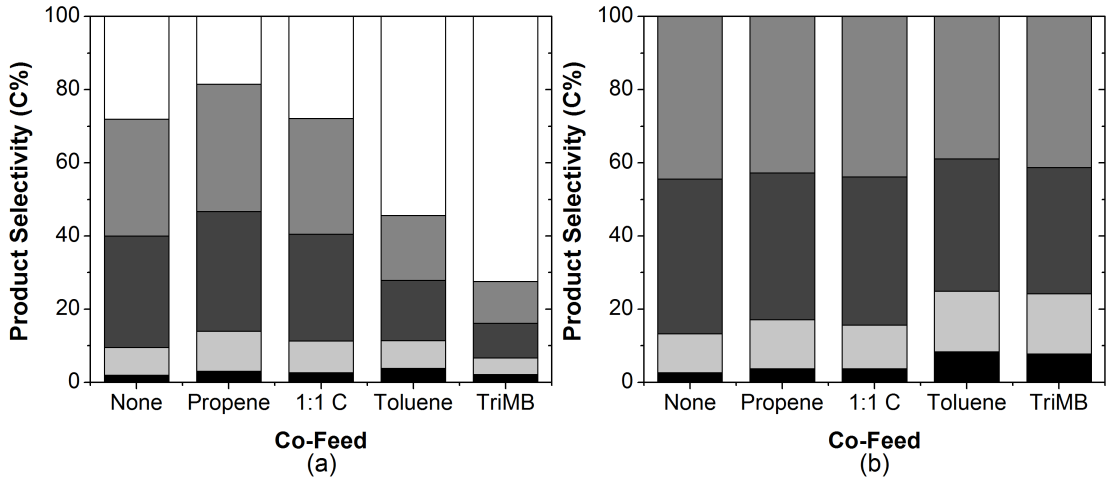

Figure 5.1: (a) The observed product selectivity and (b) the product selectivity on an aromatic-free basis of the reaction 70 kPa of DME with 4 kPa of various co-feeds at 623 K on H-BEA (Si/Al=12) and $WHSV_{DME}$=96 g (g catalyst h)$^{-1}$; ■ C_2, ■ C_3, ■ C_4, ■ C_5-C_7, □ C_{8+}.

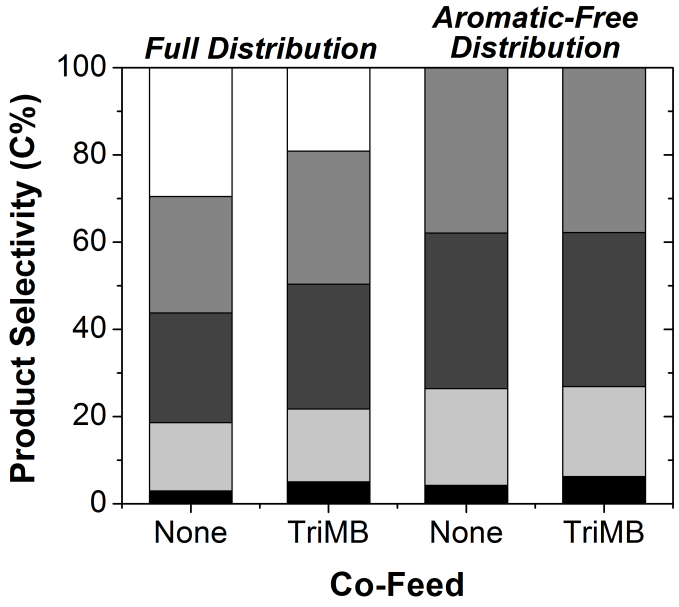

Figure 5.2: The observed product selectivity and the product selectivity on an aromatic-free basis of the reaction 70 kPa of DME with 4 kPa 1,2,4-triMB at 723 K on H-BEA (Si/Al=12) and $WHSV_{DME}$=212 g (g catalyst h)$^{-1}$; ■ C_2, ■ C_3, ■ C_4, ■ C_5-C_7, □ C_{8+}.

al.[40] at 623 K and conversions greater than 50 C% shows that both ethene and propene contain carbons originating from the aromatic. Therefore, ethene, propene, and isobutene can all come from the aromatic-based cycle in MTH on H-BEA. Based on the co-reaction of ^{13}C-DME with unlabeled C_5-C_7 olefins, Simonetti et al.,[27] however, calculated β-scission rates of C_5-C_7 olefins to form ethene, propene, n-butene, and isobutene at 473 K on H-BEA to be between 0.66 to 1.9 μmol (mol Al s)$^{-1}$, showing that ethene, propene, and isobutene can all be formed the olefin-based cycle as well. Unlike H-ZSM-5, where ethene was predominantly a product of the aromatic-based cycle and ethene selectivity increased systematically with increased propagation of the aromatic-based cycle, there are no clear olefin products of the aromatic-based cycle that increase in selectivity with increased propagation of the aromatic-based cycle.

Using the ethene/2MB yield for the reaction of various feed compositions at 623 and 723 K to determine the relative propagation of the olefin- and aromatic-based cycles, it is clear the addition of a pure aromatic co-feed increases the propagation of the aromatic-based cycle, based on the increased ethene/2MB yield for these co-feed compositions compared to ethene/2MB yield for the reaction of DME in the absence of a co-feed (Figure 5.3). However, the ethene/2MB yield for the co-reaction of DME with toluene at 623 K was higher than that of DME co-reacted with 1,2,4-triMB at 623 K even though the product selectivity to aromatics was higher for the co-reaction of 1,2,4-triMB with DME (Figure 5.1 and Figure 5.3). To determine if aromatic methylation and dealkylation contributed to the product selectivity to C_2-C_7, the aromatic-free selectivity of DME with various co-feeds at 623 K on H-BEA was determined (Figure 5.1b). The selectivity on an aromatic-free basis increased for both ethene and propene but decreased for C_4 hydrocarbons when toluene and 1,2,4-triMB were used as co-feeds compared to the propene co-feed and DME reacted in the absence of a co-feed on H-BEA. Surprisingly, the selectivity on an aromatic-free basis to ethene and propene for the 1:1 C mixed propene:toluene co-feed with DME was similar to that of the co-reaction of DME with propene and the reaction of DME alone. The increased aromatic-free selectivity to ethene and propene suggest that at the conditions used in this work, the aromatic-based cycle contributes to propene and ethene formation, but the majority of C_4 hydrocarbons come from the olefin-based cycle. Comparatively, the product distribution of DME reacted in the absence of a co-feed and DME co-reacted with 1,2,4-triMB are more similar at 723 K that at 623 K. At 723 K and 80-90 C% conversion, only ethene selectivity on an aromatic-free basis increases slightly, from 4.2 to 6.2 C% and selectivity on an aromatic free-basis to all other C_3-C_7 when 1,2,4-triMB co-fed with DME compared to the reaction of DME alone,(Figure 5.2) suggesting that at higher temperatures, the aromatic-based cycle no longer contributes significantly to light olefin products.

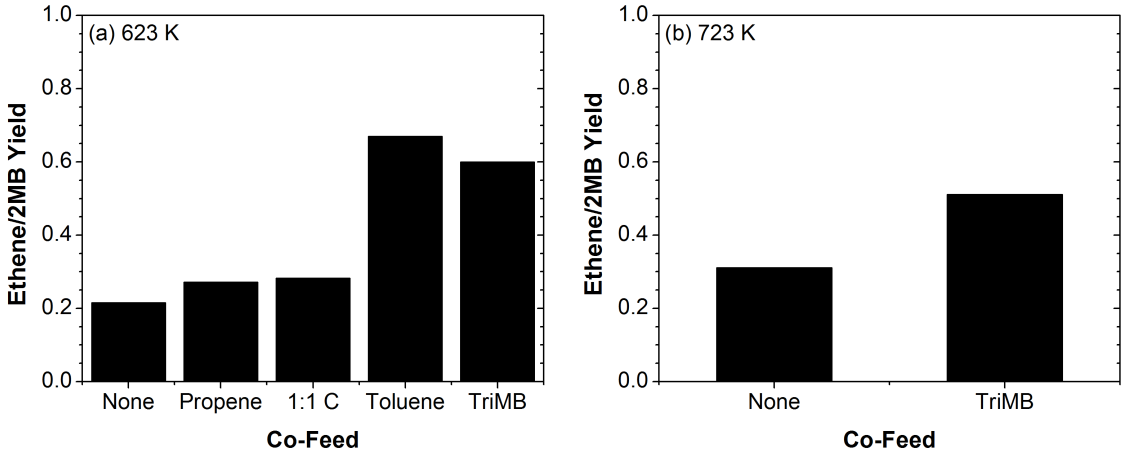

Figure 5.3: The ethene/2MB yield for the reaction of 70 kPa DME with 4 kPa of various co-feeds on H-BEA (Si/Al=12) at (a) 623 K and WHSV$_{DME}$=96 g (g catalyst h)$^{-1}$ and (b) 723 K and WHSV$_{DME}$=212 g (g catalyst h)$^{-1}$.

5.3.2 The MTH Hydrocarbon Pool on H-BEA

In the hydrocarbon pool mechanism of MTH, olefins and aromatics undergo repeated methylation and cracking. The identity of the hydrocarbon pool species, however, depends on the catalyst structure as well as the operating conditions. By co-reacting 4 kPa of ^{13}C-propene and ^{13}C-toluene with ^{12}C-DME on H-BEA at 623 K, the identity of active hydrocarbon pool species at these conditions was determined. Isotopologue distribution of the co-reaction of ^{12}C-DME with ^{13}C-labeled propene or toluene (1:1 C) is shown in Section 5.5.2 of the Supplemental Information, along with the isotopologue distributions of olefins for the co-reaction of ^{12}C-DME with ^{13}C-toluene and the aromatic isotopologue distribution for the co-reaction of ^{12}C-DME with ^{13}C-propene. When ^{13}C-toluene is co-reacted with ^{12}C-DME, a monotonic decrease in the fraction of isotopologues with seven ^{13}C-atoms with increasing aromatic size is observed, showing that the majority (>80%) of MBs with 2-4 methyl groups are formed primarily from methylation of toluene (Figure 5.4). The increasing incorporation of ^{12}C-atoms from DME into larger aromatics, particularly penta- and hexaMB, shows that these aromatics are both formed from methylation of toluene and rebuilt from successive methylations and dealkylations, resulting in a significant fraction of penta- (31.5%) and hexaMB (65.5%) that contain fewer than seven ^{13}C-atoms (Figure 5.4). The increased scrambling of ^{12}C/^{13}C-atoms in penta- and hexaMB compared with that of smaller polyMBs, shows that on large-pore H-BEA zeolite, larger aromatics are the active aromatic hydrocarbon pool species. In contrast, in Chapter 3, it is shown that on medium-pore H-ZSM-5 zeolite, aromatics with 2-4 methyl groups are the active hydrocarbon pool species, suggesting that increased zeolite pore size allows for larger intermediates

to participate in the hydrocarbon pool.

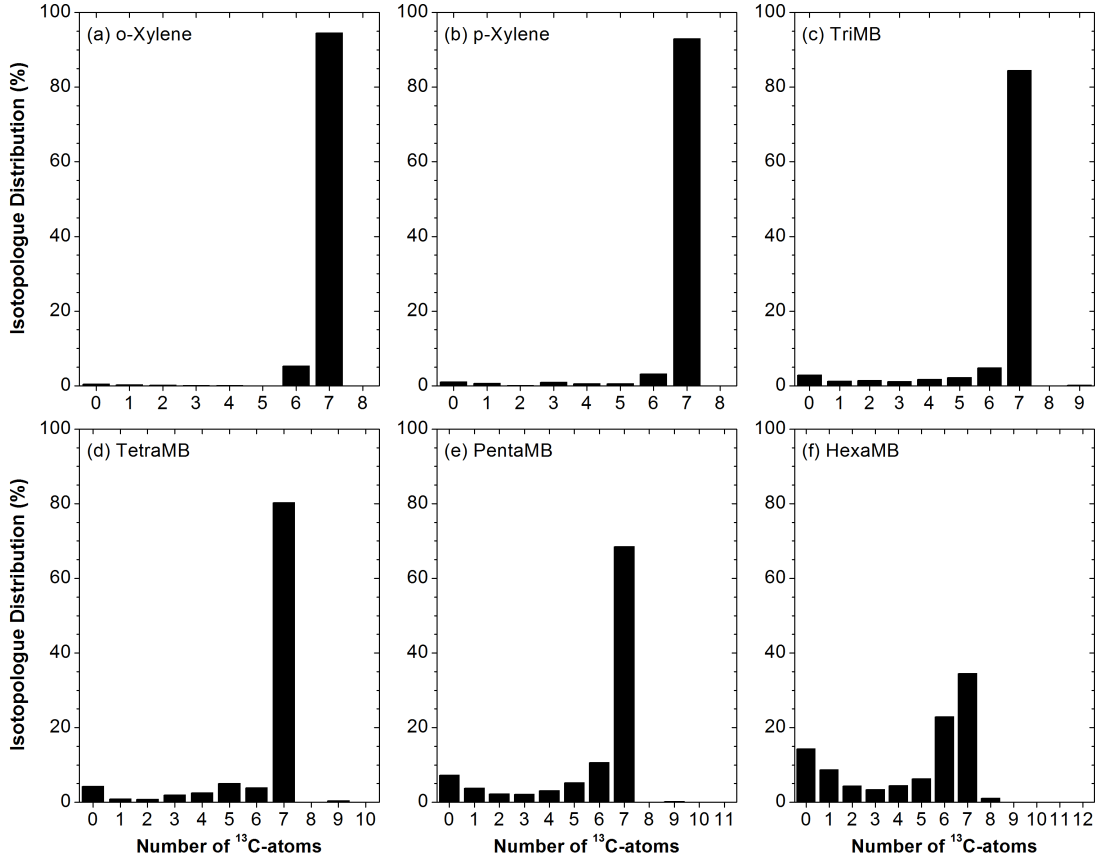

Figure 5.4: Product isotopologue distributions of (a) o-xylene, (b) p-xylene, (c) triMB, (d) tetraMB, (e) pentaMB, and (f) hexaMB for the co-reaction of 70 kPa ^{12}C-DME with 4 kPa of ^{13}C-toluene on H-BEA (Si/Al=12) at 623 K and WHSV$_{DME}$=96 g (g catalyst h)$^{-1}$.

The ^{13}C-content of C_2-C_7 olefins for the co-reaction of 70 kPa ^{12}C-DME with 4 kPa of ^{13}C-propene on H-BEA at 623 K is shown in Figure 5.5a. The observed ^{13}C content is compared with the expected ^{13}C-content based on methylation of the $(n-1)$ olefin, where n is the olefin carbon number. In Figure 5.5, the ^{13}C-content of propene is the highest of the olefins because ^{13}C-propene is also a reactant in this system. The isotopologue distribution of propene also shows that 23.4% of propene contains no ^{13}C-atoms and the expected ^{13}C-content of propene based on methylation of ethene is an order-of-magnitude lower than what is observed, indicating that propene is formed from other routes, such as aromatic dealkylation and olefin cracking (Figure 5.5b). The experimentally observed ^{13}C-content of butene and pentene is lower than the expected ^{13}C-content based on methylation of the $(n-1)$ olefin, suggesting that these olefins are also formed as cracking products of higher olefins. In contrast, the experimentally observed ^{13}C-content of hexene and heptene matches

the expected ^{13}C-content, showing that these higher olefins are formed predominantly by methylation reactions. The ^{13}C-content of ethene is similar to that hexene and heptene, suggesting that ethene, in addition to being a product of aromatic dealkylation, may also be a cracking product of higher olefins (Figure 5.5). The observed ^{13}C-contents of the product olefins compared to the expected ^{13}C-contents of these olefins based on methylation of $(n-1)$ olefin show that on large-pore zeolite H-BEA, C_3-C_5 olefins are cracking products of higher olefins, whereas on medium-pore zeolite H-ZSM-5, C_3 and C_4 olefins were cracking products, showing that the larger pore size allows for larger olefin cracking products to form.

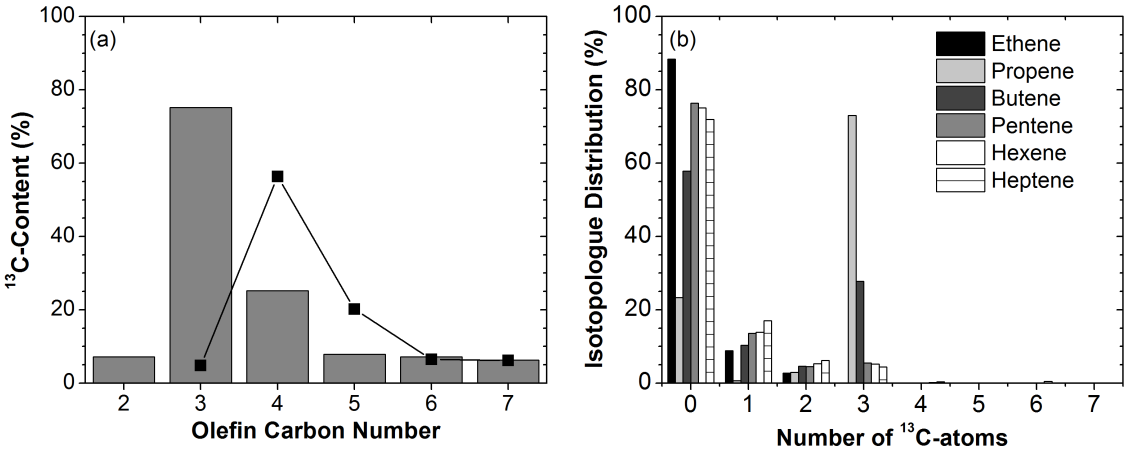

Figure 5.5: (a) Total ^{13}C-content of and (b) isotopologue distribution of olefins for the co-reaction of 70 kPa ^{12}C-DME with 4 kPa of ^{13}C-propene on H-BEA (Si/Al=12) at 623 K and WHSV$_{DME}$=96 g (g catalyst h)$^{-1}$; for (a) ■ experimentally observed ^{13}C-content and -■- expected ^{13}C-content of olefins based on methylation of the $(n-1)$ olefin.

To understand the hydrocarbon pool in the absence of an aromatic or olefin co-feed, ^{12}C-DME was reacted on H-BEA at 623 K for 10 minutes and then switched to a ^{13}C-DME feed under steady-state conditions so that the flow of DME was not interrupted by a switch to ^{13}C-DME. After the switch, the ^{13}C-content of the C_2-C_7 olefins are all similar, indicating that these species are all mechanistically linked (Figure 5.6). The ^{13}C-content of penta- and hexaMB is slightly lower than that of the olefins, suggesting that these polyMBs are mechanistically distinct from the olefins (Figure 5.6). A similar experiment on H-BEA was previously performed by Svelle, Bjørgen, and co-workers,[44,45] at 623 K and 53% methanol conversion on a catalyst sample with Si/Al=120. Their results showed that the ^{13}C-content of C_{2+} olefins, penta-, and hexaMB were similar, indicating that all olefins are mechanistically linked to to penta- and hexaMB, suggesting that either all olefins come from the aromatics, or the aromatics are being formed from the olefins. In the results shown in Figure 5.6, the ^{13}C-content of the aromatics is slightly lower than the ^{13}C-content of the

olefins. Based on this result and the similar ^{13}C-contents of olefins and aromatics in the experiments by Svelle, Bjørgen, and co-workers[44,45], it is more likely that the aromatics are formed from olefins, but aromatic dealkylation to form light olefins does not contribute significantly to the MTH product selectivity on H-BEA.

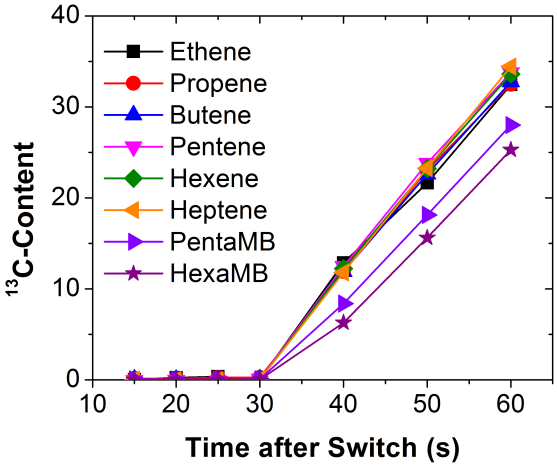

Figure 5.6: Incorporation of ^{13}C-atoms into the olefin and aromatic products of the reaction of 70 kPa ^{12}C-DME followed by a switch to at 623 K and WHSV$_{DME}$=175 g (g catalyst h)$^{-1}$.

5.3.3 Effect of feed composition, temperature, and times-on-stream on MTH conversion on H-SAPO-34

Similar to the work presented on tuning the selectivity of MTH on H-ZSM-5 and H-BEA through use of aromatic and olefin co-feeds, propene and 2-pentene were co-reacted with DME on H-SAPO-34 to determine if the selectivity of MTH conversion could be tuned on this catalyst. Propene was used to propagate the olefin-based cycle and 2-pentene was used to propagate the aromatic-based cycle. 2-pentene was used as a co-feed instead of an aromatic because aromatics are too large to diffuse in the small 8-MR windows (3.4 $\AA$ in diameter) of H-SAPO-34. Therefore, 2-pentene was fed as an aromatic precursor - an olefin that upon methylation, can undergo dehydrocyclization to form aromatics. Figure 5.7 shows the product selectivity as a function of conversion for the reaction of DME alone and for DME co-reacted with propene or 2-pentene. The results shown in Figure 5.7 are recorded between 0.3 and 3.6 ks time-on-stream, with the highest conversion for each reaction at 0.3 ks time-on-stream and the lowest conversion at 3.6 ks time-on-stream. For the co-reaction of DME with propene, the concentration of propene in the effluent was greater than that in the feed, and therefore, the only the net propene produced in included in the assessment of product selectivity. For all the results shown in this work on H-SAPO-34, ethene accounted

for >99% of C_2 hydrocarbons and propene accounted for >90% of C_3 hydrocarbons. For the co-reaction of DME with 2-pentene, the concentration of 2-pentene was lower in the effluent compared to the feed, and so it was assumed to that the 2-pentene in the effluent was unreacted feed. The product selectivity of MTH conversion on H-SAPO-34 at 623 K does not change significantly with the addition of propene or 2-pentene as co-feeds, showing that under these conditions, the use of olefins co-feeds does not increase propagation of either the olefin- or aromatic-based on H-SAPO-34.

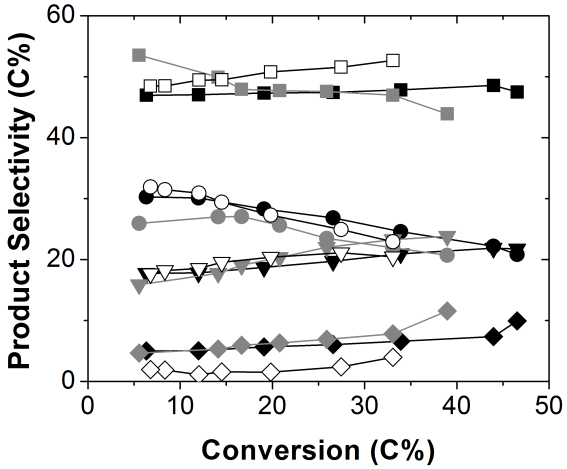

Figure 5.7: Product selectivity for the reaction of 70 kPa DME (WHSV=17.2 g $(g_{cat}\ h)^{-1}$) on H-SAPO-34 at 623 K with no co-feed (filled black symbols), 4.1 kPa of propene (filled gray symbols), and 5.3 kPa of 2-pentene (open black symbols); ● C_2, ■ C_3, ▼ C_4, and ◆ C_{5+}.

The effect of reaction temperature (548-723 K) on the selectivity of MTH conversion of H-SAPO-34 is shown in Figure 5.8. At both 548 and 623 K (Figure 5.8), product distributions for the reaction of 70 kPa DME over SAPO-34 are similar and the selectivity to propene is $1.4 - 2.4$ times higher than the selectivity to ethene. Additionally, selectivity to ethene increases from 25.1 to 32.5 C% at 548 K and from 20.8 to 30.3 C% at 623 K with increasing time-on-stream, and a corresponding decrease in the selectivity to C_{4+} hydrocarbons is observed with increasing times-on-stream, suggesting that C_{4+} hydrocarbons may be formed from ethene oligomerization reactions at short times-on-stream. The selectivity to propene, however, remains constant with time-on-stream at 548 and 623 K. At 723 K, the product selectivity remains relatively constant after 1 ks time-on-stream, after which, the selectivity to ethene is approximately the same as the selectivity to propene (37-44 C%), where as at lower temperatures, selectivity to propene was 1.4-2.4 times higher than the selectivity to ethene. Additionally, the ethene selectivity increases from 15.2 to 44.2 C% between 0.3 and 0.9 ks time-on-stream. A corresponding decrease in selectivity

to C_{4+} hydrocarbons is also observed between 0.3 and 0.9 ks time-on-stream. This rapid increase in ethene selectivity is most likely a result of fast deactivation of the catalyst, with conversion decreasing from 63.7 to 13.7 C% in the same time-on-stream interval. At all temperatures, increases in selectivity to ethene with a corresponding decrease in selectivity to C_{4+} hydrocarbons is observed at early times-on-stream, when the catalyst is the least deactivated.

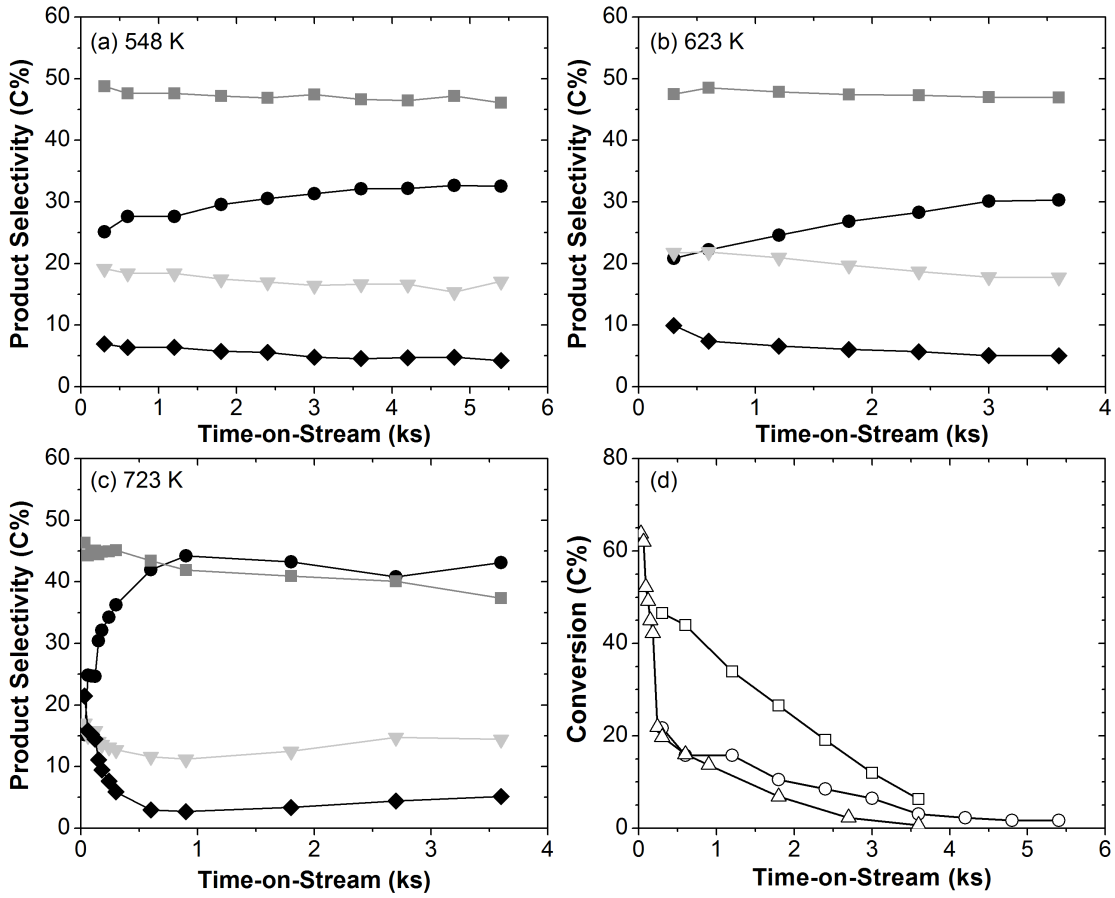

Figure 5.8: Product selectivity at (a) 548 K and WHSV=34.3 g_{DME} $(g_{cat}\ h)^{-1}$), (b) 623 K and WHSV=17.2 g_{DME} $(g_{cat}\ h)^{-1}$), and (c) 723 K and WHSV=86 g_{DME} $(g_{cat}\ h)^{-1}$) and (d) conversion for the reaction of 70 kPa DME on H-SAPO-34; ● C_2, ■ C_3, ▼ C_4, ◆ C_{5+}, ○ 548 K, □ 623 K, and ◇ 723 K.

Due to the rapid deactivation of the catalyst at 723 K for the reaction of 70 kPa DME over H-SAPO-34 (Figure 5.8d), additional reactions of DME at 723 K were performed and samples of the reaction effluent were collected at shorter intervals. Figure 5.9 shows the product selectivity and conversion for the reaction of DME over H-SAPO-34 at 723 K between 0 and 0.3 ks time-on-stream at WHSV of 86.2 and 327.6 g $(g_{cat}\ h)^{-1}$. At both space velocities, there are two different induction periods observed - one in which the conversion

increases and then remains relatively constant for 0.2 ks and another induction period in which ethene selectivity increases and then remains relatively constant after 0.1-0.2 ks time-on-stream. The ethene selectivity increases even during the 0.2 ks of steady-state DME conversion on H-SAPO-34, showing that the increase in ethene selectivity with time-on-stream shown in Figure 5.8 is not a result of only catalyst deactivation. Most likely, the aromatic hydrocarbon pool is changing even at constant conversion of DME, resulting in a changing ethene to propene selectivity.

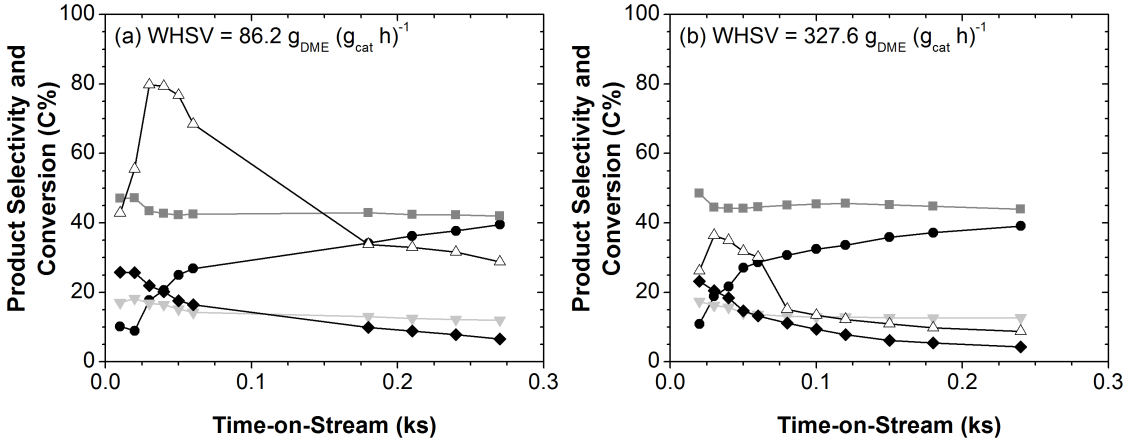

Figure 5.9: Product selectivity and conversion of the reaction of 70 kPa DME on H-SAPO-34 at 723 K, (a) WHSV=86.2 g $(g_{cat}\ h)^{-1}$) and (b) WHSV=327.6 g $(g_{cat}\ h)^{-1}$); ● C_2, ■ C_3, ▼ C_4, ◆ C_{5+}, and △ DME conversion.

5.4 Conclusions

The relative propagation of the olefin- and aromatic-based cycle on H-BEA could be tuned through the use of olefin and aromatic co-feeds. Under the conditions studied in this work, we show that by co-processing olefins or aromatics with DME, we can control the composition of the organic hydrocarbon pool and therefore its catalytic consequences for MTH selectivity on H-BEA. The addition of propene resulted in a four-fold increase in selectivity for C_3-C_7 aliphatics compared to the addition of 1,2,4-triMB at 623 K. By changing the ratio of olefins and aromatics in the co-feed, the selectivity of MTH over H-BEA can be systematically tuned at iso-conversion. The total ^{13}C-content of C_6-C_7 olefins matched the expected ^{13}C-content based on methylation of the $(n-1)$ olefin for the co-reaction of ^{12}C-DME with ^{13}C-propene on H-BEA. In contrast, the total ^{13}C-content of C_3-C_5 did not match the expected ^{13}C-content based on methylation of the $(n-1)$ olefin, showing that C_6-C_7 olefins are formed primarily from methylation reactions while C_3-C_5 olefins can be formed from cracking of larger olefins. For the co-reaction of ^{12}C-DME with

^{13}C-toluene on H-BEA, penta- and hexaMB have a significant fraction of isotopologues with fewer than seven ^{13}C-atoms compared to lower polyMBs, showing that larger polyMBs are more active than smaller polyMBs for aromatic dealkylation on H-BEA. Overall, the isotopic results show that C_3-C_5 olefins are cracking products and penta- and hexaMBs participate in the aromatic hydrocarbon pool on large-pore H-BEA, whereas our discussion in Chapter 3 showed that on medium-pore H-ZSM-5, C_3-C_4 olefins are cracking products and di-, tri-, and tetraMBs participate in the aromatic hydrocarbon pool. Isotopic switching experiments on show that the ^{13}C-content of C_2-C_7 olefins are similar while the ^{13}C-content of penta- and hexaMB are lower, suggesting that in the absence of an olefin or aromatic co-feed, the aromatic dealkylation does not contribute significantly to the product distribution of MTH on H-BEA.

On H-SAPO-34, the product selectivity of MTH conversion could not be tuned through the use of propene and 2-pentene co-feeds. For the reaction of DME alone H-SAPO-34, the propene/ethene selectivity decreased from 1.4-2.4 at 548 and 623 K to approximately 1 at 723 K. Additionally two separate induction periods are observed at short (<60 s) times-on-stream – one in which the conversion increases with increasing time on stream and a second in which the hydrocarbon pool evolves and a 3-fold increase in ethene selectivity is observed. The results in this chapter show that tuning the selectivity of MTH through the use of olefin and aromatic co-feeds is not unique to H-ZSM-5 – the selectivity on H-BEA can also be tuned. On H-SAPO-34, however, the selectivity of MTH could not be tuned, showing that the catalyst structure influences the ability to tune the selectivity of MTH.

5.5 Supplemental Information

5.5.1 Catalyst Characterization of H-BEA

Determination of the number of Brønsted Acid Sites

Chemical titration using dimethyl ether (DME) over the H-BEA sample used in this study was performed previously by Chiang et al.[136] in a tubular packed-bed quartz reactor (10 mm inner diameter) under atmospheric pressure. A mixture of DME/Ar/He (0.17 cm^3 s^{-1}; 24.9% DME, 25.1% Ar and 50% He; Praxair) was introduced by He (0.67 cm^3 s^{-1}, ultrapure, Minneapolis oxygen) during each pulse with 90s intervals. The physisorbed DME and water formed were subsequently removed by He (1.67 cm^3 s^{-1}) for 1.5 to 2.5 hours.

The DME uptake ratio per Al site for the sample of H-BEA used in this study was found to be 0.42.[136] Cheung et al.[61] showed that each Brønsted acid site in zeolites can adsorb 0.5 DME molecules because DME reacts with surface hydroxyl groups to form persistent methyl groups. Therefore, the concentration of Brønsted acid sites in the zeolite used in

this study is nearly identical to that inferred from the framework aluminum content in this material.

Nitrogen adsorption experiments

Nitrogen adsorption/desorption measurements for the H-BEA sample used in this work were previously carried out at 77 K on an Autosorb-1 analyzer (Quantachrome Instruments). Prior to the measurement, the sample was evacuated overnight at 573 K and 1 mm Hg. The specific surface area and the pore size distribution were calculated using the Brunauer Emmett Teller (BET) and BJH method, respectively. Conventional t-plot methods were also used for extracting micropore volume and external surface area from the nitrogen adsorption data over t ranges from 3 to 5 Å. The BET equation was used to calculate the BET specific surface area from the adsorption data obtained at P/P_0 between 0.1 and 0.3.

Table 5.2: Characterization information for the catalyst sample used in this study. Si/Al was determined from ICP-OES elemental analysis as performed by Galbraith Laboratories.

		BET surface	BET micropore	
	Si/Al	DME/Al	Area (m^2g^{-1})	volume (cc g^{-1})
H-BEA	12.0	0.42 [136]	579	0.19

X-ray diffraction pattern

The powder X-ray diffraction (XRD) pattern for the sample of H-BEA used in this work was collected on a Bruker AXS D5005 diffractometer using Cu- Kα radiation. Data were collected with a step size of 0.04° and a step time of 3 s. This diffraction pattern confirms the crystallinity and identity of the H-BEA sample used in this work (Figure 5.10).

5.5.2 Isotopic results for the co-reaction of ^{12}C-DME with ^{13}C-labeled toluene and propene

The isotopologue distribution of the co-reaction of ^{12}C-DME with ^{13}C-toluene and ^{12}C-propene (1:1 C) is shown in Figure 5.11. The isotopologue distribution of the co-reaction of ^{12}C-DME with ^{12}C-toluene and ^{13}C-propene (1:1 C) is shown in Figure 5.12. The isotopologue distributions of olefins for the co-reaction of ^{12}C-DME with ^{13}C-toluene is shown in Figure 5.13 and the aromatic isotopologue distribution for the co-reaction of ^{12}C-DME with ^{13}C-propene is shown in Figure 5.14.

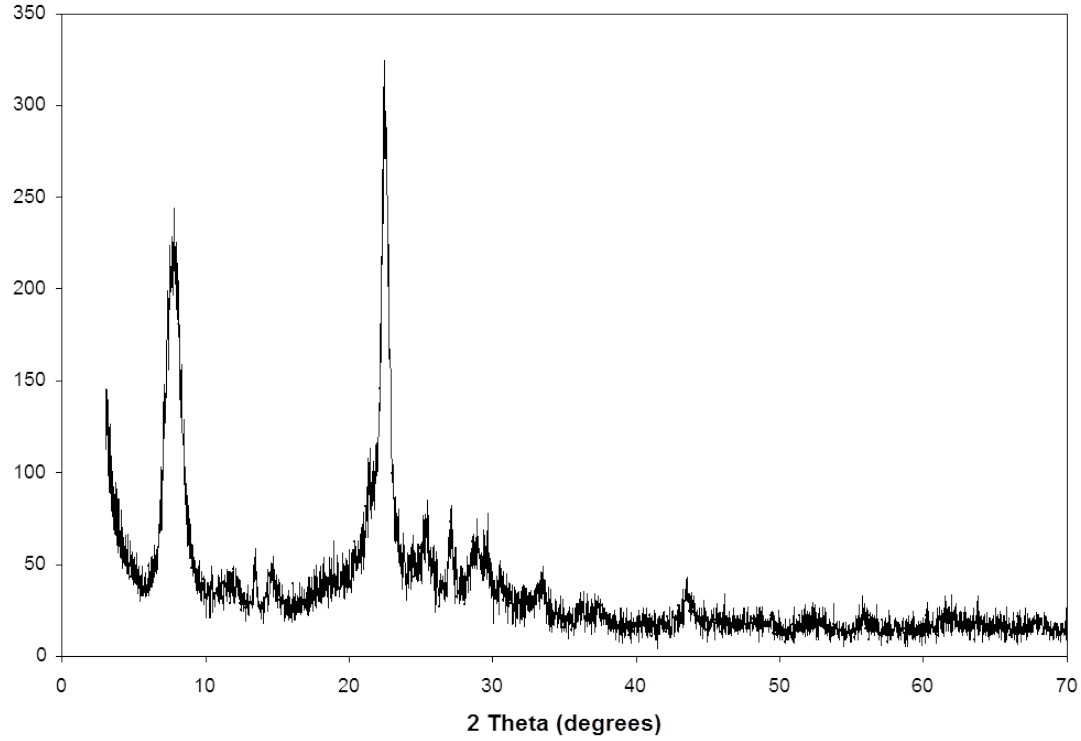

Figure 5.10: XRD pattern for H-BEA.

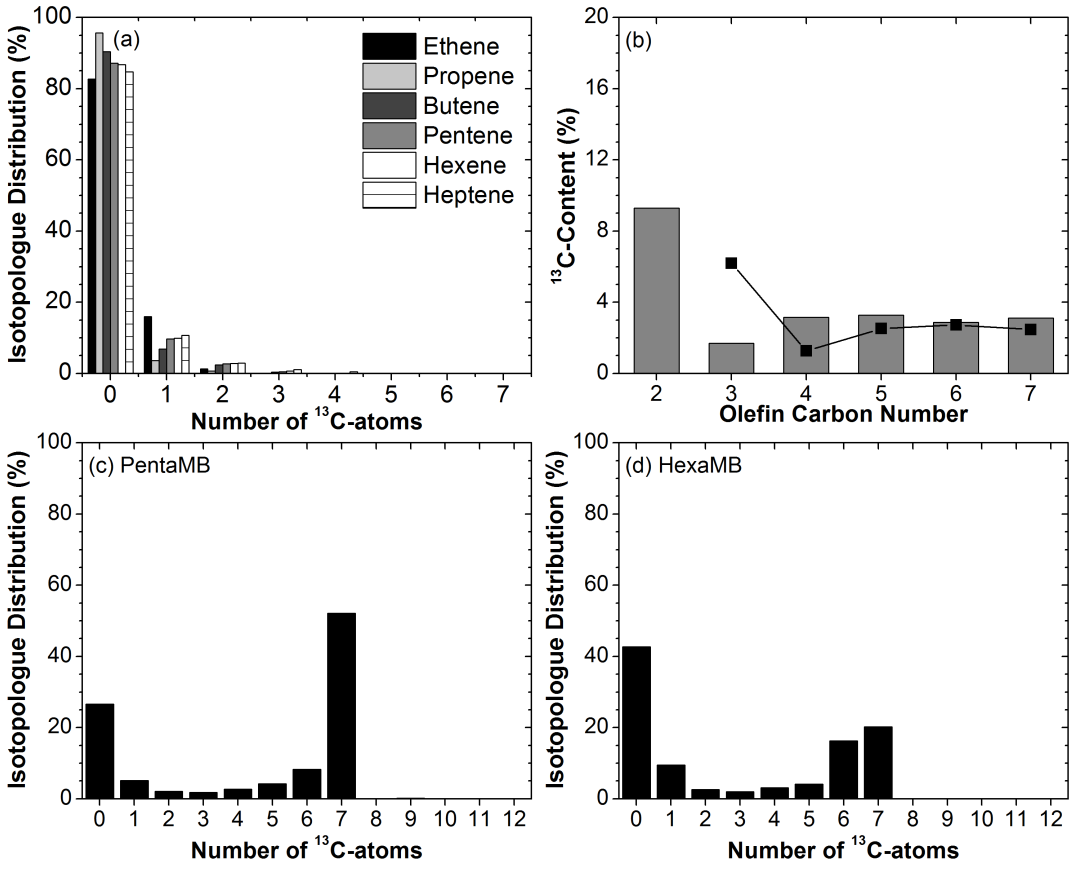

Figure 5.11: (a) Isotopologue distribution of olefins, (b) total ^{13}C-content of olefin, (c) isotopologue distribution of pentaMB, and (d) isotopologue distribution of hexaMB for the co-reaction of 70 kPa ^{12}C-DME with 1.3 kPa of ^{13}C-toluene and 2.8 kPa of ^{12}C-propene on H-BEA (Si/Al=12) at 623 K and WHSV$_{DME}$=96 g (g catalyst h)$^{-1}$; for (b) ■ experimentally observed ^{13}C-content and -■- expected ^{13}C-content of olefins based on methylation of the $(n-1)$ olefin.

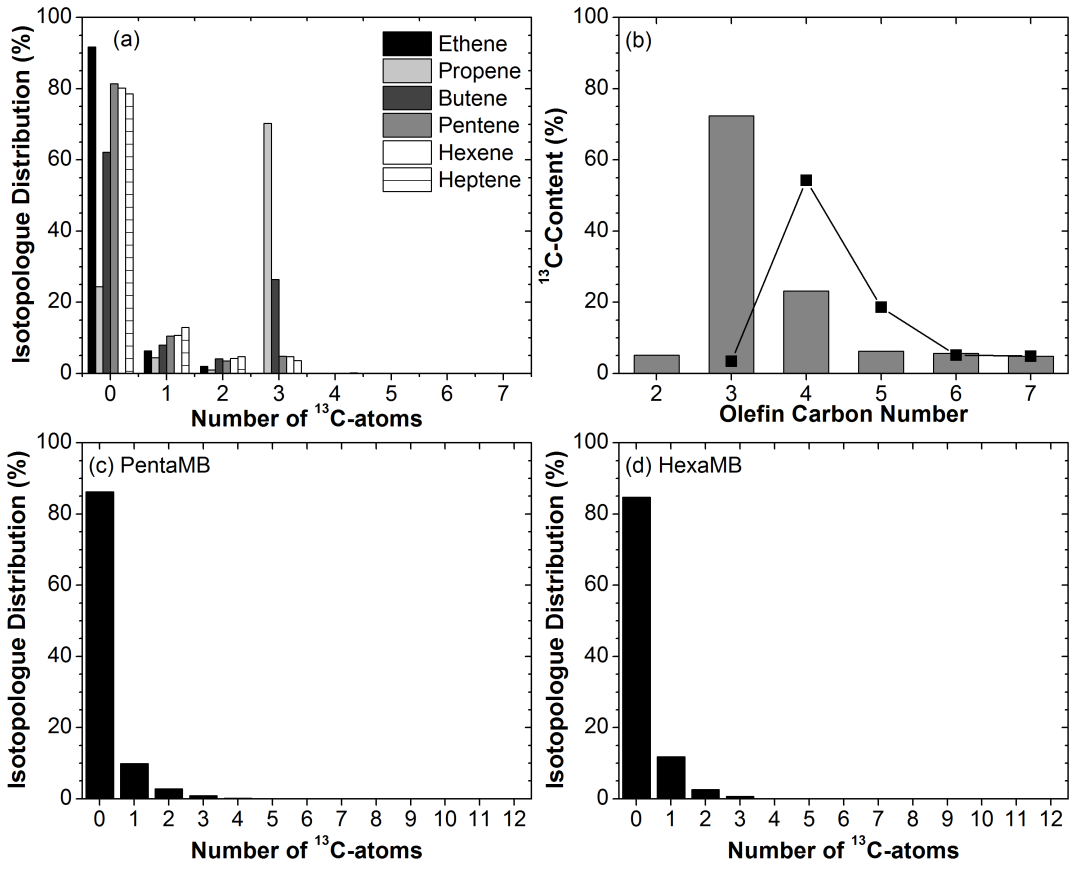

Figure 5.12: (a) Isotopologue distribution of olefins, (b) total ^{13}C-content of olefin, (c) isotopologue distribution of pentaMB, and (d) isotopologue distribution of hexaMB for the co-reaction of 70 kPa ^{12}C-DME with 1.3 kPa of ^{12}C-toluene and 2.8 kPa of ^{13}C-propene on H-BEA (Si/Al=12) at 623 K and WHSV$_{DME}$=96 g (g catalyst h)$^{-1}$; for (b) ■ experimentally observed ^{13}C-content and -■- expected ^{13}C-content of olefins based on methylation of the $(n-1)$ olefin.

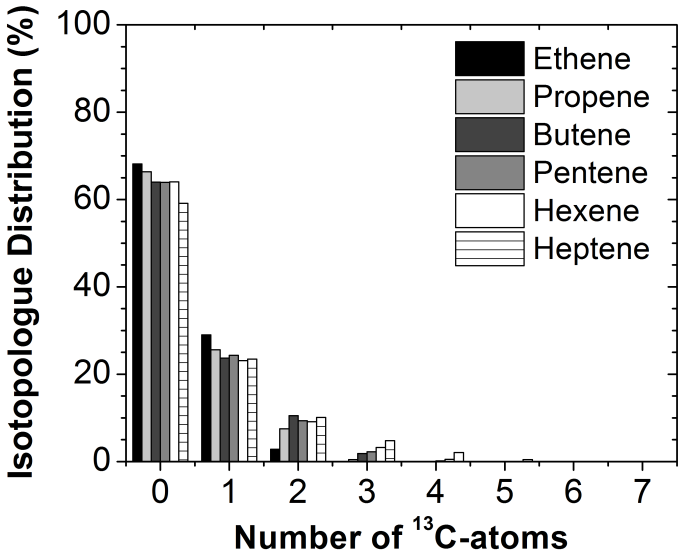

Figure 5.13: (a) Isotopologue distribution of olefins for the co-reaction of 70 kPa ^{12}C-DME with 4 kPa of ^{13}C-toluene on H-BEA (Si/Al=12) at 623 K and WHSV$_{DME}$=96 g (g catalyst h)$^{-1}$.

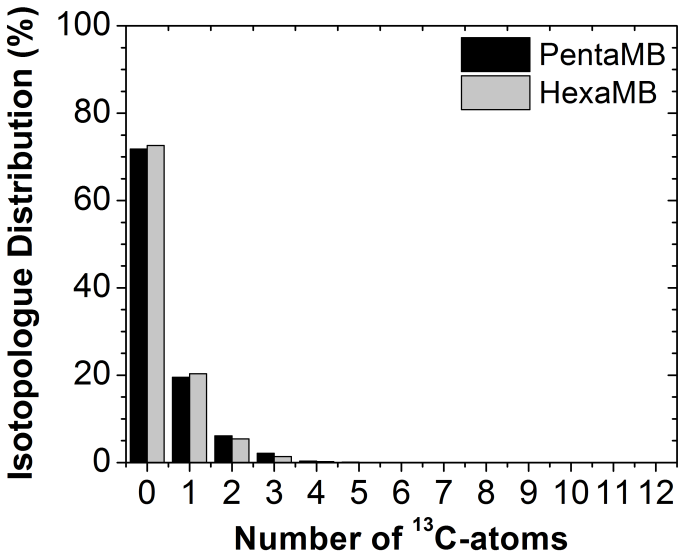

Figure 5.14: (a) Isotopologue distribution of penta- and hexaMB for the co-reaction of 70 kPa ^{12}C-DME with 4 kPa of ^{13}C-propene on H-BEA (Si/Al=12) at 623 K and WHSV$_{DME}$=96 g (g catalyst h)$^{-1}$.

5.5.3 Retained hydrocarbons on H-SAPO-34

The hydrocarbons retained within the catalyst were analyzed with GC-MS after 0.24 ks of reaction of 70 kPa DME (327.6 g $(g_{cat}\ h)^{-1}$) over H-SAPO-34. After 0.24 ks, the reactor was quenched to room temperature with liquid nitrogen at a rate of approximately 75 K s^{-1}. The catalyst was removed from the reactor and dissolved in a 1-mL aqueous solution of 15 wt% HF. After 1 hour, 1 mL of CH_2Cl_2 was added to extract the dissolved organic material from the aqueous phase. The organic phase was then analyzed with GC-MS. The GC chromatogram showed that variety of polyMB and polymethylnapthalenes were retained on the catalyst (Figure 5.15).

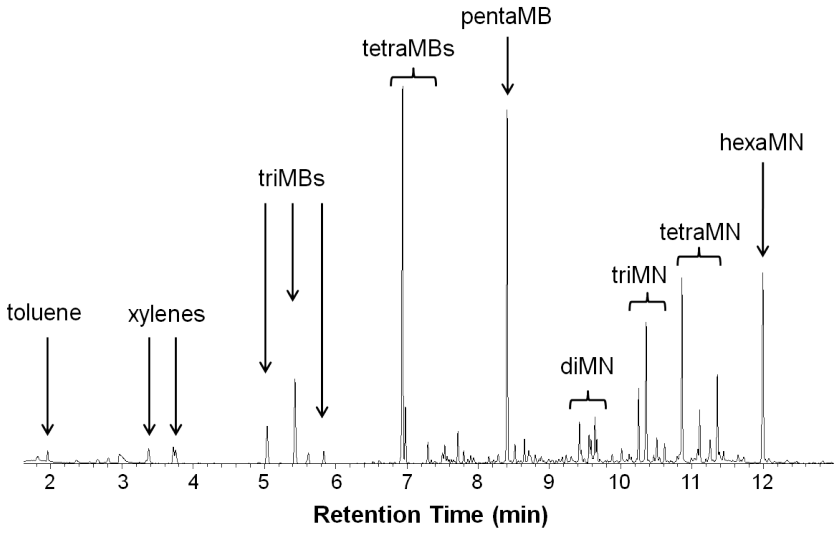

Figure 5.15: GC chromatogram of retained hydrocarbons in SAPO-34 after 4 minutes of reaction with 70 kPa DME on H-SAPO-34 at 723 K and WHSV=328 g $(g_{cat}\ h)^{-1}$.

CHAPTER

SIX

THE MECHANISM OF AROMATIC DEALKYLATION IN METHANOL-TO-HYDROCARBONS CONVERSION ON H-ZSM-5

6.1 Introduction

The conversion of methanol over acid zeolite catalysts to a wide variety of hydrocarbons, including gasoline-range hydrocarbons (methanol-to-gasoline, MTG) and light olefins (methanol-to-olefins, MTO) has been extensively studied because methanol can be produced from any carbon-based feedstock, such as natural gas, coal, and biomass, via a syngas ($CO+H_2$) intermediate.[13–15] Methanol-to-hydrocarbons (MTH) proceeds through an indirect mechanism, known as the hydrocarbon pool mechanism, in which hydrocarbon formation occurs through repeated methylation and cracking of olefins and aromatics entrained within the zeolite pores.[16–18,29] Isotopic switching experiments in which a ^{12}C-methanol feed is switched with a ^{13}C-methanol feed during steady-state reaction on H-ZSM-5 at 623 K have shown that after the switch the ^{13}C-incorporation of ethene matched that of methylbenzenes (MBs), while the ^{13}C-incorporation of C_{3+} olefins matched each other.[19,20] This result showed that two different catalytic cycles are at work on H-ZSM-5, one involving ethene and polymethylbenzenes (polyMBs) and another involving C_{3+} olefins. Similar work has also been done on other zeolite and zeotype frameworks, either showing the presence of both cycles or showing the dominance of one cycle over another.[42–45] Isotopic experiments on H-ZSM-5, H-BEA, and H-MOR in which methanol/dimethyl ether (DME) is co-reacted with aromatics have also shown that ethene and propene contain carbon atoms originating from the aromatic co-feed.[39,40,89] While these results show that both ethene and propene are mechanistically linked to polyMBs, the mechanism of aromatic dealkylation to form light olefins is still debated.

Experimental and theoretical work have postulated that light olefin formation from polyMBs occurs through a paring, side-chain, or ring expansion mechanism (Figure 6.1 and

Figure 6.2). The paring mechanism, first proposed by Sullivan et al.[113] for the hydrocracking of hexaMB on a nickel sulfide catalyst, is initiated by gem-methylation of a MB which is followed by ring contraction to a 5-membered ring. As a result, an alkyl group is formed, which can subsequently crack to form propene or isobutene, containing one aromatic ring carbon. Arstad et al.[137] proposed a ring expansion mechanism for ethene and propene formation from heptamethylbenzenium. Similar to the paring mechanism, the ring expansion mechanism is also initiated by gem-methylation of a polyMB and the eliminated olefin contains one aromatic ring carbon. Experimental work form Bjørgen et al.[90] in which ^{13}C-methanol is co-reacted with ^{12}C-benzene on H-BEA reported that at 543 K at least 50% of propene and isobutane (coming from isobutene) molecules contained one ^{12}C-atom, showing that an aromatic ring carbon is incorporated into light olefins. Similar experiments by Erichsen et al.[138] at 523 K on H-SAPO-5 showed that at least 60% of ethene and propene molecules also contained one ^{13}C-atom. Although the incorporation of an aromatic ring carbon into light olefins show that on these large-pore catalysts at low temperatures, aromatic dealkylation occurs via either a paring or ring-expansion mechanism, the experimental results reported by Bjørgen et al. and Erichsen et al. did not distinguish between the two mechanisms and the mechanism of aromatic dealkylation was not discernible for similar isotopic experiments on H-BEA at 330 K.[90,138]

The side-chain mechanism is also initiated by gem-methylation of a MB, however, in this mechanism gem-methylation is followed by deprotonation and results in the formation of an exo-cyclic double bond. The exo-cyclic double bond can then undergo side-chain methylation to form a side-chain that can crack to form ethene or propene. Work by Sassi et al.[120] at 723 K on H-BEA shows that pulse reactions of ^{13}C-methanol with various ^{12}C-MBs result in ethene and propene having similar ^{13}C-contents as the overall ^{13}C-content of the methanol and aromatic methyls in the feed, suggesting that olefin formation at these conditions occurs via a side-chain mechanism. Reactions of ^{13}C-methanol with ^{12}C-ethyl, propyl, and butylbenzenes on H-BEA at 623 K produced high fractions (<50%) of completely ^{12}C-labeled ethene, propene, and butenes, respectively[120,121] While the high fractions of completely ^{12}C-labeled olefins show that the side-chain mechanism does occur under conditions where aromatics with C_{2+} alkyl groups are co-fed with methanol, it is unclear to what extent the side-chain mechanism contributes to olefin formation under typical MTH conditions where the majority of aromatics are methylbenzenes.[44] Work by Sassi et al. at temperatures above 623 K on H-BEA suggest that the side-chain mechanism is occurring while work by Bjorgen et al. at temperatures below 573 K suggest that either the paring or ring expansion mechanism contribute to olefin formation. These results are reconcilable if a change in the dealkylation mechanism occurs with temperature.

Theoretical studies by McCann, Lesthaeghe, and co-workers[98] using ONIOM methods

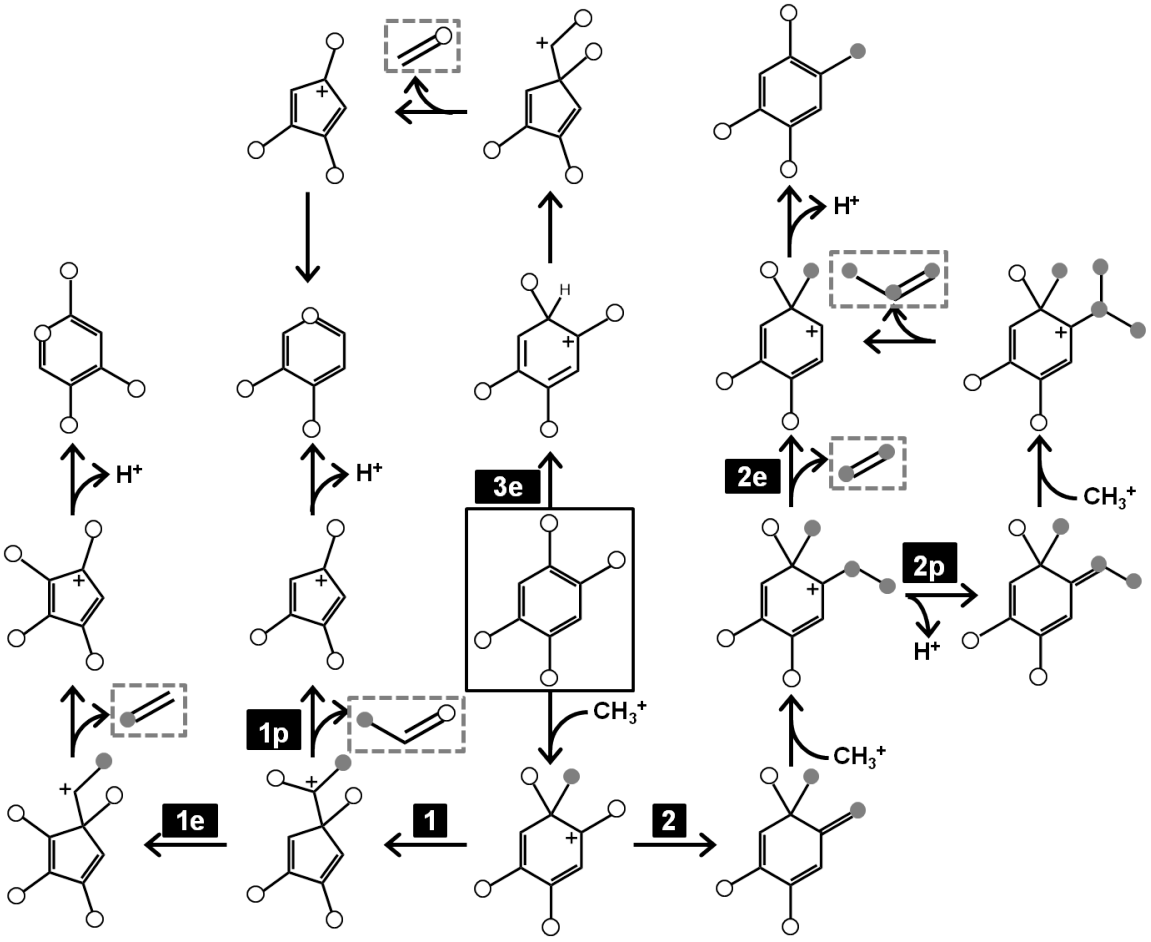

Figure 6.1: Several mechanisms have been proposed for ethene and propene formation from MBs. The paring mechanism for ethene (1e) and propene (1p) formation from 1,2,4,5-tetraMB is shown in path 1. The side-chain mechanism for ethene (2e) and propene (2p) formation from 1,2,4,5-tetraMB is shown in path 2. Path 3e shows an alternative paring-type mechanism for ethene formation from 1,2,4,5-tetraMB that only requires protonation, not methylation; - aromatic ring carbon, ○ aromatic methyl carbon, and ● methyl carbon from DME/methanol.

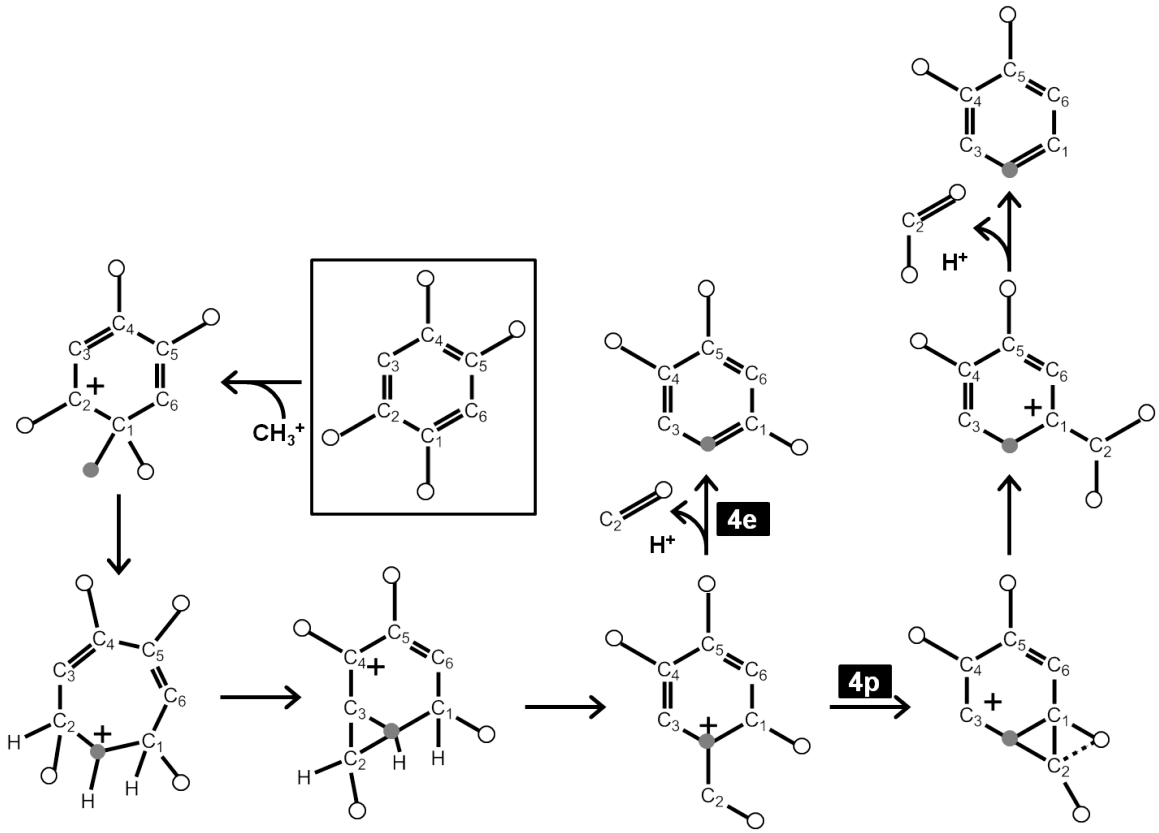

Figure 6.2: Ring expansion mechanism for ethene (4e) and propene (4p) formation; - aromatic ring carbon, ○ aromatic methyl carbon, and ● methyl carbon from DME/methanol

on 46T clusters of H-ZSM-5 show that the highest barriers for isobutene formation from toluene are aromatic methylation steps (E_a=150-162 kJ mol^{-1}). Lesthaeghe et al.[11] investigated the side-chain mechanism for ethene formation from *o*-xylene on 46T clusters of H-ZSM-5 using ONIOM methods and found that the ethene elimination step had the highest barrier (E_a≈200 kJ mol^{-1}). The high barrier to ethene elimination led Lesthaeghe et al.[11] to hypothesize that side-chain may grow longer to eliminate propene or may eventually cause deactivation of the catalyst. Additionally, Seiler et al.[139] used *in situ* ^{13}C-NMR for the continuous flow reaction of ^{13}C-methanol followed by a switch to ^{12}C-methanol on H-ZSM-5 at 548-573 K and observed that the peak at 10-30 ppm decreased by 40% after the switch. This range in chemical shift was assigned to alkyl groups on aromatics and therefore, this 40% reduction in peak area was attributed to olefin formation via the side-chain mechanism. Alternatively, the 10-30 ppm region can also be assigned to methyl groups on aromatics,[106] hence, the paring, side-chain, and ring expansion mechanism are all consistent with the peak reduction following a switch to ^{12}C-methanol. While theoretical work suggests that barriers to aromatic dealklylation are lower for the paring mechanism on H-ZSM-5, experimental evidence has not been able to distinguish between the different aromatic dealkylation mechanisms on this zeolite.

Understanding the mechanism of aromatic dealkylation to form light olefins in MTH is key to understanding how ethene and propene selectivity can be controlled. In this work, we use the effluent isotopologue distributions of 1,2,4-triMB and 1,2,4,5-tetraMB for the co-reactions of DME with toluene, p-xylene, and 4-ethyltoluene, where either DME or the aromatic co-feed are labeled with ^{13}C-atoms, on H-ZSM-5 at 523-723 K to predict the ^{13}C-contents of ethene and propene based on the paring, side-chain, and ring expansion mechanisms. The predicted ^{13}C-content of ethene and propene from the paring mechanism mostly closely matches the experimentally observed ^{13}C-content of ethene and propene, showing for the first time that aromatic dealkylation in MTH converison on H-ZSM-5 occurs through the paring mechanism at 523-723 K.

6.2 Materials and Methods

6.2.1 Catalyst Preparation

The catalyst, H-ZSM-5 (CBV8014), Si/Al=42.6, was obtained in the ammonium form from Zeolyst International. Structural and chemical characterization of the commercial H-ZSM-5 sample used in this study is reported in Section 3.5.1. The silicon to aluminum ratio of the commercial H-ZSM-5 sample was determined by ICP-OES elemental analysis (performed by Galbraith Laboratories). The ammonium-form zeolite was sieved to obtain aggregate particle sizes between 180 and 425 μm (40-80 mesh) and treated in 1.67 cm^3 s^{-1} of dry air

(20-21% O_2, <10 ppm H_2O, Minneapolis Oxygen) at 773 K for 4 hours (heating rate of 0.0167 K s^{-1}) to convert it to the proton-form zeolite. The catalyst was pre-treated in-situ in 1.67 cm^3 s^{-1} of helium flow (99.995% purity, Minneapolis Oxygen) at 773 K overnight using a heating rate of 0.0167 K s^{-1} prior to reaction.

6.2.2 Catalytic reactions of DME with aromatic co-feeds over H-ZSM-5

A stainless steel packed bed reactor (0.25 in o.d.; 0.215 in i.d.) equipped with a concentric thermal well (0.0625 in o.d.; 0.0485 in i.d.) aligned along the tube center was used for the conversion of DME. The catalyst bed was supported between quartz wool plugs and operated at isothermal conditions using an ARI heating coil regulated by a Watlow Temperature Controller (96 Series). Reactions were performed using 10 mg of catalyst mixed with approximately 0.15 g of quartz sand at 523 K with either $^{12}C_2$- or $^{13}C_2$-DME at 7.5-9.3 kPa ($^{12}C_2$-DME from Matheson Tri-Gas, 99.5% purity; $^{13}C_2$-DME from Aldrich Chemistry, 99% ^{13}C-atom purity; 0.024-0.030 cm^3 s^{-1}) with 4 kPa of an aromatic co-feed and a balance of helium so that the total feed flowrate was 0.417 cm^3 s^{-1}. The aromatic co-feeds used were $^{12}C_8$-p-xylene (Sigma Aldrich, ≥99% purity), $^{13}C_2$-p-xylene where the ^{13}C-atoms were on the methyl groups (Isotec, 99% ^{13}C-atom purity), $^{12}C_7$-toluene (Sigma Aldrich, ≥99.9% purity), and $^{12}C_9$-4-ethyltoluene (Fluka Analytical, ≥95.0% purity). ^{13}C NMR was performed on the p-xylene sample from Isotec to confirm that the ^{13}C-atoms were located only on the methyl carbons (Section 6.5.1 of the Supplemental Information). The aromatic co-feeds were fed as a liquid using a Cole Parmer EW-74900-00 syringe pump at rates of 0.61, 0.67, and 0.72 μL s^{-1} for toluene, p-xylene, and 4-ethyltoluene, respectively. Heat traced lines (423 K) were used to transfer the aromatic co-feed to the reactor and the reactor effluent to a gas chromatograph-mass spectrometer (GC-MS, Agilent 7890-5975C) equipped with a methyl-siloxane capillary column (HP-1, 50.0 m × 320 μm × 0.52 μm) connected to a flame ionization detector and a 5% diphenyl, 95% methyl-siloxane capillary column (HP-5, 50.0 m × 320 μm × 0.52 μm) connected to a mass spectrometer. The total pressure of the reactor was 130 kPa. Similar reactions were also performed at 623 K and 723 K, using 0.5 and 0.1 mg of catalyst, respectively, diluted in approximately 150 mg of quartz sand. Isotopologue distributions were determined from mass fragmentation patterns using the method outlined by Price and Iglesia.

6.2.3 Predicting ^{13}C-content of ethene and propene from aromatics

In Section 6.1, three different proposed mechanisms for aromatic dealkylation in MTH were discussed and these mechanisms are examined in this work. For both the side-chain mechanism and the ring expansion mechanisms, routes for ethene and propene formation have been previously proposed.[39,120,137] For the paring mechanism, however, only routes for

propene and isobutene formation have been proposed.[90,113] Arstad et al. also performed calculations involving free carbocations investigating if a paring mechanism depicited in 3e of Figure 6.1 was possible, but determined that the secondary carbenium ion formed was not stable, and therefore this mechanism will not form ethene.[140] Recent work from Erichsen et al.[138] on the co-reaction of ^{13}C-methanol with ^{12}C-benzene on SAPO-5 shows that 60% of the ethene produced contains one ring carbon, which is consistent with the ring expansion mechanism or a paring-type mechanism. We propose mechanism 1e (Figure 6.1) to account for the possibility of ethene coming from a paring-type mechanism. In mechanism 1e, a methyl from the isopropyl group on the 5-membered ring shifts to the ring accompanied by a simultaneous hydrogen shift from the ring to the isopropyl group. Note that in this mechanism, ethene should always contain one ring carbon, but the other carbon may come from either methyl carbon on the isopropyl group.

In this work, multiple dealkylation mechanisms for ethene and propene formation are compared to determine which mechanism best fits the experimentally observed ^{13}C-content of ethene and propene based on the effluent isotopic composition of 1,2,4-trimethylbenzene, 1,2,4,5-tetramethylbenzene, and 4-ethyltoluene. The ^{13}C-content of aromatic ring carbons and methyl carbons must be known to correlate the ^{13}C-content of these aromatic precursors to that of ethene and propene. To determine the ^{13}C-content of the ring and methyl carbons, we assume that methyl carbons on aromatics are the first to incorporate DME carbons. For a particular MB with a total of t methyl groups, m_i is the number of ^{13}C methyl carbons, and r_i is the number of ^{13}C ring carbons in a particular isotopologue of the MB with i ^{13}C-atoms. For $i \leq t$, $m_i = t$ and $r_i = 0$. For $i > t$, $m_i = t$ and $r_i = i - t$. If the overall fraction of the the aromatic species with i ^{13}C-atoms is x_i, then the total ^{13}C-content of the methyl groups (^{13}M) is

$$\frac{\sum_{i=0}^{t+6} m_i x_i}{t}, \tag{6.1}$$

and the total ^{13}C-content of the ring carbons (^{13}R) is

$$\frac{\sum_{i=0}^{t+6} r_i x_i}{6}. \tag{6.2}$$

This method is also used to calculate the ^{13}C-content of the ring carbons and the exocyclic carbons for 4-ethyltoluene. In the specific case of 4-ethyltoluene, ^{13}M is the total ^{13}C-content of methyl and ethyl carbons.

Based on the four mechanisms for ethene formation (1e,2e,3e, and 4e) and the three mechanisms for propene formation (1p, 2p, 4p) shown in in Figure 6.1 and Figure 6.2 and the effluent isotopologue distributions for the three aromatic precursors, the ^{13}C-contents for ethene and propene can be predicted. The prediction depends on both the mechanism and

the aromatic precursor. For example, 4-ethyltoluene, if protonated, has the same structure as an intermediate of the side-chain mechanism and the ring expansion mechanism. Therefore, in both these mechanisms, the predicted ^{13}C-content of ethene from 4-ethyltoluene would simply be ^{13}M, the overall ^{13}C-content of the exocyclic carbons in 4-ethyltoluene. In the ring expansion mechanism, the ^{13}C-content of ethene will depend on which methyl in the gem-methyl group is inserted into the 7-membered ring as well as if there is a methyl group ortho to the gem-methyl group. The equations used for the predicted ^{13}C-contents of ethene and propene for each of the aromatic precursors and mechanisms examined in this work are summarized in Table 6.1, where ^{13}D is the fraction of ^{13}C-atoms in the methylating agent (DME or methanol). The absolute error for the predicted ^{13}C-content of the olefin formed ($^{13}C_{pred}$) compared to the experimentally observed ^{13}C-content of the olefin formed ($^{13}C_{obs}$)is

$$|^{13}C_{obs} - ^{13}C_{pred}|, \tag{6.3}$$

and the relative error is

$$\frac{|^{13}C_{obs} - ^{13}C_{pred}|}{^{13}C_{obs}}. \tag{6.4}$$

Table 6.1: Models used to predict the ^{13}C-content of olefins formed from 1,2,4-triMB, 1,2,4,5-tetraMB, and 4-ethyltoluene via different aromatic dealkylation mechanisms.

		Olefin Formed:	
Mechansism	**Aromatic Precursor**	**Ethene (e)**	**Propene (p)**
Paring 1	All	$\frac{^{13}M+^{13}D+2^{13}R}{4}$	$\frac{^{13}M+^{13}D+^{13}R}{3}$
Side Chain 2	1,2,4-tri- & 1,2,4,5-tetraMB	$\frac{^{13}M+^{13}D}{2}$	$\frac{^{13}M+2^{13}D}{3}$
	4-ethyltoluene	^{13}M	$\frac{2^{13}M+^{13}D}{3}$
Paring 3	All	$\frac{^{13}M+^{13}R}{2}$	–
Ring Exp. 4	1,2,4-triMB	$\frac{7^{13}M+5^{13}D+12^{13}R}{24}$	$\frac{3^{13}M+^{13}D+2^{13}R}{6}$
	1,2,4,5-tetraMB	$\frac{5^{13}M+3^{13}D+8^{13}R}{16}$	$\frac{3^{13}M+^{13}D+2^{13}R}{6}$
	4-ethyltoluene	^{13}M	$\frac{2^{13}M+^{13}D}{3}$

6.3 Results and Discussion

Three different isotopic feed compositions of 4 kPa of toluene, p-xylene, and 4-ethyltoluene were co-reacted with 7.5-9.3 kPa of ^{13}C-DME in which the number of ^{12}C-methyls on the aromatic feed was varied:

1. $^{13}C_2$-p-xylene: 0 ^{12}C-aromatic methyls
2. $^{12}C_7$-toluene: 1 ^{12}C-aromatic methyl
3. $^{12}C_8$-p-xylene: 2 ^{12}C-aromatic methyls
4. $^{12}C_8$-4-ethyltoluene: 1 ^{12}C-aromatic methyl and 1 ^{12}C-aromatic ethyl

Reaction 3 and 4 were also performed at higher temperatures (623 K-723 K). Additionally, $^{13}C_2$-p-xylene was co-reacted with ^{12}C-DME at 523 K so that the only ^{13}C-methyls were the two methyls on p-xylene. The total carbon converted in these experiments was less than 10 C% for all reactions. For all the reactions performed, at 1 minute time-on stream, ethene, propene, and C_{8+} hydrocarbons accounted for 90-96% of the products formed, indicating that olefin methylation and cracking were suppressed. Unless otherwise specified, all results shown in this work were collected at 1 minute time-on-stream. While results at 1 minute time-on-stream may still be in the induction period for MTO, the isotopologue distributions for the aromatic precursors examined at this time-on-stream contain fewer DME carbons incorporated into the aromatic ring compared to later times-on-stream. It is important to minimize the incorporation of DME carbons into the aromatic rings because it is unlikely that the incorporation of DME and aromatic methyl carbons into the ring is random. The models used for predictions of the ^{13}C-contents of ethene and propene, however, assume that ^{13}C-atoms in the aromatic ring follow a statistical distribution, and therefore, only isotopic results at 1 minute-time-on-stream are used.

6.3.1 Aromatic dealkylation mechanisms for ethene formation

Co-reaction of ^{13}C-DME with $^{13}C_2$-p-xylene at 523 K

A major observable difference distinguishing the side-chain mechanism from either the paring or ring expansion mechanisms for aromatic dealkylation reactions is that the paring and ring expansion mechanisms result in the incorporation of an aromatic ring carbon into the olefin formed whereas the side-chain mechanism only incorporates aromatic methyl carbons and carbons from the methylating agent (DME or methanol) into the olefin formed. In the reaction of ^{13}C-DME with $^{13}C_2$-p-xylene, all methyl carbons in the feed are ^{13}C-labeled and aromatic ring carbons in the feed are ^{12}C-atoms. For this reaction at 523 K, both 1,2,4-triMB and 1,2,4,5-tetraMB are predominantly methylation products of $^{13}C_2$-p-xylene and

the majority of ethene (64%) contains 1 ^{13}C-atoms (Figure 6.3), indicating that a majority of ethene contains only 1 aromatic ring carbon, which is consistent with paring mechanisms 1e, 3e, and the ring expansion mechanism 4e in Figure 6.1. Additionally, even though 93% of triMB and 86% of tetraMB are all methylation products (containing only 3 and 4 ^{13}C-atoms, respectively), there is a significant fraction of ethene isotopologues that contain 2 ^{12}C-atoms (17%) or all ^{13}C-atoms (19%, Figure 6.3). This suggests that there may be some scrambling between the ring and methyl carbons that is independent of dealkylation or that the side-chain mechanism may contribute to the fraction of all ^{13}C-ethene.

Isotopic co-reactions of DME with p-xylene and toluene at 523 K

Both proposed paring mechanisms (1e and 3e in Figure 6.1) and the ring expansion mechanism (4e in Figure 6.1) for ethene incorporate an aromatic ring carbon into ethene. These mechanisms differ in how they incorporate methyl carbons, either from the methylating agent or from the aromatic. For the paring 1e mechanism, there is an equal probability of one carbon in ethene coming from a DME carbon or from a methyl carbon on already on the aromatic. For the ring expansion mechanism, the probability of containing an aromatic methyl carbon or a DME carbon depends on the aromatic precursor; for 1,2,4-trimethylbenzene 7/12 ethene molecules should contain one carbon from aromatic methyls and 5/12 ethene molecules should contain one carbon from DME and for 1,2,4,5-tetraMB, 5/8 ethene molecules should contain one carbon from aromatic methyls and 3/8 ethene molecules should contain one carbon from DME. In the paring 3e mechanism, all ethene molecules should contain one carbon originating from aromatic methyls. To distinguish between these three mechanisms, ^{13}C-DME was co-reacted with toluene or p-xylene containing 0-2 ^{12}C-methyl groups and all ^{12}C-aromatic rings at 523 K. Additionally, $^{13}C_2$-p-xylene was co-reacted with ^{12}C-DME so that the only ^{13}C-atoms present in the reaction were from methyl groups on the p-xylene feed. At these conditions, the majority of 1,2,4-triMB and 1,2,4,5-tetraMB isotopologues were methylation products of the aromatic co-feed (Figure 6.3). As the number of ^{12}C-methyls groups on the aromatic co-feed increased, the fraction of ethene containing only 1 ^{13}C decreased and concurrently the fraction of ethene containing 0 ^{13}C-atoms increased, showing that the aromatic methyl groups are incorporated into ethene (Figure 6.3). For these reactions at 523 K, both the mean absolute and relative errors for ethene coming from 1,2,4-trimethylbenzene, 1,2,4,5-tetraMB, and 4-ethyltoluene via the paring 1e mechanism were the lowest compared to the other mechanisms (Figure 6.10 in the Supplemental Information).

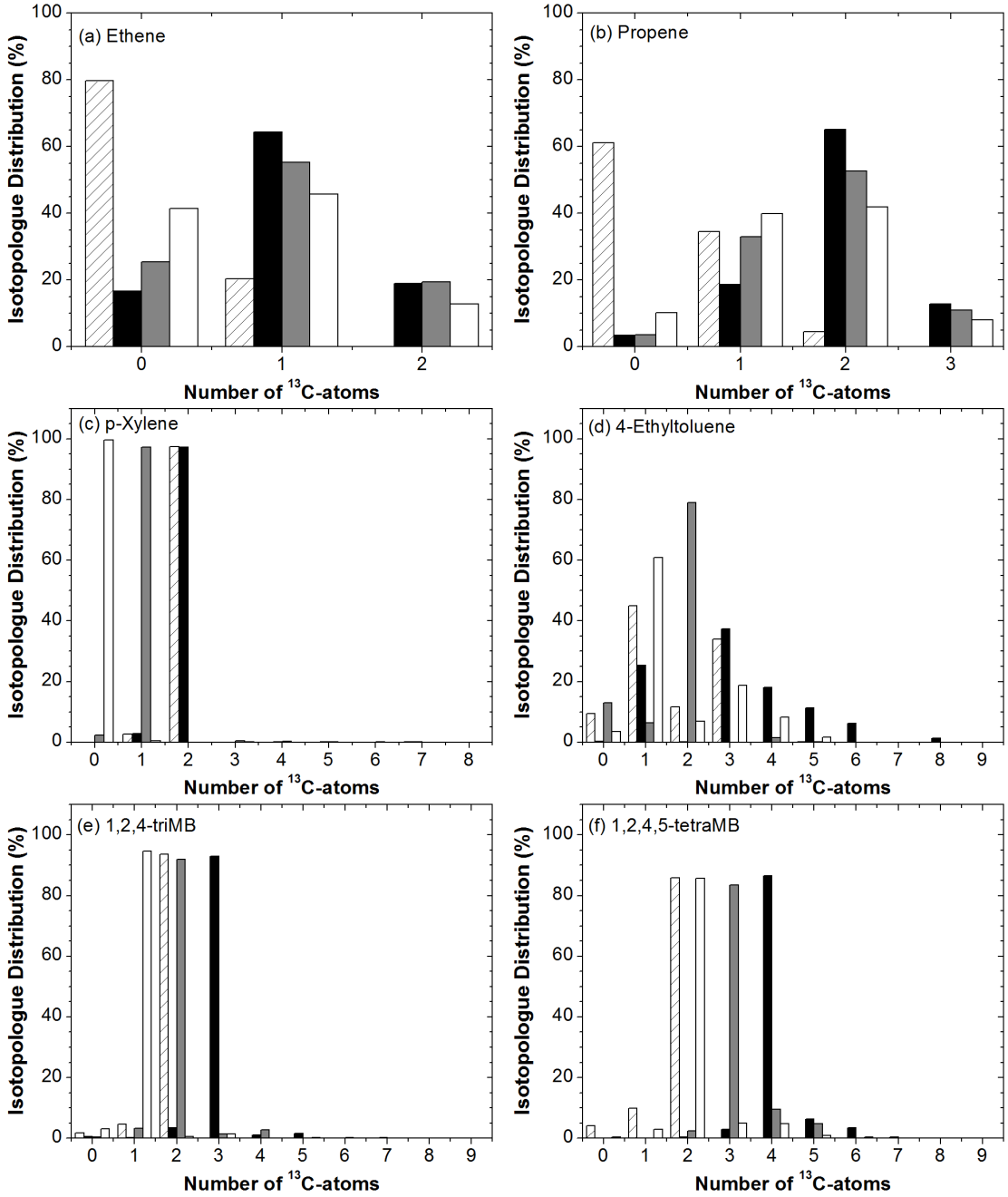

Figure 6.3: Isotopologue distributions for the co-reaction of ▨ ^{12}C-DME with $^{13}C_2$-p-xylene, ■ ^{13}C-DME with $^{13}C_2$-p-xylene, ■ ^{13}C-DME with $^{12}C_7$-toluene, and □ ^{13}C-DME with $^{12}C_8$-p-xylene at 523 K for (a) ethene, (b) propene, (c) p-xylene, (d) 1,2,4-triMB, (e) 4-ethyltoluene, and (f) 1,2,4,5-tetraMB.

Effect of temperature on the mechanism of ethene formation

For the co-reaction of ^{13}C-DME with $^{13}C_2$-p-xylene, increasing the reaction temperature from 523 K to 723 K, the fraction of ethene containing only one aromatic ring carbon (^{12}C) decreases from approximately 65% to 50% (Figure 6.4). Concurrently, the ^{13}C-content of both 1,2,4-triMB and 1,2,4,5-tetraMB increases by approximately 10 percentage points with the 200 K increase in temperature (Figure 6.4). The co-reaction of ^{13}C-DME with $^{12}C_8$-p-xylene was also performed at 623 K. For the reaction conditions used at 623 K, only 35% of ethene contained 1 ^{13}C-atoms and 44% contained all ^{13}C-atoms (Figure 6.12 in the Supplemental Information). Aromatics at 623 K also showed increased ^{13}C-contents compared to 523 K (Figure 6.12). When the error for the model predictions of the co-reaction of ^{13}C-DME with $^{13}C_2$-p-xylene at 723 K and ^{13}C-DME with ^{12}C-p-xylene at 623 K are included in the error calculations, the overall results do not differ qualitatively from those for the reactions at 523 K only. For all the reactions in which p-xylene or toluene were used as co-feeds, the mean absolute and relative errors for ethene from 1,2,4-triMB, 1,2,4,5-tetraMB and 4-ethyltoluene are the lowest for the paring 1e mechanism (Table 6.2). Despite the overall increase in the fractions of 1,2,4-tri- and 1,2,4,5-tetraMB that are not methylation products of the aromatic co-feed and decrease in the fraction of ethene containing only 1 ^{13}C-atom, the model predictions show that there is no change in the aromatic dealkylation mechanism for ethene formation over a 200 K temperature change. This is the first time that it has been experimentally shown that the mechanism of aromatic dealklylation does not change over a 200 K temperature range and at commercial operating temperatures for MTO.

Parity plots of the the different dealkylation mechanisms comparing the experimentally observed ^{13}C-content of ethene to the predicted ^{13}C-content of ethene from 1,2,4-tri-, 1,2,4,5-tetraMB, and 4-ethyltoluene from the different aromatic dealkylation mechanisms are shown in Figure 6.5. For the parity plots for ethene formation, results are only shown for the reactions in which in toluene or p-xylene were used co-feeds at temperatures from 523 K and 723 K. The effect of 4-ethyltoluene co-feeds on ethene and propene formation will be discussed in section 6.3.3. Based on Figure 6.5 and the mean absolute and relative errors shown in Table 6.2, it is clear that ethene is formed from the paring 1e mechanism from 1,2,4-triMB and 1,2,4,5-tetraMB. Surprisingly, both mean absolute and relative error for ethene from 4-ethyltoluene from the paring 1e mechanism is also the lowest compared to ethene from 4-ethyltoluene from the other mechanisms, showing that at these reaction conditions, 4-ethyltoluene most likely reacts via the paring 1e mechanism, and not the side-chain 2e mechanism.

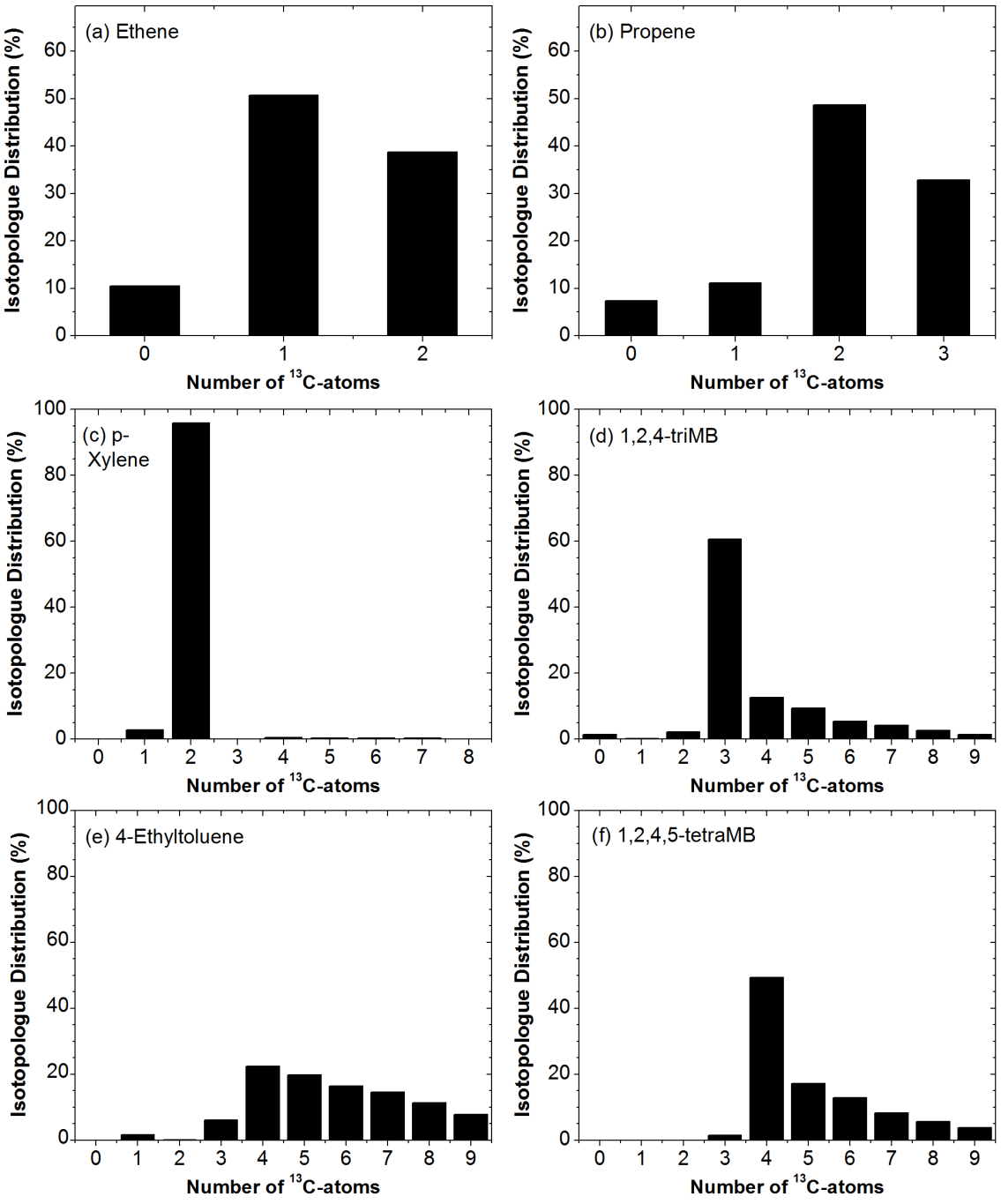

Figure 6.4: Isotopologue distributions for the co-reaction of ^{13}C-DME with of $^{13}C_2$-p-xylene at 723 K for (a) ethene, (b) propene, (c) p-xylene, (d) 1,2,4-triMB, (e) 4-ethyltoluene, and (f) 1,2,4,5-tetraMB.

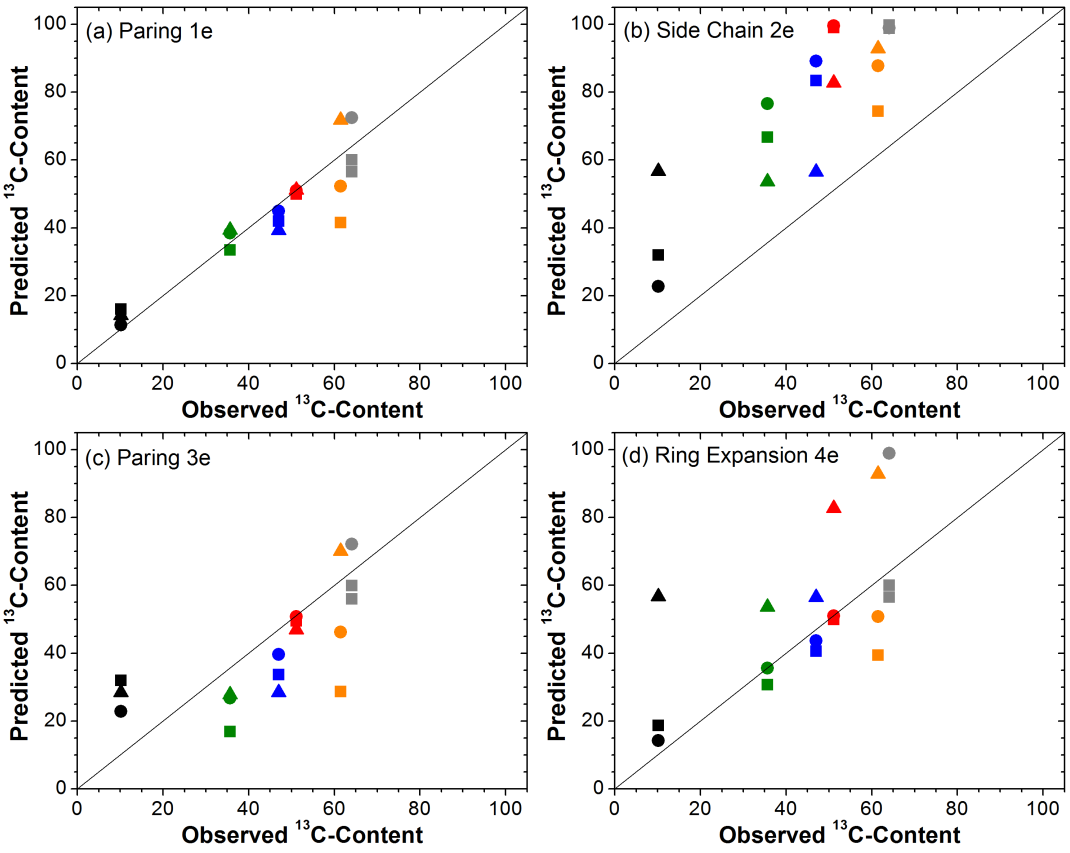

Figure 6.5: Parity plot for the predicted vs. experimentally observed ^{13}C-content for ethene from ■ 1,2,4-triMB, ● 1,2,4,5-tetraMB, and ▲ 4-ethyltoluene for the co-reactions of ■ ^{12}C-DME with $^{13}C_2$-p-xylene, ■ ^{13}C-DME with $^{13}C_2$-p-xylene, ■ ^{13}C-DME with $^{12}C_7$-toluene, ■ ^{13}C-DME with $^{12}C_8$-p-xylene at 523 K, ■ ^{13}C-DME with ^{12}C-p-xylene at 623 K, and ■ ^{13}C-DME with $^{13}C_2$-p-xylene at 723 K.

Table 6.2: Absolute and relative error for the model predictions of the ^{13}C-content of ethene formed from various aromatic precursors via the different aromatic dealkylation mechanisms compared to the experimentally observed ^{13}C-content of ethene when varying isotopic compositions of DME are co-reacted with p-xylene or toluene at 523 K-723 K. Units of absolute and relative error are percentage points of ^{13}C and %, respectively.

	Absolute Error			**Relative Error**		
Mechanism	124triMB	1245tetraMB	4ET	124triMB	1245tetraMB	4ET
Paring 1e	6.9	3.2	5.7	20.1	7.6	16.1
Side Chain 2e	30.8	34.4	28.6	91.4	87.0	115.9
Paring 3e	16.1	8.1	11.0	60.8	32.8	46.0
Ring Exp. 4e	8.5	3.8	28.6	26.9	12.0	115.9

6.3.2 Aromatic dealkylation mechanisms for propene formation

The trends in the isotopologue distribution of propene for the different co-reactions of DME with p-xylene and toluene are similar to that of ethene (Section 6.3.1) and so will not be discussed in detail. Briefly, in the co-reaction of ^{13}C-DME with $^{13}C_2$-p-xylene at 523 K, 65% of propene contains only 1 ^{12}C-atom (Figure 6.3), showing that aromatic ring carbons are incorporated into propene. When the number of ^{12}C-methyl groups on the aromatic co-feed increases from 0-2, the fraction of propene with only 1 ^{12}C-atom decreases as the fraction of propene with only 1 ^{13}C-atom increases, showing that the aromatic methyl carbons are also incorporated into propene (Figure 6.3). Additionally, when ^{13}C-DME is co-reacted with $^{13}C_2$-p-xylene at 723 K, the most abundant isotopologue of propene still contains only 1 ^{12}C-atom (Figure 6.4), again, showing that the mechanism of aromatic dealkylation for propene formation does not change over a 200 K temperature range. Parity plots for the three different mechanisms for propene formation are shown in Figure 6.6. This parity plot includes experimentally observed ^{13}C-contents for propene for the co-reaction of DME with toluene, p-xylene, and 4-ethyltoluene at both 523 and 723 K. For propene formation from both 1,2,4-triMB and 1,2,4,5-tetraMB, the model predictions for the paring 1p mechanism fits the best with the observed ^{13}C-content of propene. Both the mean absolute and relative errors for propene formation from the paring 1p mechanism are the lowest compared to the side-chain 2p and ring expansion 4p mechanisms (Table 6.3). This result is in agreement with ethene formation occurring through paring 1e mechanism, as both the paring 1e and 1p mechanisms share common intermediates. Similar to ethene, for paring 1p mechanism, the mean absolute and relative error for 1,2,4,5-tetraMB is lower than that of 1,2,4-triMB and 4-ethyltoluene, indicating that 1,2,4,5-tetraMB is either present in higher concentrations in the zeolite pores and/or that the rate of propene formation from 1,2,4,5-tetraMB is faster compared to the other two aromatics.

Table 6.3: Absolute and relative error for the model predictions of the ^{13}C-content of propene formed from various aromatic precursors via the different aromatic dealkylation mechanisms compared to the experimentally observed ^{13}C-content of propene when varying isotopic compositions of DME are co-reacted with p-xylene, toluene, or 4-ethyltoluene at 523 K-723 K. Units of absolute and relative error are percentage points of ^{13}C and %, respectively.

	Absolute Error			**Relative Error**		
Mechanism	124triMB	1245tetraMB	4ET	124triMB	1245tetraMB	4ET
Paring 1p	6.1	3.7	11.3	14.3	6.3	21.0
Side Chain 2p	26.6	28.6	24.0	49.0	48.3	54.4
Ring Exp. 4p	12.8	6.9	24.0	43.6	27.6	54.4

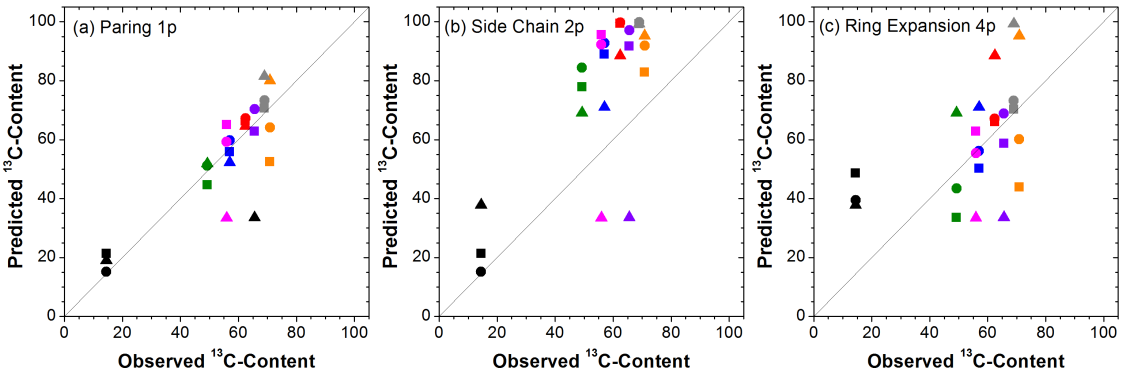

Figure 6.6: Parity plot for the predicted vs. experimentally observed ^{13}C-content for propene from ■ 1,2,4-triMB, ● 1,2,4,5-tetraMB, and ▲ 4-ethyltoluene for the co-reactions of ■ ^{12}C-DME with $^{13}C_2$-*p*-xylene, ■ ^{13}C-DME with $^{13}C_2$-*p*-xylene, ■ ^{13}C-DME with $^{12}C_7$-toluene, ■ ^{13}C-DME with $^{12}C_8$-*p*-xylene, ■ ^{13}C-DME with $^{12}C_9$-4-ethyltoluene at 523 K, ■ ^{13}C-DME with ^{12}C-*p*-xylene at 623 K, ■ ^{13}C-DME with $^{13}C_2$-*p*-xylene, and ■ ^{13}C-DME with $^{12}C_9$-4-ethyltoluene at 723 K.

6.3.3 Isotopic labeling results of DME co-reacted with 4-ethyltoluene

4-Ethyltoluene was used as a co-feed to understand if and to what extent the side-chain mechanism contributes to light olefin production in MTH. The isotopologue distributions for light olefins and aromatics are shown for reaction of ^{13}C-DME and ^{12}C-4-ethyltoluene at 523 K are shown in Figure 6.7 at 1, 5 and 10 minutes time-on-stream. Based on the side-chain mechanism (2e in Figure 6.1), ^{12}C-4-ethyltoluene should dealkylate and form all ^{12}C-ethene or the side-chain may undergo methylation by ^{13}C-DME and subsequently eliminate propene with only 1 ^{13}C-atom. In Figure 6.7 at 1 minute time-on-stream, 83% of ethene does have only ^{12}C-atoms and 39% of propene contains only 1 ^{13}C-atom, which is consistent with the side-chain mechanism. For propene, however, the most abundant isotopologue contains 2 ^{13}C-atoms, which would be consistent with the paring mechanism assuming the ^{12}C-atom came from the aromatic ring. At this time-on-stream, 99% of 4-ethyltoluene has no ^{13}C-atoms, showing that the 4-ethyltoluene in the effluent is just unreacted feed. In contrast, 85% of 1,2,4,5-tetraMB at 1 minute time-on-stream has 3 ^{13}C-atoms, suggesting that 4-ethyltoluene eliminates ethene to form toluene, which subsequently is methylated 3 times by ^{13}C-DME to form $^{13}C_3$-1,2,4,5-tetraMB. However, p-xylene and 1,2,4-triMB do not follow this same pattern and have a significant fraction of isotopologues with 1-4 and 2-5 ^{13}C-atoms, respectively. It is unclear what mechanistic pathways form p-xylene and 1,2,4-triMB here. At increasing time-on-streams, the ^{13}C-content of ethene, propene, p-xylene, 1,2,4-triMB, and 1,2,4,5-tetraMB all increase. The ^{13}C-content of 4-ethyltoluene

remains unchanged with increasing time-on-stream. The changing isotopologue distributions with time-on-stream show that the methylbenzenes in the aromatic hydrocarbon pool evolves with time-on-stream and becomes more ^{13}C-rich. In contrast, 99% of isotopologues of a methylation product of 4-ethyltoluene contained only 1 ^{13}C-atom at all times-on-stream. This product was determined to be a methylation product of 4-ethyltoluene based on its isotopologue distribution and because its concentration increased significantly when 4-ethyltoluene was co-fed with DME, compared to the co-reaction of DME with other methylbenzenes. The absence of ^{13}C-atoms in 4-ethyltoluene and one of its methylation products show that these aromatics are not reformed at a rate as fast as 1,2,4-triMB or 1,2,4,5-tetraMB, suggesting that these ethylated aromatics are not co-catalytic. While the side-chain mechanism can occur in the presence of a 4-ethyltoluene, ethylated aromatics do not participate as co-catalysts in MTH hydrocarbon pool mechanism.

The co-reaction of ^{13}C-DME and ^{12}C-4-ethyltoluene was also performed at 723 K. Due to the rapid deactivation of the catalyst at these conditions (within 3 minutes of reaction), the product isotopologue distributions are only shown at 1 minute time-on-stream (Figure 6.8). For ethene, the isotopologues with 0 and 1 ^{13}C-atoms have a similar fraction (43% and 35%, respectively), which is consistent with both the side-chain and paring mechanism. Additionally, for propene, the most abundant isotopologue has only 1 ^{13}C-atom, consistent with the paring mechanism. This indicates that while the side-chain mechanism does occur when 4-ethyltoluene is co-reacted, the paring mechanism is also occurring in parallel. Most abundant isotopologue of p-xylene, 1,2,4-triMB, and 1,2,4,5-tetraMB containe 1, 2, and 3 ^{13}C-atoms, respectively, indicating that these methylbenzenes are most likely the result of ethene elimination from 4-ethyltoluene to form toluene, followed by sequential methylations by ^{13}C-DME. Due to the fast deactivation of the catalyst at 723 K when 4-ethyltoluene is co-reacted with DME, it is more likely that 4-ethyltoluene is a precursor to coke on H-ZSM-5, which is in agreement to results from Schulz[124] showing that at ethylated and propylated benzenes were the most predominant aromatics retained inside of the deactivated H-ZSM-5 catalyst after the reaction of methanol at 543 K. Results for the co-reaction of ^{13}C-DME and ^{12}C-4-ethyltoluene at both 523 K and 723 K suggest that while the side-chain mechanism does occur, evidenced by the fraction of all ^{12}C-labeled ethene, a paring mechanism is also occurring in parallel, supported by the high fraction of ethene and propene containing both ^{13}C and ^{12}C-atoms.

6.4 Conclusions

In summary, effluent isotopologue distributions of 1,2,4-triMB, 1,2,4,5-tetraMB, and 4-ethyltoluene were used to predict the ^{13}C-content of ethene and propene for co-reactions

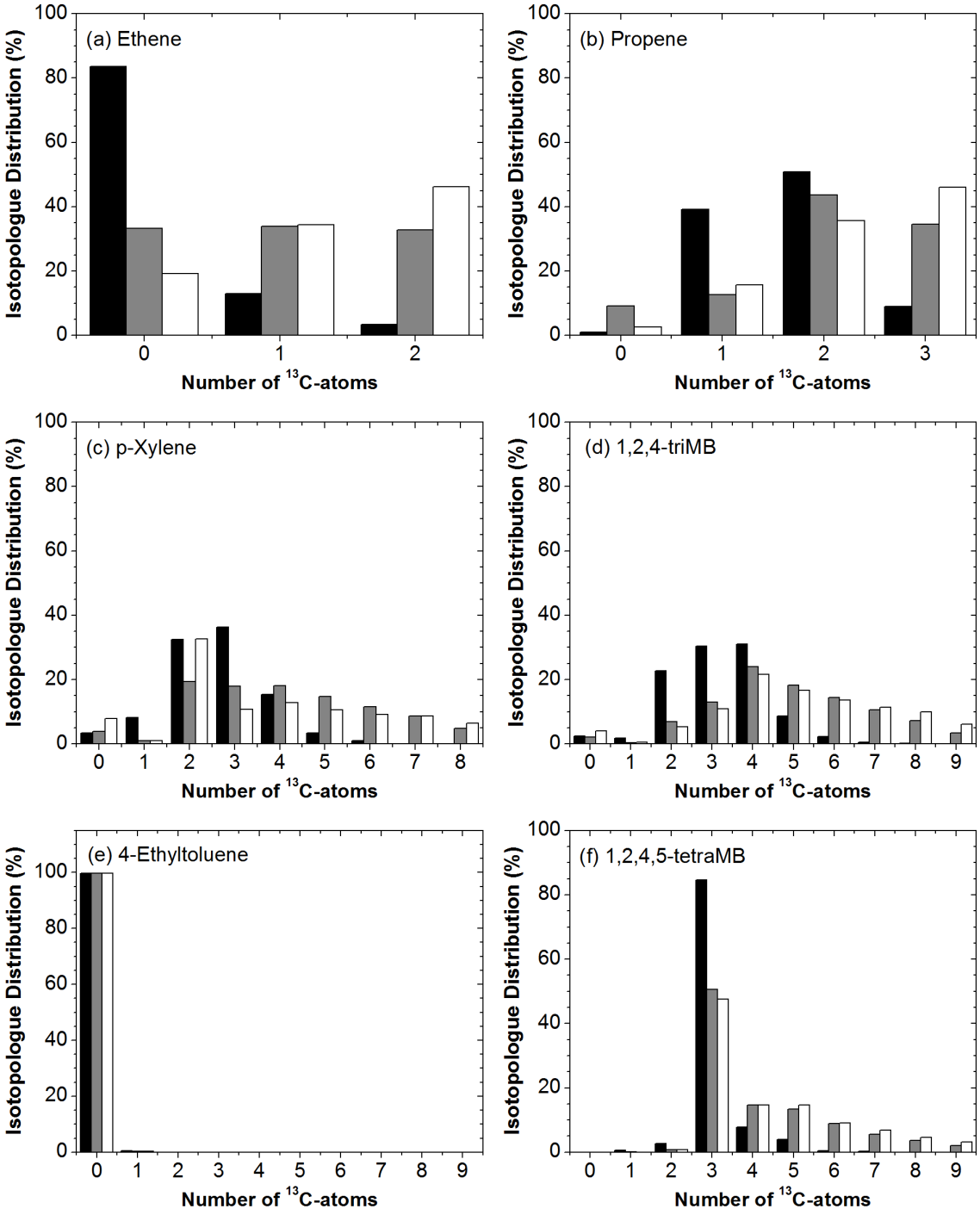

Figure 6.7: Isotopologue distributions for the reaction of ^{13}C-DME with ^{12}C-4-ethyltoluene at 523 K for (a) ethene, (b) propene, (c) p-xylene, (d) 1,2,4-triMB, (e) 4-ethyltoluene, and (f) 1,2,4,5-tetraMB at ■ 1, ■ 5, and □ 10 minutes time-on-stream.

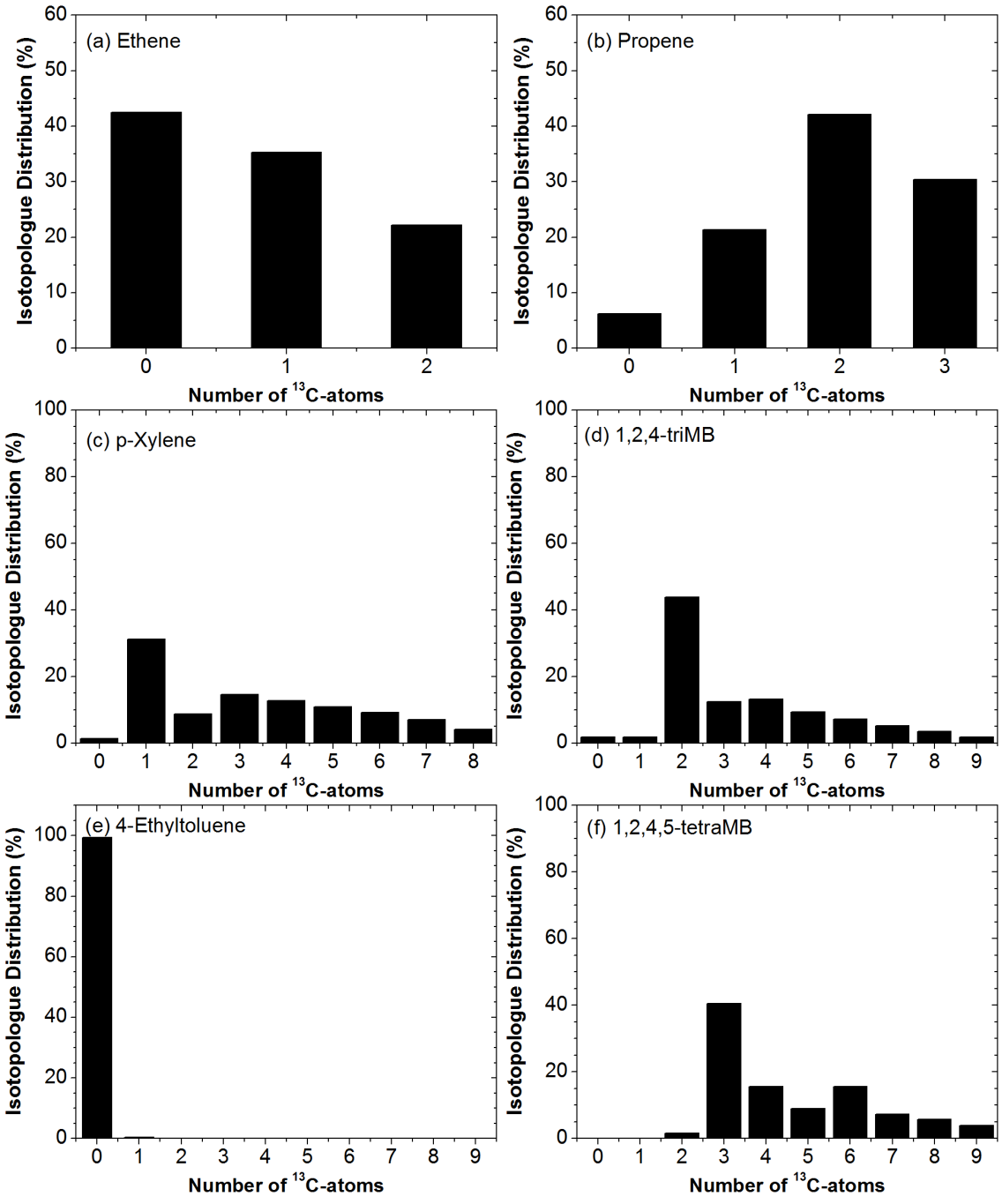

Figure 6.8: Isotopologue distributions for the reaction of ^{13}C-DME with ^{12}C-4-ethyltoluene at 723 K for (a) ethene, (b) propene, (c) p-xylene, (d) 1,2,4-triMB, (e) 4-ethyltoluene, and (f) 1,2,4,5-tetraMB.

of DME with toluene, p-xylene, and 4-ethyltoluene where either DME or the aromatic was ^{13}C-labeled. Predictions were made using models for 4 different aromatic dealkylation mechanisms for ethene and 3 aromatic dealkylation mechanisms for propene and compared to the experimentally observed ^{13}C-content of ethene and propene. Based on the mean absolute and relative errors for these mechanisms, the experimentally observed ^{13}C-content of ethene and propene were best predicted using the paring 1e and 1p mechanisms, respectively. Additionally, for both the paring 1e and 1p mechanisms, predictions using 1,2,4,5-tetraMB as the aromatic precursor to ethene and propene had the lowest mean absolute and relative error compared to the 1,2,4-triMB and 4-ethyltoluene, suggesting either that the rate of dealkylation from 1,2,4,5-tetraMB is faster or that 1,2,4,5-tetraMB has a higher concentration within the zeolite pore compared to 1,2,4-triMB and 4-ethyltoluene. For the co-reaction of ^{13}C-DME and ^{12}C-4-ethyltoluene at 523 K and 723 K, the high fraction of ethene with only ^{12}C-atoms suggest that ethene can be formed via the side-chain mechanism, however, both 4-ethyltoluene and its methylation product incorporated negligible amounts of ^{13}C-atoms, indicating that while these species can undergo side-chain dealkylation, they are not co-catalytic in that they are not reformed fast enough to participate in the aromatic hydrocarbon pool.

These results, for the first time show that the paring mechanism for light olefin formation in MTO is occurring on H-ZSM-5 over a 200 K temperature range. While the paring 1e and 1p mechanisms may not be the exact mechanism for ethene and propene formation, the results in this work show that ethene is formed from one aromatic ring carbon and the other carbon has a 50% chance of coming from the methylating agent and a 50% chance of coming from an aromatic methyl carbon. Propene is formed from one aromatic ring carbon, one aromatic methyl carbon, and one carbon coming from the methylating agent. Computational studies investigating aromatic dealkylation on H-ZSM-5 will be helpful in determining the mechanistic pathways most likely to result in these specific ethene and propene compositions.

6.5 Supplemental Information

6.5.1 ^{13}C NMR of $^{13}C_2$-p-xylene

^{13}C NMR spectra was recorded for a sample of 400 mg of $^{13}C_2$-p-xylene dissolved in 1.24 g of $CDCl_3$ at ambient temperature using a VAC-300 spectrometer at 75.4 MHz with ^{1}H decoupling at 300 MHz to confirm that the p-xylene only had ^{13}C-atoms on the methyl groups. The spectra (Figure 6.9) shows a large peak at 21.7 ppm, representing the methyl carbons and a smaller peaks at 110 and 130 representing the ring carbons. A triplet around 78 represents the solvent. Based on this spectra, the majority of the ^{13}C-atoms in the

$^{13}C_2$-p-xylene sample are located on the methyl groups.

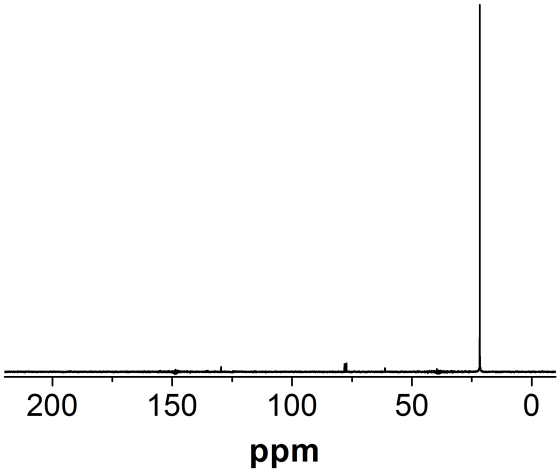

Figure 6.9: ^{13}C NMR spectra of $^{13}C_2$-p-xylene.

6.5.2 Model error for predicting the ^{13}C-content of ethene and propene

The absolute and relative error for the predicted ^{13}C-content of ethene and propene coming from 1,2,4-triMB, 1,2,4,5tetraMB, and 4-ethyltoluene via the different aromatic dealkylation mechanisms compared to the experimentally observed ^{13}C-contents of ethene and propene are shown in Figure 6.10 and Figure 6.11 for the co-reactions of DME with toluene, p-xylene, and 4-ethyltoluene.

6.5.3 Isotopic results for the co-reaction of ^{13}C-DME with $^{12}C_8$-p-xylene at 623 K

Figure 6.12 shows isotopologue distributions for ethene, propene, p-xylene, 4-ethyltoluene, 1,2,4-triMB, and 1,2,4,5-tetraMB in the effluent for the co-reaction of ^{13}C-DME with $^{12}C_8$-p-xylene at 623 K.

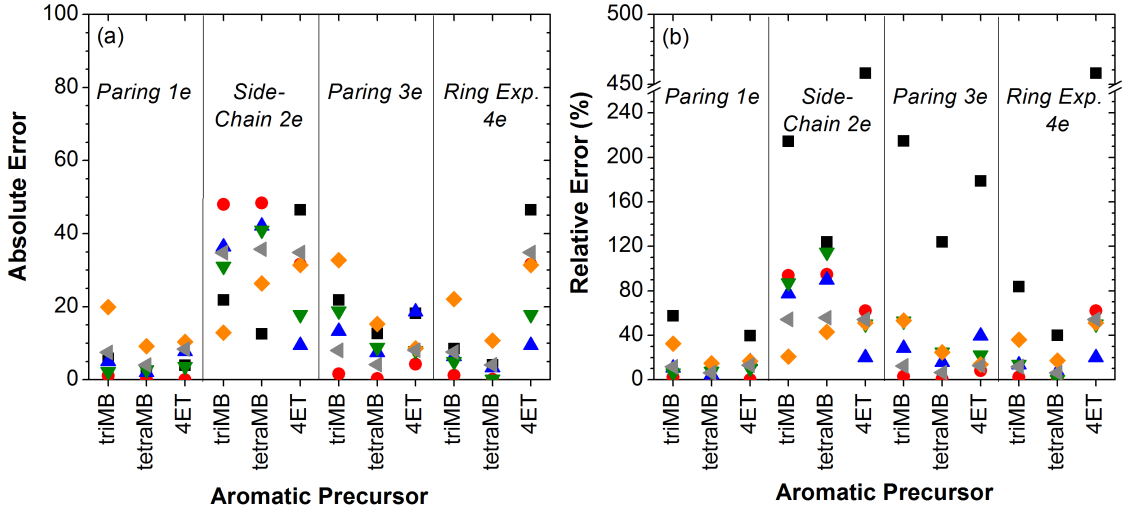

Figure 6.10: (a) Absolute and (b) relative errors in predictions of the ^{13}C-content of ethene coming from different aromatic precursors and different mechanisms for the co-reactions of (■) ^{12}C-DME + $^{13}C_2$-p-xylene at 523 K, (●) ^{13}C-DME + $^{13}C_2$-p-xylene at 523 K, (▲) ^{13}C-DME + ^{12}C-toluene at 523 K, (▼) ^{13}C-DME + ^{12}C-p-xylene at 523 K, (◆) ^{13}C-DME + ^{12}C-p-xylene at 623 K, (◄ ^{13}C-DME + $^{13}C_2$-p-xylene at 723 K.

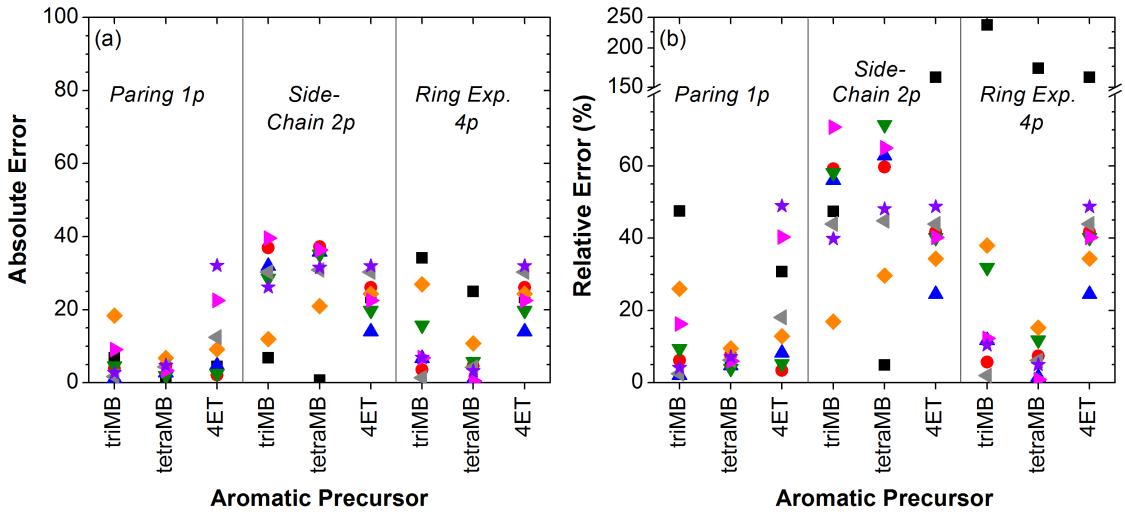

Figure 6.11: (a) Absolute and (b) relative errors in predictions of the ^{13}C-content of propene coming from different aromatic precursors and different mechanisms for the co-reactions of (■) ^{12}C-DME + $^{13}C_2$-p-xylene at 523 K, (●) ^{13}C-DME + $^{13}C_2$-p-xylene at 523 K, (▲) ^{13}C-DME + ^{12}C-toluene at 523 K, (▼) ^{13}C-DME + ^{12}C-p-xylene at 523 K, (◆) ^{13}C-DME + ^{12}C-p-xylene at 623 K, (◄ ^{13}C-DME + $^{13}C_2$-p-xylene at 723 K, (►) ^{13}C-DME + ^{12}C-4-ethyltoluene at 523 K, and (★) ^{13}C-DME + ^{12}C-4-ethyltoluene at 723 K.

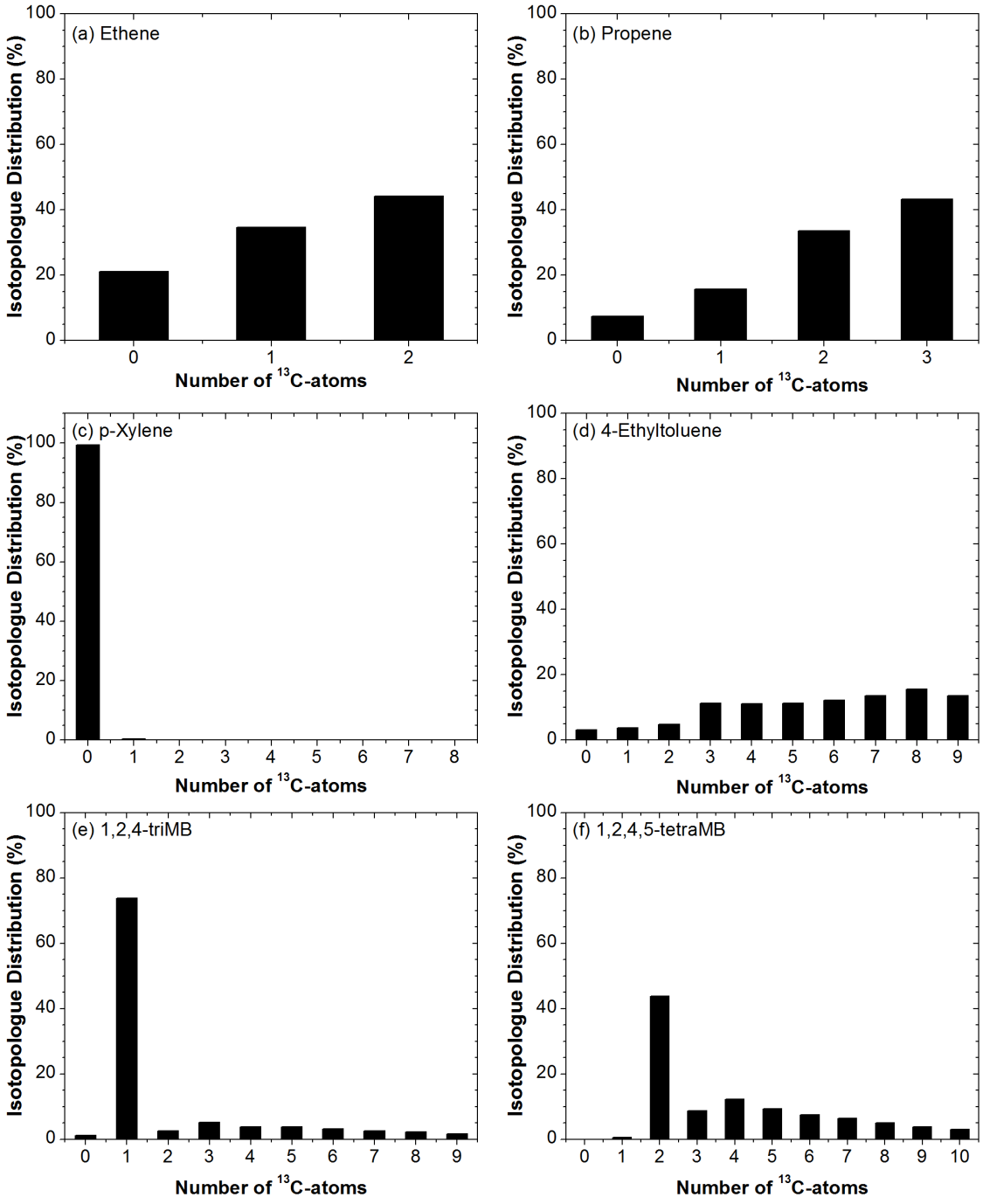

Figure 6.12: Isotopologue distributions for the reaction of ^{13}C-DME with ^{12}C-p-xylene at 623 K for (a) ethene, (b) propene, (c) p-xylene, (d) 1,2,4-triMB, (e) 4-ethyltoluene, and (f) 1,2,4,5-tetraMB.

CHAPTER

SEVEN

FUTURE DIRECTIONS

The selectivity of MTH conversion was systematically tuned through the use of olefin and aromatic co-feeds on both H-ZSM-5 and H-BEA and was reported in Chapters 3 and 5. While the pore size of H-BEA is large enough that significant amounts of hexaMB can be observed in the reaction effluent for MTH conversion on H-BEA, on H-ZSM-5, negligible amounts of penta- and hexaMB are observed in the effluent of MTH conversion. Analysis of hydrocarbons retained within the pores of H-ZSM-5 has shown that penta- and hexaMB are formed inside the catalyst, however, these aromatics have kinetic diameters larger that the 5.1-5.6 $\AA$ pore diameters of H-ZSM-5 and cannot diffuse out of the catalyst.[141,142] The conversion of MTH on 17-μm crystals of H-ZSM-5, reported in Chapter 4, showed that the ethene/2MB yield was approximately a factor of two greater that the ethene/2MB yield of MTH conversion on the the commercial H-ZSM-5 sample. Increased diffusion limitations due to larger crystal sizes, therefore, result in increased propagation of the aromatic-based cycle compared to the olefin-based cycle, evidenced by the higher ethene/2MB ratio for MTH conversion on 17-μm crystals of H-ZSM-5 compared to the commercial H-ZSM-5 sample. A quantitative study on the effect of diffusion limitation on MTH conversion is recommended. While penta- and hexaMB are too large to exit the channels of H-ZSM-5, aromatic methylation and dealkylation reactions of 1,2,4-triMBs and 1,2,4,5-tetraMBs may be diffusion-limited. Understanding the effects of aromatic diffusion on the relative propagation of the aromatic- and olefin-based cycles may provide another parameter that can be manipulated to systematically control the selectivity of MTH conversion on H-ZSM-5.

On H-ZSM-5, predictions of the isotopic composition of ethene and propene from dealkylation of 1,2,4-triMB and 1,2,4,5-tetraMB via the paring mechanism most closely matched the experimentally observed isotopic composition of ethene and propene compared to other aromatic dealkylation mechanisms for the co-reaction of the DME and toluene, p-xylene,

4-ethyltoluene with varying $^{13}C/^{12}C$ feed compositions at 523-723 K and were reported in Chapter 6. The ability to predict the isotopic composition of ethene and propene based on the paring mechanism shows that the paring mechanism is most likely the mechanism of aromatic dealkylation on H-ZSM-5. Co-reactions of ^{13}C-methanol with ^{12}C-benzene have previously shown that at low temperatures (<573 K), greater than 50% of light olefins incorporate one ^{12}C-atom on H-BEA and H-SAPO-5, showing that aromatic ring carbons are incorporated into light olefins.[90,138] While the incorporation of aromatic ring carbons imply that that either the paring or ring-expansion mechanisms are occurring on these catalysts, these two mechanisms have not been quantitatively distinguished from each other on H-BEA or H-SAPO-5. The methodology reported in Chapter 6 should be extended to the study of aromatic dealkylation mechanisms on other catalyst used in MTH conversion. By doing so, the effect of catalyst structure on the mechanism of aromatic dealkylation can be further understood.

In Chapter 6, a new mechanism for ethene formation from the paring mechanism is shown (Paring 1e in Figure 6.1) in which a gem-methylated aromatic undergoes ring contraction and forms an exocyclic isopropyl group. The isopropyl group shrinks to an ethyl group by a methyl shift from the isopropyl group to the 5-membered ring and subsequent scission of the ethyl groups results in ethene formation. Theoretical work has not previously investigated the energetics involved in the methyl shift from the isopropyl group to the ring. Computational studies on the paring 1e mechanism are recommended to help understand if this mechanism is energetically feasible. If the the paring 1e mechanism is not energetically feasible, then the results presented in Chapter 6 can be used to postulate a different dealklyation mechanism that still results in 50% of ethene molecules containing one aromatic ring carbon and one aromatic methyl carbon and the other 50% of ethene molecules containing one aromatic ring carbon and one carbon from DME/methanol. By combining theoretical work with the experimental results discussed in Chapter 6, the mechanism of aromatic dealkylation can be further understood and verified.

BIBLIOGRAPHY

[1] Svelle, S., Rønning, P. O., and Kolboe, S. *Journal of Catalysis* **224**(1), 115–123 (2004).

[2] Svelle, S., Rønning, P. O., Olsbye, U., and Kolboe, S. *Journal of Catalysis* **234**(2), 385–400 (2005).

[3] Hill, I. M., Hashimi, S. A., and Bhan, A. *Journal of Catalysis* **285**(0), 115–123 (2012).

[4] Hill, I. M., Hashimi, S. A., and Bhan, A. *Journal of Catalysis* **291**(0), 155–157 (2012).

[5] Hill, I. M., Ng, Y. S., and Bhan, A. *ACS Catalysis* , 1742–1748 (2012).

[6] Van Speybroeck, V., Van der Mynsbrugge, J., Vandichel, M., Hemelsoet, K., Lesthaeghe, D., Ghysels, A., Marin, G. B., and Waroquier, M. *Journal of the American Chemical Society* **133**(4), 888–899 (2011).

[7] Weitkamp, J., Jacobs, P. A., and Martens, J. A. *Applied Catalysis* **8**(1), 123–141 (1983).

[8] Buchanan, J. S., Santiesteban, J. G., and Haag, W. O. *Journal of Catalysis* **158**(1), 279–287 (1996).

[9] Joshi, Y. V. and Thomson, K. T. *Journal of Catalysis* **230**(2), 440–463 (2005).

[10] Vandichel, M., Lesthaeghe, D., Mynsbrugge, J. V. d., Waroquier, M., and Van Speybroeck, V. *Journal of Catalysis* **271**(1), 67–78 (2010).

[11] Lesthaeghe, D., Horrẽ, A., Waroquier, M., Marin, G. B., and Van Speybroeck, V. *Chemistry - A European Journal* **15**(41), 10803 – 10808 (2009).

[12] Chang, C. D. and Silvestri, A. J. *Journal of Catalysis* **47**(2), 249–259 (1977).

[13] Olsbye, U., Svelle, S., Bjørgen, M., Beato, P., Janssens, T. V. W., Joensen, F., Bordiga, S., and Lillerud, K. P. *Angewandte Chemie International Edition* **51**(24), 5810–5831 (2012).

[14] Støcker, M. *Microporous and Mesoporous Materials* **29**(1-2), 3–48 (1999).

[15] Ilias, S. and Bhan, A. *ACS Catalysis* **3**, 18–31 (2013).

[16] Dahl, I. M. and Kolboe, S. *Catalysis Letters* **20**(3), 329–336 (1993).

[17] Dahl, I. M. and Kolboe, S. *Journal of Catalysis* **149**(2), 458–464 (1994).

[18] Dahl, I. M. and Kolboe, S. *Journal of Catalysis* **161**(1), 304–309 (1996).

[19] Svelle, S., Joensen, F., Nerlov, J., Olsbye, U., Lillerud, K.-P., Kolboe, S., and Bjørgen, M. *Journal of the American Chemical Society* **128**(46), 14770–14771 (2006).

[20] Bjørgen, M., Svelle, S., Joensen, F., Nerlov, J., Kolboe, S., Bonino, F., Palumbo, L., Bordiga, S., and Olsbye, U. *Journal of Catalysis* **249**(2), 195–207 (2007).

[21] Hickman, D. A. and Schmidt, L. D. *Science* **259**(5093), 343–346 (1993).

[22] Laurendeau, N. M. *Progress in Energy and Combustion Science* **4**(4), 221–270 (1978).

[23] Wen, W. Y. *Catalysis Reviews-Science and Engineering* **22**(1), 1–28 (1980).

[24] Asadullah, M., Ito, S., Kunimori, K., Yamada, M., and Tomishige, K. *Journal of Catalysis* **208**(2), 255–259 (2002).

[25] Sutton, D., Kelleher, B., and Ross, J. R. H. *Fuel Processing Technology* **73**(3), 155–173 (2001).

[26] Ahn, J. H., Temel, B., and Iglesia, E. *Angewandte Chemie* **121**(21), 3872–3874 (2009).

[27] Simonetti, D. A., Ahn, J. H., and Iglesia, E. *Journal of Catalysis* **277**(2), 173–195 (2011).

[28] Mikkelsen, O. and Kolboe, S. *Microporous and Mesoporous Materials* **29**(1-2), 173–184 (1999).

[29] Haw, J. F., Song, W., Marcus, D. M., and Nicholas, J. B. *Accounts of Chemical Research* **36**(5), 317–326 (2003).

[30] Lesthaeghe, D., Van Speybroeck, V., Marin, G. B., and Waroquier, M. *Angewandte Chemie-International Edition* **45**(11), 1714–1719 (2006).

[31] Lesthaeghe, D., Van Speybroeck, V., Marin, G. B., and Waroquier, M. *Industrial & Engineering Chemistry Research* **46**(26), 8832–8838 (2007).

[32] Song, W., Marcus, D. M., Fu, H., Ehresmann, J. O., and Haw, J. F. *Journal of the American Chemical Society* **124**(15), 3844–3845 (2002).

[33] Marcus, D. M., McLachlan, K. A., Wildman, M. A., Ehresmann, J. O., Kletnieks, P. W., and Haw, J. F. *Angewandte Chemie International Edition* **45**(19), 3133–3136 (2006).

[34] Ono, Y. and Mori, T. *Journal of the Chemical Society-Faraday Transactions* **77**, 2209–2221 (1981).

[35] Langner, B. E. *Applied Catalysis* **2**(4-5), 289–302 (1982).

[36] Dessau, R. M. and LaPierre, R. B. *Journal of Catalysis* **78**(1), 136–141 (1982).

[37] Dessau, R. M. *Journal of Catalysis* **99**(1), 111–116 (1986).

[38] Song, W., Haw, J. F., Nicholas, J. B., and Heneghan, C. S. *Journal of the American Chemical Society* **122**(43), 10726–10727 (2000).

[39] Mole, T., Bett, G., and Seddon, D. *Journal of Catalysis* **84**(2), 435–445 (1983).

[40] Mikkelsen, O., Ronning, P. O., and Kolboe, S. *Microporous and Mesoporous Materials* **40**(1-3), 95–113 (2000).

[41] Tau, L. M., Fort, A. W., Bao, S., and Davis, B. H. *Fuel Processing Technology* **26**(3), 209–219 (1990).

[42] Teketel, S., Olsbye, U., Lillerud, K.-P., Beato, P., and Svelle, S. *Microporous and Mesoporous Materials* **136**(1-3), 33–41 (2010).

[43] Hereijgers, B. P. C., Bleken, F., Nilsen, M. H., Svelle, S., Lillerud, K.-P., Bjørgen, M., Weckhuysen, B. M., and Olsbye, U. *Journal of Catalysis* **264**(1), 77–87 (2009).

[44] Bjørgen, M., Joensen, F., Lillerud, K.-P., Olsbye, U., and Svelle, S. *Catalysis Today* **142**(1-2), 90–97 (2009).

[45] Svelle, S., Olsbye, U., Joensen, F., and Bjørgen, M. *Journal of Physical Chemistry C* **111**(49), 17981–17984 (2007).

[46] Cui, Z. M., Liu, Q., Song, W. G., and Wan, L. J. *Angewandte Chemie-International Edition* **45**(39), 6512–6515 (2006).

[47] Cui, Z.-M., Liu, Q., Ma, Z., Bian, S.-W., and Song, W.-G. *Journal of Catalysis* **258**(1), 83–86 (2008).

[48] Teketel, S., Svelle, S., Lillerud, K.-P., and Olsbye, U. *ChemCatChem* **1**(1), 78–81 (2009).

[49] Teketel, S., Skistad, W., Benard, S., Olsbye, U., Lillerud, K. P., Beato, P., and Svelle, S. *ACS Catalysis* **2**(1), 26–37 (2012).

[50] Svelle, S., Visur, M., Olsbye, U., Saepurahman, S., and Bjørgen, M. *Topics in Catalysis* **54**(13-15), 897–906 (2011).

[51] Bercaw, J. E., Diaconescu, P. L., Grubbs, R. H., Kay, R. D., Kitching, S., Labinger, J. A., Li, X., Mehrkhodavandi, P., Morris, G. E., Sunley, G. J., and Vagner, P. *Journal of Organic Chemistry* **71**(23), 8907–8917 (2006).

[52] Bercaw, J. E., Diaconescu, P. L., Grubbs, R. H., Hazari, N., Kay, R. D., Labinger, J. A., Mehrkhodavandi, P., Morris, G. E., Sunley, G. J., and Vagner, P. *Inorganic Chemistry* **46**(26), 11371–11380 (2007).

[53] Bercaw, J. E., Grubbs, R. H., Hazari, N., Labinger, J. A., and Li, X. *Chemical Communications* (28), 2974–2976 (2007).

[54] Bercaw, J. E., Hazari, N., Labinger, J. A., Scott, V. J., and Sunley, G. J. *Journal of the American Chemical Society* **130**(36), 11988–11995 (2008).

[55] Simonetti, D. A., Ahn, J. H., and Iglesia, E. *ChemCatChem* **3**(4), 704–718 (2011).

[56] Svelle, S., Tuma, C., Rozanska, X., Kerber, T., and Sauer, J. *Journal of the American Chemical Society* **131**(2), 816–825 (2009).

[57] Mazar, M. N., Al-Hashimi, S., Bhan, A., and Cococcioni, M. *Journal of Physical Chemistry C* **116**, 19053–19612 (2012).

[58] Lee, C. C., Gorte, R. J., and Farneth, W. E. *Journal of Physical Chemistry B* **101**(19), 3811–3817 (1997).

[59] Stich, I., Gale, J. D., Terakura, K., and Payne, M. C. *Journal of the American Chemical Society* **121**(14), 3292–3302 (1999).

[60] Forester, T. R. and Howe, R. F. *Journal of the American Chemical Society* **109**(17), 5076–5082 (1987).

[61] Cheung, P., Bhan, A., Sunley, G. J., Law, D. J., and Iglesia, E. *Journal of Catalysis* **245**(1), 110–123 (2007).

[62] Yamazaki, H., Shima, H., Imai, H., Yokoi, T., Tatsumi, T., and Kondo, J. N. *Angewandte Chemie International Edition* **50**, 1–5 (2011).

[63] Bosacek, V. *Journal of Physical Chemistry* **97**(41), 10732–10737 (1993).

[64] Wang, W. and Hunger, M. *Accounts of Chemical Research* **41**(8), 895–904 (2008).

[65] Jiang, Y., Hunger, M., and Wang, W. *Journal of the American Chemical Society* **128**(35), 11679–11692 (2006).

[66] Boronat, M., Martinez, C., and Corma, A. *Physical Chemistry Chemical Physics* **13**(7), 2603–2612 (2011).

[67] Blaszkowski, S. R. and van Santen, R. A. *Journal of Physical Chemistry* **99**(30), 11728–11738 (1995).

[68] Blaszkowski, S. R. and van Santen, R. A. *Journal of the American Chemical Society* **118**(21), 5152–5153 (1996).

[69] Blaszkowski, S. R. and van Santen, R. A. *Journal of Physical Chemistry B* **101**(13), 2292–2305 (1997).

[70] Ivanova, I., Pomakhina, E. B., Rebrov, A. I., Hunger, M., Kolyagin, Y. G., and Weitkamp, J. *Journal of Catalysis* **203**(2), 375–381 (2001).

[71] Frash, M. V., Kazansky, V. B., Rigby, A. M., and van Santen, R. A. *Journal of Physical Chemistry B* **102**(12), 2232–2238 (1998).

[72] Rigby, A. M., Kramer, G. J., and van Santen, R. A. *Journal of Catalysis* **170**(1), 1–10 (1997).

[73] Frash, M. V. and van Santen, R. A. *Topics in Catalysis* **9**(3-4), 191–205 (1999).

[74] Hay, P. J., Redondo, A., and Guo, Y. J. *Catalysis Today* **50**(3-4), 517–523 (1999).

[75] Kazansky, V. B., Frash, M. V., and van Santen, R. A. *Catalysis Letters* **48**(1-2), 61–67 (1997).

[76] Kazansky, V. B., Frash, M. V., and van Santen, R. A. *Studies in Surface Science and Catalysis* **105**, 2283–2290 (1997).

[77] Boronat, M., Viruela, P., and Corma, A. *Journal of Physical Chemistry B* **103**(37), 7809–7821 (1999).

[78] Boronat, M., Viruela, P., and Corma, A. *Physical Chemistry Chemical Physics* **2**(14), 3327–3333 (2000).

[79] Bao, S., Tau, L. M., and Davis, B. H. *Journal of Catalysis* **111**(2), 436–439 (1988).

[80] Hazari, N., Labinger, J. A., and Scott, V. J. *Journal of Catalysis* **263**(2), 266–276 (2009).

[81] Frash, M. V., Solkan, V. N., and Kazansky, V. B. *Journal of the Chemical Society-Faraday Transactions* **93**(4), 515–520 (1997).

[82] Boronat, M., Viruela, P., and Corma, A. *Journal of Physical Chemistry A* **102**(48), 9863–9868 (1998).

[83] Boronat, M., Zicovich-Wilson, C. M., Corma, A., and Viruela, P. *Physical Chemistry Chemical Physics* **1**(4), 537–543 (1999).

[84] Janik, M. J., Davis, R. J., and Neurock, M. *Journal of Catalysis* **244**(1), 65–77 (2006).

[85] Mullen, G. M. and Janik, M. J. *ACS Catalysis* **1**(2), 105–115 (2011).

[86] Jasra, R. V., Bhatt, B. D., Garg, V. N., and Bhat, S. G. T. *Applied Catalysis* **39**(0), 49–60 (1988).

[87] Dass, D. V. and Odell, A. L. *Journal of Catalysis* **113**(1), 259–262 (1988).

[88] Joshi, Y. V. and Thomson, K. T. *Journal of Physical Chemistry C* **112**(33), 12825–12833 (2008).

[89] Ilias, S. and Bhan, A. *Journal of Catalysis* **290**(0), 186–192 (2012).

[90] Bjørgen, M., Olsbye, U., Petersen, D., and Kolboe, S. *Journal of Catalysis* **221**(1), 1–10 (2004).

[91] Van der Mynsbrugge, J., Visur, M., Olsbye, U., Beato, P., Bjørgen, M., Van Speybroeck, V., and Svelle, S. *Journal of Catalysis* **292**(0), 201–212 (2012).

[92] Mirth, G. and Lercher, J. A. *Journal of Physical Chemistry* **95**(9), 3736–3740 (1991).

[93] Saepurahman, Visur, M., Olsbye, U., Bjorgen, M., and Svelle, S. *Topics in Catalysis* **54**(16-18), 1293–1301 (2011).

[94] Arstad, B., Kolboe, S., and Swang, O. *Journal of Physical Chemistry B* **106**(49), 12722–12726 (2002).

[95] Svelle, S., Kolboe, S., Olsbye, U., and Swang, O. *Journal of Physical Chemistry B* **107**(22), 5251–5260 (2003).

[96] Svelle, S., Kolboe, S., Swang, O., and Olsbye, U. *Journal of Physical Chemistry B* **109**(26), 12874–12878 (2005).

[97] Vos, A. M., Nulens, K. H. L., De Proft, F., Schoonheydt, R. A., and Geerlings, P. *Journal of Physical Chemistry B* **106**(8), 2026–2034 (2002).

[98] McCann, D. M., Lesthaeghe, D., Kletnieks, P. W., Guenther, D. R., Hayman, M. J., vanSpeybroeck, V., Waroquier, M., and Haw, J. F. *Angewandte Chemie International Edition* **47**(28), 5179–5182 (2008).

[99] Mantha, R., Bhatia, S., and Rao, M. S. *Industrial & Engineering Chemistry Research* **30**(2), 281–286 (1991).

[100] Rabiu, S. and Al-Khattaf, S. *Industrial & Engineering Chemistry Research* **47**(1), 39–47 (2008).

[101] Vinek, H., Derewinski, M., Mirth, G., and Lercher, J. A. *Applied Catalysis* **68**(1), 277–284 (1991).

[102] Jentys, A., Tanaka, H., and Lercher, J. A. *Journal of Physical Chemistry B* **109**(6), 2254–2261 (2004).

[103] Pope, C. G. *Journal of Physical Chemistry* **88**(25), 6312–6313 (1984).

[104] Lesthaeghe, D., DeSterck, B., VanSpeybroeck, V., B. Marin, G., and Waroquier, M. *Angewandte Chemie International Edition* **46**(8), 1311–1314 (2007).

[105] Barger, P. T., Vora, B. V., Pujad, P. R., and Chen, Q. *Studies in Surface Science and Catalysis* **145**, 109–114 (2003).

[106] Song, W., Fu, H., and Haw, J. F. *Journal of the American Chemical Society* **123**(20), 4749–4754 (2001).

[107] Bjørgen, M., Olsbye, U., Svelle, S., and Kolboe, S. *Catalysis Letters* **93**(1-2), 37–40 (2004).

[108] Xu, T., Barich, D. H., Goguen, P. W., Song, W., Wang, Z., Nicholas, J. B., and Haw, J. F. *Journal of the American Chemical Society* **120**(16), 4025–4026 (1998).

[109] Bjørgen, M., Olsbye, U., and Kolboe, S. *Journal of Catalysis* **215**(1), 30–44 (2003).

[110] Bjørgen, M., Bonino, F., Kolboe, S., Lillerud, K.-P., Zecchina, A., and Bordiga, S. *Journal of the American Chemical Society* **125**(51), 15863–15868 (2003).

[111] Wang, C. M., Wang, Y. D., Xie, Z. K., and Liu, Z. P. *Journal of Physical Chemistry C* **113**(11), 4584–4591 (2009).

[112] Lesthaeghe, D., Van Speybroeck, V., and Waroquier, M. *Physical Chemistry Chemical Physics* **11**(26), 5222–5226 (2009).

[113] Sullivan, R. F., Egan, C. J., Langlois, G. E., and Sieg, R. P. *Journal of the American Chemical Society* **83**(5), 1156–1160 (1961).

[114] Xu, T. and Haw, J. F. *Journal of the American Chemical Society* **116**(17), 7753–7759 (1994).

[115] Stepanov, A. G., Luzgin, M. V., Arzumanov, S. S., Ernst, H., and Freude, D. *Journal of Catalysis* **211**(1), 165–172 (2002).

[116] Luzgin, M. V., Stepanov, A. G., Arzumanov, S. S., Rogov, V. A., Parmon, V. N., Wang, W., Hunger, M., and Freude, D. *Chemistry - A European Journal* **12**(2), 457–465 (2006).

[117] Long, J. F., Wang, X. X., Ding, Z. X., Xie, L. L., Zhang, Z. Z., Dong, J. G., Lin, H. X., and Fu, X. Z. *Journal of Catalysis* **255**(1), 48–58 (2008).

[118] Song, W. G., Nicholas, J. B., and Haw, J. F. *Journal of Physical Chemistry B* **105**(19), 4317–4323 (2001).

[119] Haw, J. F., Nicholas, J. B., Song, W., Deng, F., Wang, Z., Xu, T., and Heneghan, C. S. *Journal of the American Chemical Society* **122**(19), 4763–4775 (2000).

[120] Sassi, A., Wildman, M. A., Ahn, H. J., Prasad, P., Nicholas, J. B., and Haw, J. F. *Journal of Physical Chemistry B* **106**(9), 2294–2303 (2002).

[121] Sassi, A., Wildman, M. A., and Haw, J. F. *Journal of Physical Chemistry B* **106**(34), 8768–8773 (2002).

[122] Anderson, M. W. and Klinowski, J. *Journal of the American Chemical Society* **112**(1), 10–16 (1990).

[123] Price, G. L. and Iglesia, E. *Industrial & Engineering Chemistry Research* **28**(6), 839–844 (1989).

[124] Schulz, H. *Catalysis Today* **154**(3-4), 183–194 (2010).

[125] Svelle, S., Arstad, B., Kolboe, S., and Swang, O. *Journal of Physical Chemistry B* **107**(35), 9281–9289 (2003).

[126] Chiang, H. and Bhan, A. *Journal of Catalysis* **271**(2), 251 – 261 (2010).

[127] Liu, D., Bhan, A., Tsapatsis, M., and Al Hashimi, S. *ACS Catalysis* **1**(1), 7–17 (2011).

[128] Bhat, Y. S., Halgeri, A. B., and Rao, T. *Industrial & Engineering Chemistry Research* **28**(7), 890–894 (1989).

[129] Sotelo, J. L., Uguina, M. A., Valverde, J. L., and Serrano, D. P. *Industrial & Engineering Chemistry Research* **32**(11), 2548–2554 (1993).

[130] Sotelo, J. L., Uguina, M. A., Valverde, J. L., and Serrano, D. P. *Industrial & Engineering Chemistry Research* **35**(4), 1300–1306 (1996).

[131] Al-Khattaf, S., Rabiu, S., Tukur, N. M., and Alnaizy, R. *Chemical Engineering Journal* **139**(3), 622–630 (2008).

[132] Odedairo, T., Balasamy, R. J., and Al-Khattaf, S. *Industrial & Engineering Chemistry Research* **50**(6), 3169–3183 (2011).

[133] Chen, S. Z., Huddersman, K., Keir, D., and Rees, L. V. C. *Zeolites* **8**(2), 106–109 (1988).

[134] Zhang, X., Liu, D., Xu, D., Asahina, S., Cychosz, K. A., Agrawal, K. V., Al Wahedi, Y., Bhan, A., Al Hashimi, S., Terasaki, O., Thommes, M., and Tsapatsis, M. *Science* **336**(6089), 1684–1687 (2012).

[135] Arstad, B. and Kolboe, S. *Journal of the American Chemical Society* **123**(33), 8137–8138 (2001).

[136] Chiang, H. and Bhan, A. *Journal of Catalysis* **283**(1), 98 – 107 (2011).

[137] Arstad, B., Kolboe, S., and Swang, O. *Journal of Physical Chemistry A* **109**(39), 8914–8922 (2005).

[138] Erichsen, M. W., Svelle, S., and Olsbye, U. *Journal of Catalysis* **298**(0), 94–101 (2013).

[139] Seiler, M., Wang, W., Buchholz, A., and Hunger, M. *Catalysis Letters* **88**(3-4), 187–191 (2003).

[140] Arstad, B., Kolboe, S., and Swang, O. *Journal of Physical Organic Chemistry* **17**(11), 1023–1032 (2004).

[141] Yoon, K. B. and Kochi, J. K. *The Journal of Physical Chemistry* **95**(9), 3780–3790 (1991).

[142] Olson, D. H., Kokotailo, G. T., Lawton, S. L., and Meier, W. M. *The Journal of Physical Chemistry* **85**(15), 2238–2243 (1981).

APPENDIX

A

LIST OF ABBREVIATIONS

The following abbreviations are used in this work:

4ET:	4-ethyltoluene
2MB:	2-methylbutane + 2-methyl-2-butene
344T2P:	3,4,4-trimethyl-2-pentene
CHD:	cyclohexadiene
DFT:	density functional theory
DME:	dimethyl ether
GC:	gas chromatography
MB:	methylbenzene
MR:	member ring
MS:	mass spectrometry
MTG:	methanol-to-gasoline
MTH:	methanol-to-hydrocarbons
MTO:	methanol-to-olefins
NMR:	nuclear magnetic resonance

APPENDIX

B

REACTOR UNIT DESIGN

A schematic of the reactor unit used for all the results presented in this work is shown in Figure B.1.

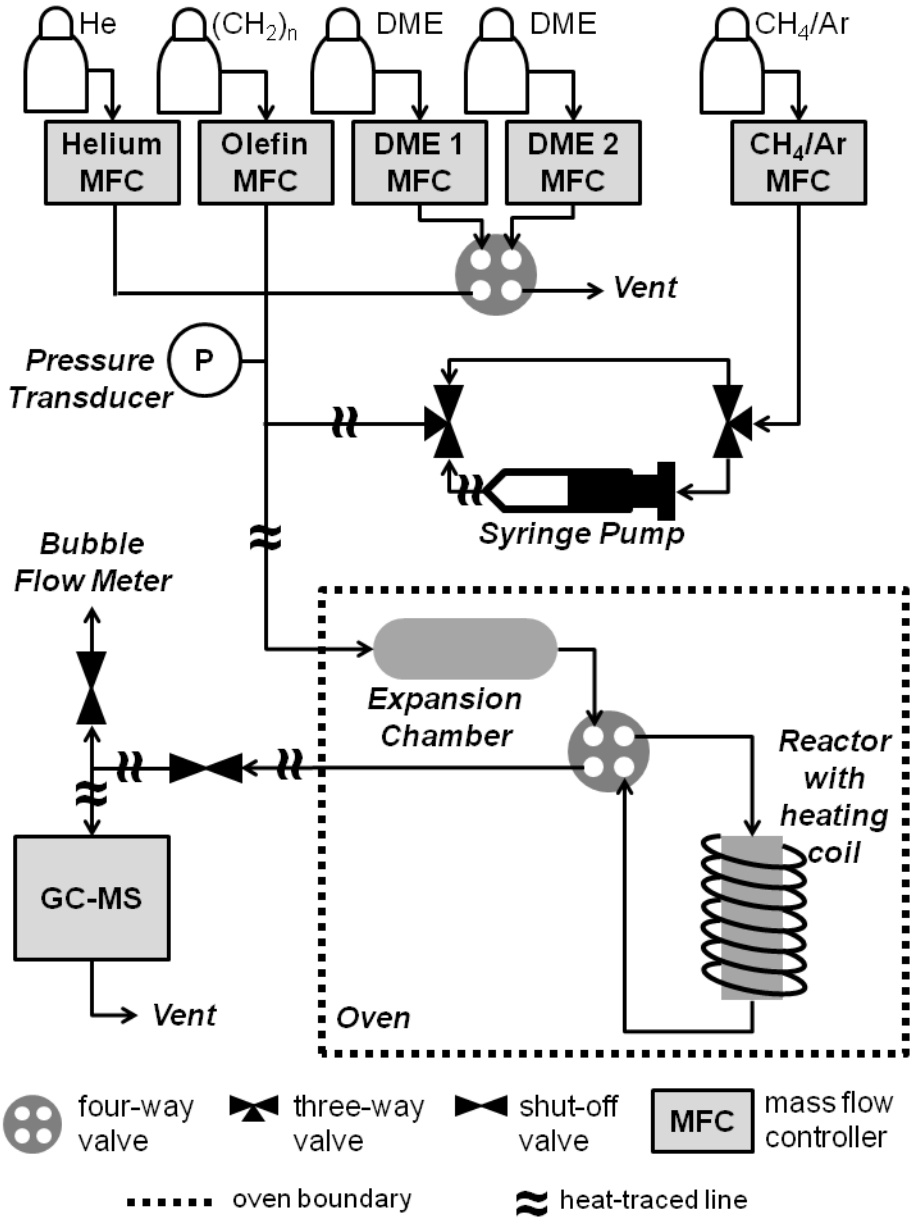

Figure B.1: A schematic of the reactor unit used for all the results presented in this work.